12-2008

CHARACTERIZATION OF VASCULAR SMOOTH MUSCLE CELL MECHANICAL AND FRICTIONAL PROPERTIES USING ATOMIC FORCE MICROSCOPY

Jason Hemmer
Clemson University, jhemmer02@yahoo.com

CHARACTERIZATION OF VASCULAR SMOOTH MUSCLE CELL MECHANICAL AND FRICTIONAL PROPERTIES USING ATOMIC FORCE MICROSCOPY

A Dissertation
Presented to
the Graduate School of
Clemson University

In Partial Fulfillment
of the Requirements for the Degree
Doctor of Philosophy
Bioengineering

---

by
Jason Douglas Hemmer
December 2008

Accepted by:
Dr. Martine LaBerge, Committee Chair
Dr. Delphine Dean
Dr. Eugene Langan, III
Dr. Jiro Nagatomi
Dr. Alexey Vertegel

ABSTRACT

A working hypothesis within the Laboratory of Vascular Research is that mechanical loading on vascular smooth muscle cells (VSMCs), especially due to solid contact from endovascular devices, contributes to the development of restenosis. In order to better understand the role of mechanical loading on VSMCs in vascular disease development, it is imperative to understand the mechanical properties of VSMCs themselves. To measure the viscoelastic and frictional properties of living VSMCs in an *in vitro* setting, an atomic force microscope (AFM) was utilized, thereby allowing for mechanical testing of living cells in a fluid environment. In the first phase of research, it was found that proliferative VSMCs, similar to those commonly found in atherosclerotic lesions, had lower stiffness and higher hysteresis values than quiescent VSMCs. Furthermore, measured stiffness values did not appear to deviate greatly within the central region of adherent cells. As VSMCs are viscoelastic, rather than purely elastic in their mechanical behavior, phase two involved the development of an AFM-based stress relaxation technique, in order to quantify VSMC viscoelastic behavior. Suitable mechanical models, including the QLV reduced relaxation function and a simple power-law model, were identified and applied to accurately describe VSMC stress relaxation. In addition, the roles of two major cytoskeletal components, actin and microtubules, in governing stress relaxation behavior, were quantified via the aforementioned mechanical models. In phase three, the surface frictional properties of VSMCs were focused upon, and a novel method to quantify surface shear forces on VSMCs using lateral force microscopy was developed. It was determined that VSMC frictional properties are

greatly influenced by cell stiffness, and elastohydrodynamic lubrication was proposed as a possible cellular lubricating mechanism. During research phase four, each of the techniques developed during the preceding phases was employed to test the effects of a clinically relevant biomolecule, oxidized low-density lipoprotein (oxLDL) on VSMC mechanical properties. It was concluded that oxLDL is associated with decreased cell stiffness, and decreased viscosity, as measured by stress relaxation and indentation tests. Furthermore, frictional coefficients were found to correlate positively with more fluid-like cells. This research project has led to a better understanding of VSMC mechanical behavior, as well as the development of AFM-based techniques and models that will be useful in determining cellular mechanical and frictional effects of various stimuli in an *in vitro* environment.

DEDICATION

This work is dedicated to my extraordinary wife Helen, whose unfailing support and encouragement has sustained me throughout the process of obtaining my doctoral degree, and to my parents, Richard and Linda, who instilled in me a love of learning, and taught me the value of an education.

ACKNOWLEDGEMENTS

I would like to acknowledge my advisor, Dr. Martine LaBerge, who showed me that patience and perseverance were the most important virtues one can have as a researcher. She has served as an outstanding role model, and I know that my career in science will be all the more rewarding as a result. In addition, my doctoral committee members, Dr. Delphine Dean, Dr. Jiro Nagatomi, Dr. Alexey Vertegel, and Dr. Gene Langan, have all been instrumental as teachers and mentors throughout the course of my research, and I owe them tremendous gratitude. I would also like to thank the laboratory of Dr. Anand Ramamurthi for harvesting and providing the cells used in this study. Lastly, Bethany Acampora and Cassie Gregory each deserve a sincere thank you, for their assistance with cell culture and day-to-day laboratory work.

TABLE OF CONTENTS

Page

Table of Contents (Continued)

Page

LIST OF TABLES

LIST OF FIGURES

CHAPTER ONE

LITERATURE REVIEW

The current doctoral research project addresses vascular restenosis following stent implantation. It is hypothesized that one of the key factors in restenosis is a shift in vascular smooth muscle cell mechanical properties, caused in part by the associated inflammatory response. Overall this research is intended to help understand this relationship both from a basic science perspective, and with a long-term goal of finding novel preventative treatments for vascular disease.

Vascular diseases, including atherosclerosis and restenosis, are among the world's most widespread, costly, and lethal medical conditions [1]. This remains true, despite recent advances in treatment, including the advent of drug eluting stents, as well as pharmaceutical treatments such as statins. At their core, atherosclerosis and restenosis are both inflammatory diseases with significant biomechanical components [2, 3]. A highly complex inflammatory process coupled with cellular mechanical environment both play crucial roles in the development and duration of vascular disease. Recent evidence has begun to demonstrate that cellular mechanical behavior, inflammation, and disease progression are inextricably linked [2, 3] . With the rapid development of the fields of bioengineering, biochemistry, and molecular biology, it is now possible to study these phenomena at the single cell or even single molecule level. It is this link between vascular disease as an inflammatory disease and a biomechanical disorder that serves as the primary motivation for this research. The literature review that follows is a summary

of current knowledge regarding vascular diseases as inflammatory and mechanical disorders, as well as cell mechanics theory and experimentation.

Atherosclerosis: An Inflammatory Disease

Atherosclerosis is the leading cause of mortality in the Western world, accounting for approximately 55% of all deaths [4]. This mortality rate remains staggeringly high, despite recent advances in treatments such as the introduction of drug eluting stents, as well as an increased understanding of preventative measures relating to diet and exercise. Atherosclerosis refers to a vascular disease characterized by accumulation of lipids and fibrous components in medium and large sized arteries, although the word itself means hardening of the arteries. It is a complex, multi-stage disease process that is associated with a number of risk factors, including elevated blood pressure (hypertension), obesity, diabetes mellitus, smoking, elevated low-density lipoprotein (LDL) cholesterol levels, family history and advanced age [2]. Many of the aforementioned factors have a strong genetic component, while others are environmental in origin [1]. In general, atherosclerosis can be thought of as a multi-stage inflammatory disease. Among the most significant phenomena observed during the pathogenesis of atherosclerosis, are endothelial dysfunction, a significant and prolonged inflammatory response, alterations in the extracellular matrix (ECM) of the affected region, and vascular cell proliferation [5, 6]. Interestingly, many dangerous lesions are often non-occlusive and therefore difficult to diagnose by angiography. However, active inflammation is evident in these non-occlusive lesions. Plaque inflammation can be detected through various screening

methods, as it is generally associated with increased plasma concentrations of fibrinogen and C-reactive protein (CRP) [6]. Local inflammation is also associated with increased temperature and lower pH levels, which can thus be used to measure inflammatory response in the plaque [6]. The information contained here regarding the progression of atherosclerosis is by no means complete. Given the complexity of the disease, such an undertaking would require a far lengthier discussion. For the purposes of this literature review, the information is meant to give a basic background and to support the idea that atherosclerosis is both an inflammatory disease and a biomechanical disorder, caused by an immune response gone awry. In addition, some, but not all, of the major biochemical players in atherosclerosis are discussed. Much remains to be learned regarding the disease's pathology, which is why there is a vast amount of ongoing research dedicated to further elucidating these disease mechanisms. The current research was motivated both by the idea of gaining a greater understanding of atherosclerosis from a basic science perspective, and by the search for more effective and targeted treatments.

Endothelial Dysfunction

The disease process is believed to begin with endothelial dysfunction, which can be the result of numerous stimuli, including smoking, hypertension, diabetes, genetic alterations, elevated homocysteine concentrations, and infectious microorganisms [6]. The vascular endothelium secretes a wide variety of active molecules (vasoactive substances, matrix products, procoaguluant factors, antithrombotic factors, growth factors, inflammatory mediators), and performs a myriad of functions including: acting as

a barrier to free passage of molecules and cells, mediating endothelium-dependent vasodilation, inhibiting leukocyte adhesion, migration, platelet adhesion, and aggregation, inhibiting VSMC migration and proliferation; inhibiting coagulation, promoting fibrinolysis, and participating in immune and inflammatory reactions [6]. An early marker of endothelial dysfunction is the reduction of nitric oxide (NO) activity, a regulator of vessel tone [6]. In animal models, an atherogenic diet causes endothelial cells (ECs) to express surface adhesion molecules (intracellular adhesion molecules (ICAMs) and vascular adhesion molecules (VCAMs)) that act as receptors for glycoconjugates and integrins present on monocytes and T-cells [6].

Onset of the Inflammatory Response

Following the changes that occur to the endothelial layer, monocytes are recruited to the affected area, and subsequently they migrate through the irregularly functioning endothelial layer with the help of chemoattractants (MCP-1 is responsible for migration of monocytes) [6, 7]. Monocytes may initially play a protective role, however, their continued accumulation is ultimately one of the key factors in the development of an atherosclerotic lesion [1]. The monocytes differentiate into macrophages under the influence of macrophage-colony stimulating factor (M-CSF) [6], take up accumulated lipids (forming foam cells, Figure 1.1), and eventually form fatty streaks, which can be found in the human aorta in the first decade of life [1].

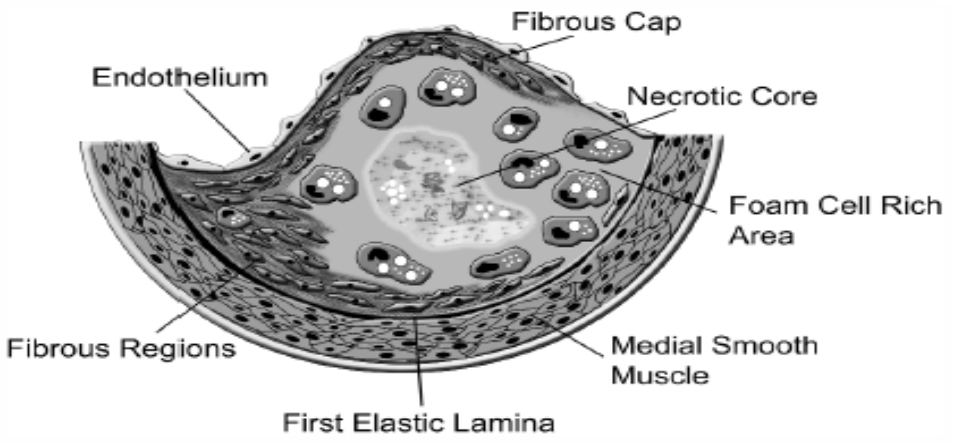

Figure 1.1. Diagram of the various components of an atherosclerotic lesion, including the necrotic core, foam cells, and fibrous regions. Figure from Jerome (2006)[8]

Foam cells eventually die, contributing their contents to what is known as the necrotic core (Figure 1.1). If the initial inflammatory response resulting from endothelial dysfunction fails, the inflammatory process continues, which leads to VSMC migration and proliferation [6]. VSMCs migrate to the intima from the media, secreting ECM components such as collagen and various proteoglycans. Lesions initially grow towards the adventitia, until a critical point is reached, when they begin to expand towards the lumen [1]. As the disease progresses, continued recruitment of inflammatory cells and lipids, and proliferation of SMCs, leads to the development of a mature atherosclerotic plaque. A fibrous cap separates this underlying conglomeration of lipids, SMCs, and ECM constituents from the luminal blood flow (Figure 1.2).

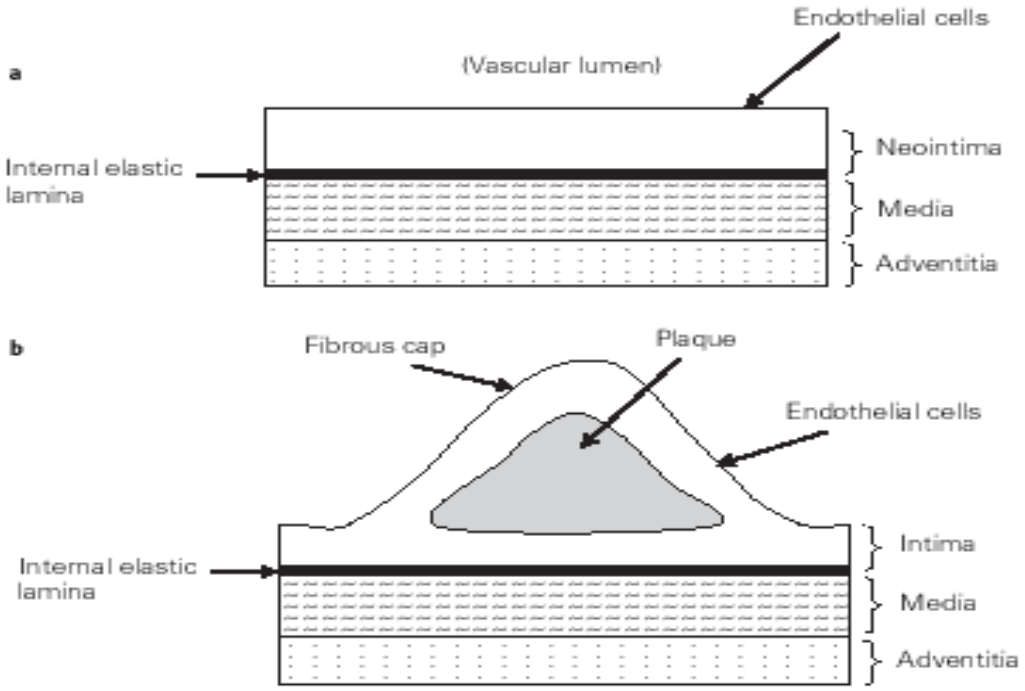

Figure 1.2. Schematic representation of a healthy artery wall (a) and an atherosclerotic lesion (b) with plaque and fibrous cap formation. Figure from Steffens and Mach (2004)[7].

The fibrous cap is most likely formed by migration of SMCs from the media, and their collagen production [6]. Thinning of this fibrous cap may lead to rupture of the plaque, and an acute ischemic event such as a cardiac infarction or stroke, depending on the origin of the lesion. Plaque rupture, which typically occurs in regions of high tangential stress and collagen depletion, sustained inflammation, macrophage accumulation, and apoptosis, (often at the shoulders of the lesion) is responsible for 80% of fatal myocardial infarctions (MI) in men [6]. Half of all infarctions occur in arteries that have < 50% stenosis, and the presence of inflammation seems to be a key characteristic. It has been found that the occurrence of acute coronary events is more

heavily dependent on the composition of the plaque, rather than the degree of stenosis caused by the lesion [1]. Additionally, the stability of atherosclerotic lesions may depend upon the degree of calcification [1].

Numerous signaling molecules and immune cells interact with one another during lesion formation. All of these components contribute to the formation of a vicious cycle, characterized by increased lesion thickening and growth (Figure 1.3) [6].

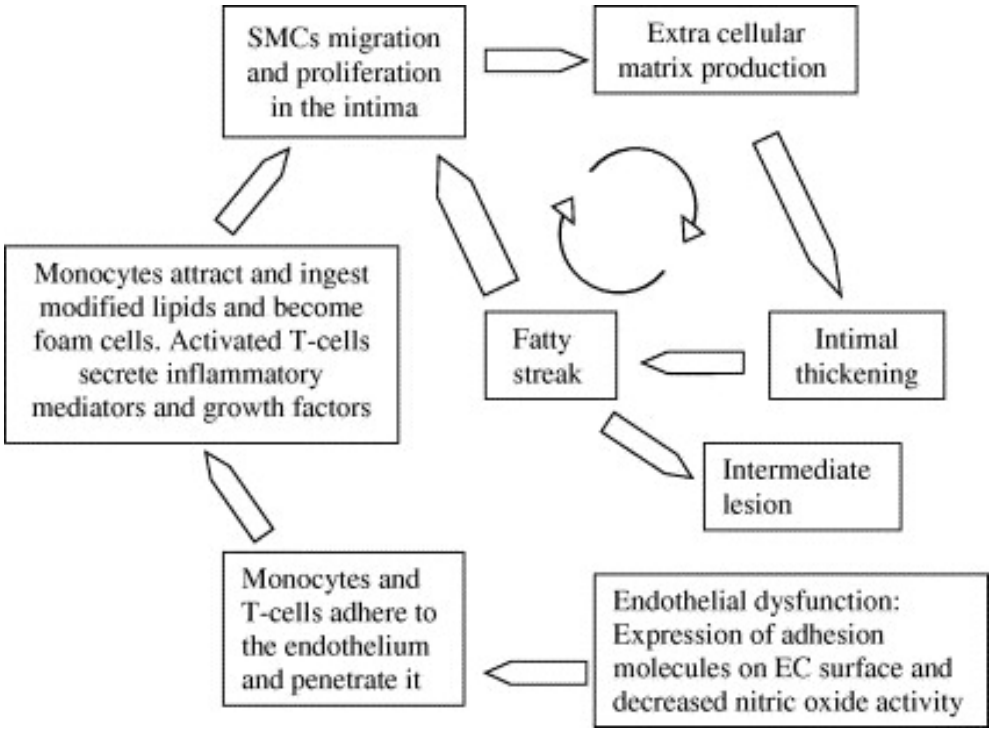

Figure 1.3. Major events occurring during development of an atherosclerotic lesion, beginning with endothelial dysfunction, and leading to a vicious cycle of ECM production, VSMC migration/proliferation, and intimal thickening. Figure from Kaperonis, et al. (2006)[6].

Among the biomolecules that play roles in atherosclerotic lesion development and inflammtion are lipoproteins, cytokines, and adhesion molecules. A brief overview of the interaction among some of these key players is given here.

Lipoproteins

One of the main culprits in the development of atherosclerosis is LDL cholesterol [9], which is present in blood plasma. Low-density lipoprotein is responsible for transport of lipids to peripheral tissues such as arteries, while high-density lipoprotein (HDL) is responsible for the removal of lipids from these tissues. Hence, HDL has an anti-atherogenic effect, while high LDL levels can be detrimental to one's health. Native LDL, is not taken up by macrophages rapidly enough to form foam cells, however oxidized LDL does contribute to foam cell formation [1]. Oxidation of the LDL takes place from a reactive oxygen species (oxidative waste) produced by endothelial cells, macrophages, and SMCs. Nitric oxide (NO) is an oxidizing agent produced by endothelial cells and macrophages, and evidence suggests that it can have either atherogenic or atheroprotective effects, depending on its source [7]. Oxidized LDL can inhibit the production of NO, possibly leading to increased lesion development due to the potential anti-atherogenic properties of NO [10]. Oxidized LDL can also penetrate the endothelium, upregulate adhesions molecules on endothelial cells, as well as induce the expression of monocyte chemoattractant protein (MCP)-1, and a number of growth factors [11, 12]. Areas of the endothelium subject to disturbed flow patterns such as bifurcated or curved regions, are susceptible to increased LDL permeability and

atherosclerotic lesion development [13]. The atheroprotective effects of HDL may be in part due to to its anti-inflammatory and anti-oxidant properties, as HDL particles can carry anti-oxidant enzymes [6].

Adhesion Molecules

As mentioned above, various adhesion molecules mediate the adherence and migration of leukocytes across the endothelial layer (Figure 1.4) [7]. A group of adhesion molecules known as selectins (including E-selectin and P-selectin) mediate the rolling of inflammatory leukocytes across the endothelial layer during the early stages of atherogenesis [14]. Intracellular adhesion molecules (ICAM-1) and vascular adhesion molecule (VCAM-1), along with integrins, play similar roles in the attachment, arrest, and subsequent migration of leukocytes [15, 16]. Macrophages and endothelial cells produce ICAM-1 in response to a number of inflammatory cytokines, including IL-6, IL-1, Tumor Necrosis Factor (TNF)-α, and interferon (IFN). On the other hand, VCAM-1 is only expressed by endothelial cells [14], and its expression precedes macrophage and T-lymphocyte recruitment [17].

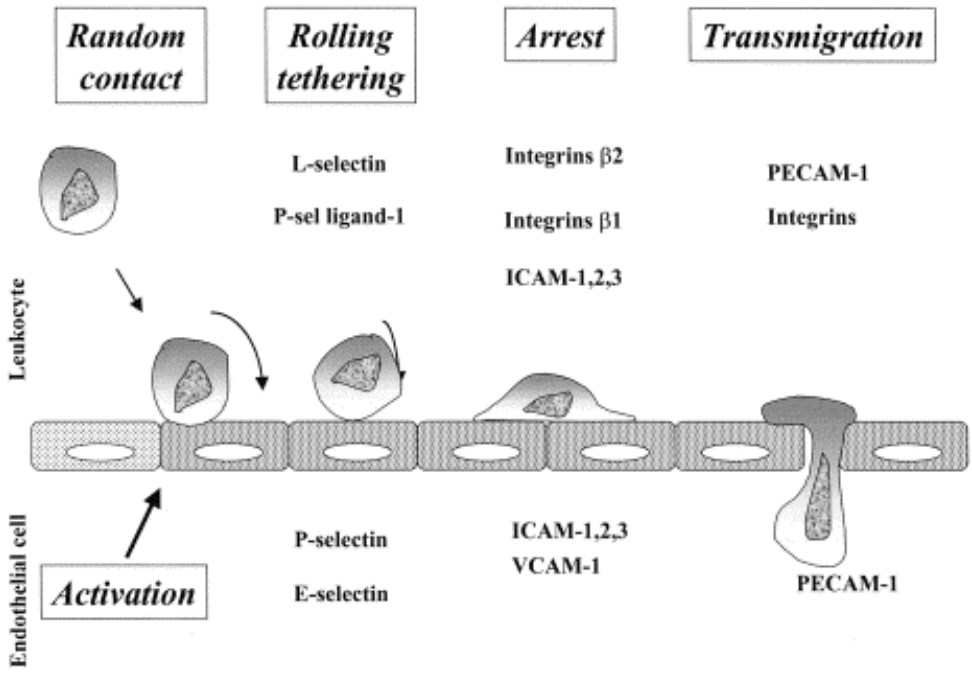

Figure 1.4. The role of various adhesion molecules in endothelial-leukocyte interactions. Figure from Blankenberg, et al. (2003)[15].

Gap Junctions

Important ion and metabolite exchange channels known as gap junctions have also been found to contribute to leukocyte migration and the development of atherosclerosis [18]. Gap junctions are formed by the connexin (Cx) family of proteins, with changes in Cx37, 40, and 43 expression all having been implicated in the development of atherosclerosis [18].

Cytokines

The elevation and modification of lipoproteins associated with atherosclerotic lesion development leads to the release of cytokines and attraction of cells expressing receptors for these cytokines [19]. Cytokines can in turn promote lesion development or

block it, depending upon which ones are involved. Opposing effects can be exerted by pro- and anti-inflammatory cytokines during the course of lesion development [20]. Some of the proinflammatory cytokines, such as TNF-α, are inducers of other cytokines and chemokines, which results in an autoamplification system that makes it difficult to distinguish the effects of each particular cytokine in the atherosclerotic process [19]. Proinflammatory cytokines can be produced by, and act on, numerous cell and tissue types (Figure 1.5) [20].

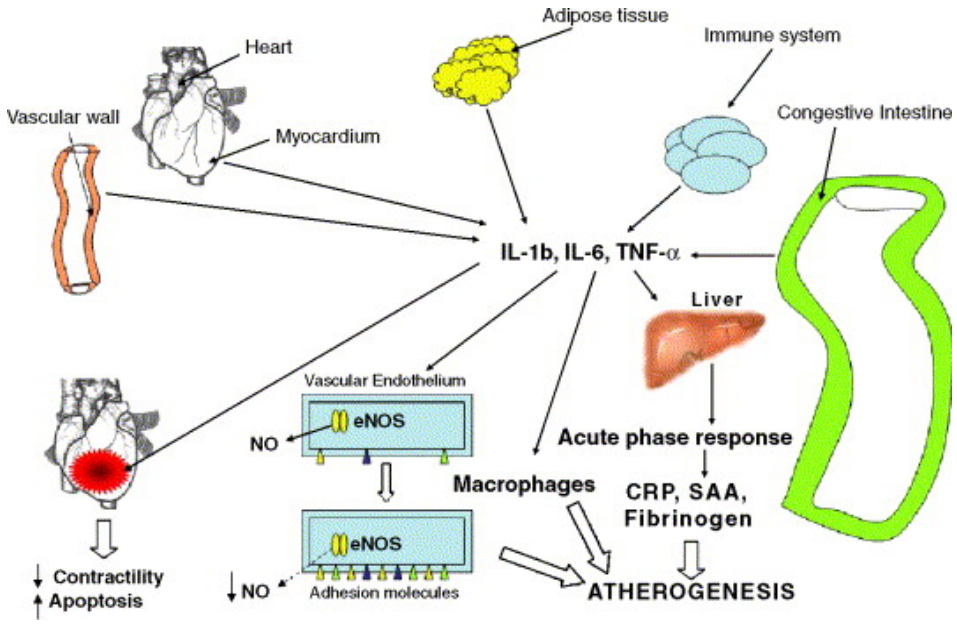

Figure 1.5. Action of the proinflammatory cytokines IL-1b, IL-6 and TNF-α on various cells and tissues. Figure from Tousoulis, et al. (2006)[20].

It has been shown that certain cytokines can alter SMC phenotype and modulate the nature of matrix synthesis and secretion [21]. The proinflammatory cytokines MCP-1,

SDF1alpha, and CCL11 have been implicated in the promotion of SMC migration and proliferation following acute injury from a balloon or wire [22]. Other injury models have found that IL-1 and TNF-α both appear to promote SMC accumulation after injury [23]. Some murine models have suggested that neither IL-1β nor TNF- α, two cytokines associated with atherosclerotic lesions, appear to strongly affect the accumulation of SMCs within those lesions. It is however, believed that TNF-α plays a significant role in the induction of SMC adhesion molecule expression [19]. Thus, discrepancies are often noted among different atherosclerotic models [19]. The cytokine MIF (macrophage migration inhibitory factor) induces disease progression as a potent stimulant of SMC accumulation and matrix deposition following vascular injury and in atherosclerosis [24]. Adipose tissue can synthesize cytokines, including TNF-α and IL-6, meaning that obesity can promote inflammation and advance atherogenesis, independently of its effect on insulin resistance and lipoprotein metabolism. Both TNF-α and IL-6 have been found to be associated with 1-year mortality in patients with critical limb ischemia [25]. In terms of negative regulation of VSMC proliferation, both IL-10 and IL-18 appear to play that role *in vivo*, with the majority of other involved cytokines leading to enhanced proliferation [26, 27]. Similarly, it should be noted that IL-10 and TGF- β are potent inhibitors of the pleiotropic (controlling several distinct and unrelated phenotypes) NF-κβ signaling pathway, which has been linked to atherosclerosis [19]. Transforming growth factor (TGF)-β is a cytokine that plays a significant role in the inflammatory component of atherosclerosis. Studies conducted under various experimental conditions have found conflicting results, but the most recent data indicate that TGF- β plays a protective role.

Other cytokines, such as M-CSF, which stimulates the proliferation and differentiation of macrophages, have been shown to play an atherogenic role and contribute to lesion formation [28]. Taken together, this suggests that certain anti-inflammatory cytokines may limit SMC modulation during the atherosclerotic and restenotic disease processes. Given the vast number of cytokines involved in vascular disease, along with their complex interactions and conflicting data regarding their roles, it is clear the further research in this area is needed.

VSMC Physiology and Phenotypic Modulation

One significant result of the physiologic action of lipoproteins, adhesion molecules, and immune cells, is an alteration in smooth muscle cell function and phenotype. In fact, the phenotypic state of VSMCs can be affected by numerous different stimuli, including humoral factors, cell-cell interactions, and mechanical forces (Figure 1.6).

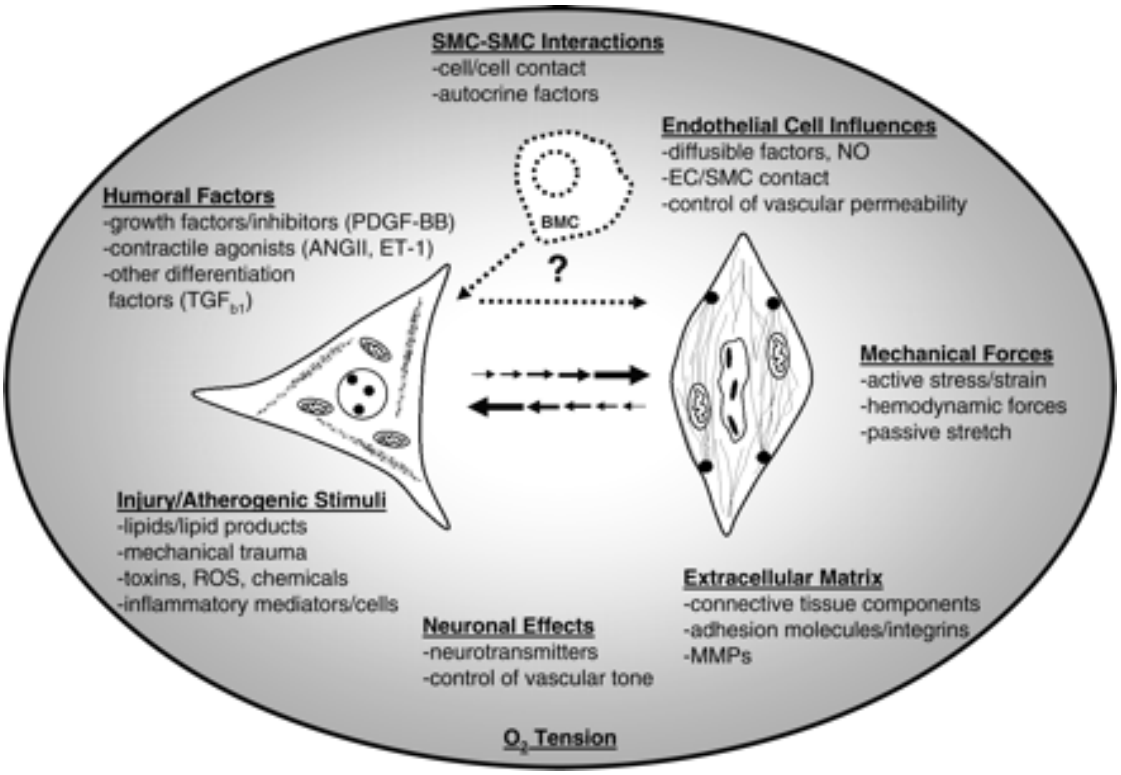

Figure 1.6. Phenotypic state of SMCs can vary greatly from fully differentiated (right) to synthetic (left) based on influence of numerous stimuli. Figure from Owens, et al. (2004)[4].

Smooth muscle cells are unique among the three major types of muscle cells (skeletal, cardiac, smooth) in their retention of phenotypic plasticity, where as both skeletal and cardiac muscle cells are terminally differentiated [4, 29]. It is likely that the plasticity of VSMCs evolved as a means of repairing damaged blood vessels and remodeling for blood pressure regulation [4]. However, with the increasing life-expectancy of humans, this reparative mechanism can often give rise to the development of atherosclerotic lesions. In the adult blood vessel, SMCs exhibit extremely low proliferation and

migration rates, and express a unique set of contractile proteins, including smooth muscle α-actin, smooth muscle γ-actin, sm-MHC (myosin heavy chain), calponin, h-caldesmon, SM22, smoothelin, and metavinculin [4, 29]. The principal function of SMCs in their healthy contractile state is the regulation of blood vessel tone, blood pressure, and blood distribution [4]. In certain cases, such as during vascular development, and in disease states such as atherosclerosis and restenosis, a shift from a contractile to a synthetic phenotypic takes place. This shift from the normal contractile state to a synthetic state is known as modulation, and is associated with a decrease in contractile protein content, as well as increased rates of proliferation, migration, and matrix production [29]. In addition to atherosclerosis, changes in SMC phenotype and function have been observed in numerous other diseases, including asthma [30] and cancer [31], as all types of SMCs can undergo modulation. According to Owens, et al. [4], the key points regarding phenotypic modulation of SMCs are that; changes in phenotype of SMC vary as a function of disease stage and location within lesion; it is difficult to identify whether lesion cells were or were not derived from preexisting SMC; environmental cues that exist within atherosclerotic lesions are different from those of a healthy vessel; and phenotypically modified SMCs contribute to alterations in ECM. These key points will now be discussed further.

Intimal SMCs found in atherosclerotic lesions are often characterized by increased DNA synthesis, decreased protein expression, alterations in contractility, and loss of myofilaments [4]. There are several protein markers expressed by SMCs that are indicative of their relative state of differentiation, including SM-α-actin, SM-MHC, h1-

calponin, SM22 α, ACLP, desmin, metavinculin, h-caldesmon, metavinculin, telokin, and smoothelin, but it must be noted that no single marker is exclusively unique to SMCs. It is also important to recognize that SMC phenotype is a continuum, with no set contractile or synthetic cells [32]. Additionally, it has been found that even within a single blood vessel, there is a great deal of heterogeneity among resident SMCs, as evidenced by differing levels of protein expression [33]. The most commonly utilized marker of SMC differentiation is SM-α-actin, due to its abundance, crucial role in SMC contraction, and the availability of its antibodies. Identification of SMC lineage on the other hand however, requires a more SMC specific marker, for which SM-MHC is suitable, due to the fact that it is not expressed in any other cell types, as is SM-α-actin [4]. A positive marker of modulated synthetic phenotype SMCs is SMemb (SM MHC embryonic), which is relatively specific for synthetic and embryonic SMCs [4]. Despite the vast amount of research in the area, very little is actually known regarding the regulation of SMC differentiation and maturation *in vivo*. Among the important factors that play a role however, are mechanical forces, contractile agonists, ECM components, neuronal factors, reactive oxygen species, endothelial-SMC interactions, and various cytokines [4]. The only factor thus far positively identified that directly promotes phenotypic modulation of SMCs is platelet derived growth factor-BB (PDGF-BB), a chemoattractant produced by activated platelets and macrophages [34] which induces proliferation and downregulation of SMC marker genes *in vitro* [35]. Other factors thought to play a role in phenotypic regulation of SMCs include TGF-β, which promotes SMC differentiation in cell culture by upregulating SM-selective markers such as SM-alpha actin and SM MHC [36], and

MMPs, which contribute to degradation and remodeling of plaque ECM, and in turn can cause SMC phenotypic switching [37]. Current understanding of the *in vivo* effects of these factors is poor, as most of our information is based on *in vitro* studies. Despite the ever-increasing library of knowledge regarding SMC physiology and its relationship to atherosclerosis, it is still not yet known if phenotypic modulation is a cause or an effect of atherosclerosis.

VSMCs and ECM Components

Some of the most noticeable changes that occur during the progression of vascular disease involve the ECM and its components. Interaction of VSMCs with surrounding ECM is mediated by several types of transmembrane receptors. The principal receptors for ECM components on vascular cells include integrins, CD44, and RHAMM [38]. There is a great deal of evidence to suggest that different ECM constituents have varying effects on vascular cell function [32, 38, 39]. A healthy artery will generally by composed of an intima (endothelial cells, minimal subendothelial ECM enriched in proteoglycans and hyaluronan); media (SMCs embedded in ECM comprising elastin, collagen, proteoglycans); and adventitia (fibrillar collagen, fibroblasts, vaso vasora) [38]. One of the main ECM constituents, collagen, is composed of a triple helix of 3 polypeptide α chains, each having a gly-x-y repeating sequence [40]. The predominant forms of collagen found in arteries are types I and III, providing tensile strength to the vessel wall [38]. While collagen provides tensile strength, it is also exhibits elastic behavior, which provides the recoil necessary in an environment with cylic pressure

pulses [41]. Elastic fibers that are synthesized by VSMCs are arranged in concentric lamellae that separate the different layers of the artery. Following balloon injury of a health artery, a neointima forms that is composed mainly of SMCs that migrate from the media to the intima. Injury of an already atherosclerotic vessel however, leads to neointimal accumulation of monocytes and lymphocytes, followed by SMC migration and proliferation [42, 43]. Lesions that are rich in lipids and macrophages typically contain less collagen, while fibrous plaques contain areas rich in collagen I and III [44]. In situ fibronectin assembly by neointimal SMCs has been observed 12 days after injury in rats. Fibronectin also assembled a fibrillar network associated with the surface of synthetic SMCs during early atherosclerotic and restenotic lesion development [45, 46]. Using 2D monolayers *in vitro*, fibronectin and collagen I have been found to induce shifts towards a synthetic state, while laminin and collagen IV induce the opposite [32, 39].

Proteoglycans and hyaluronan are hydrophilic molecules that represent another main ECM constituent. These proteoglycans consist of a core protein linked to one or more polysaccharides that have diverse roles in regulating connective tissue structure and permeability. Hyaluronan is a large molecule consisting of many repeats of a simple disaccharide stretched end to end, which binds a large amount of water forming a viscous hydrate gel. This allows the ECM to resist compressive forces. In addition, proteoglycans and HA are known to interact with vascular cells [38].

The adhesive glycoproteins fibronectin and laminin form connections between other ECM and cells via specific integrin receptors. Fibronectin is a multifunctional adhesive protein present in plasma and synthesized by vascular cells. It is a large

disulphide-linked, glycoprotein dimer that binds collagen, fibrin, and proteoglycans via specific domains as well as vascular cells through specific integrins. Laminin is the most abundant glycoprotein in endothelial and SMC basement membranes. Cells are bound to laminin through specific integrins and interacts with other ECM, such as collagen IV and heparin sulphate [38].

Atherosclerosis: Biomechanical Phenomena

Vascular smooth muscle cells are continuously exposed to cyclic mechanical stretch from arterial blood pressure [3]. When the mechanical environment acting on VSMCs changes, a number of contractile proteins are downregulated, including SM-MHC isoforms, α -actin, h-caldesmon, and calponin [3]. Increased stresses resulting from hypertension lead to myofilament loss, the development of extensive endoplasmic reticulum, and large Golgi complexes, which are all events indicative of the shift towards a synthetic phenotype. In addition, contractile ability is lost, protein secretion is increased, and the cells become more responsive to autocrine and paracrine growth factors that are produced in response to mechanical stress. These growth factors can then lead to further hypertrophy and/or hyperplasia [42]. Biomechanical stress on arterial walls can be increased as much as 30% in cases of severe hypertension, leading to significant changes in the arterial tissue structure [47]. Evidence of the important role of stress states in the development of atherosclerosis is also provided by the fact that lesions occur most frequently in areas of bifurcation or otherwise disturbed stress states [48]. Given the abundant evidence implicating altered stress states in the development of atherosclerosis and restenosis, it has been hypothesized that physical forces can initiate signaling pathways which in turn lead to cell death, an inflammatory response, and VSMC proliferation. A proposed mechanism for this sequence of events is the altering of receptor conformation that may be cause by mechanical stresses [3].

VSMC Mechanosensors

A number of different types of mechanosensors exist on the surface of SMCs. Perhaps the most important in terms of mechanical signal transduction are integrins. These are a family of transmembrane receptors that mediate cell attachment to the ECM at focal contact sites [49]. Integrins are heterodimeric, and consist of non-covalently bound transmembrane α and β subunits, of which there are at least 15 α and 8 β that can heterodimerise to produce more than 20 different receptors (Figure 1.7).

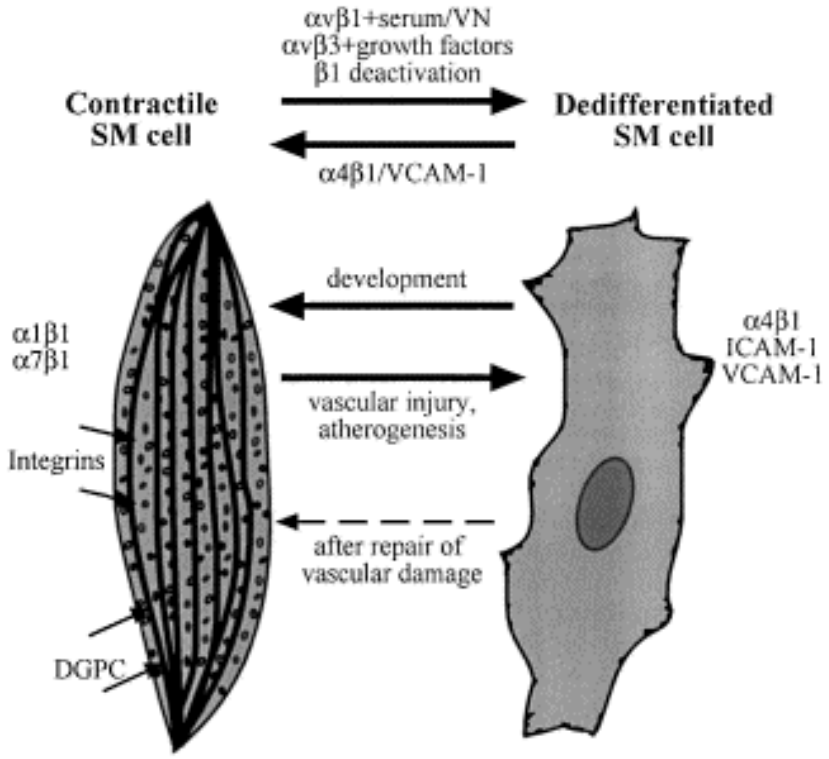

Figure 1.7. Involvement of different of α / β integrin pairings in forming adhesions to various ECM components, and regulating phenotype. Figure from Moiseeva (2001)[50].

Importantly, integrins also transmit extracellular mechanical stimuli to intracellular signaling events [42], in turn activating numerous downstream signals potentially leading to phenomena such as cell migration and cytoskeletal reorganization [3]. In cultured VSMCs, mechanical stress has been shown to increase DNA synthesis when the substrate is collagen, fibronectin, or vitronectin, but not laminin or elastin. This suggests some level of specificity in the cell-ECM interactions that lead to biochemical responses when external stresses are applied [3]. Integrin signaling is also associated with the formation of new focal adhesion complexes consisting of clustered integrins with various cytoskeletal proteins, such as talin and paxillin [3]. It has been shown that focal adhesion kinase (FAK) binds both to the cytoplasmic regions of integrins and to cytoskeletal proteins, providing a direct linkage for signal transduction leading to MAPK activation [51]. Integrin mediated autophosphorylation of FAK can lead to subsequent tyrosine phosphorylation of various cytoskeletal proteins and cytoskeletal remodeling, as a result of mechanical stimuli [3].

Mechanical stresses have been shown to alter the structure and organization of intracellular actin (Figure 1.8) [52]. Vascular SMCs contain a reservoir of unpolymerized globular (G) actin, which their skeletal and cardiac counterparts do not possess. Intravascular pressure leads to a decrease in G-actin concentration, and in increase in filamentous (F) actin [53]. Depolymerization of F-actin with substances such as cytochalasin D leads to an increase in G-actin content, and cell relaxation, while polymerization of F-actin causes cell contraction and decreased G-actin content [52]. Such formation of F-actin could very well be involved in mechanical signal transduction

and increased force production. The exact mechanism by which mechanical forces induce actin polymerization is not known, but it most likely involves integrin-mediated signal transduction.

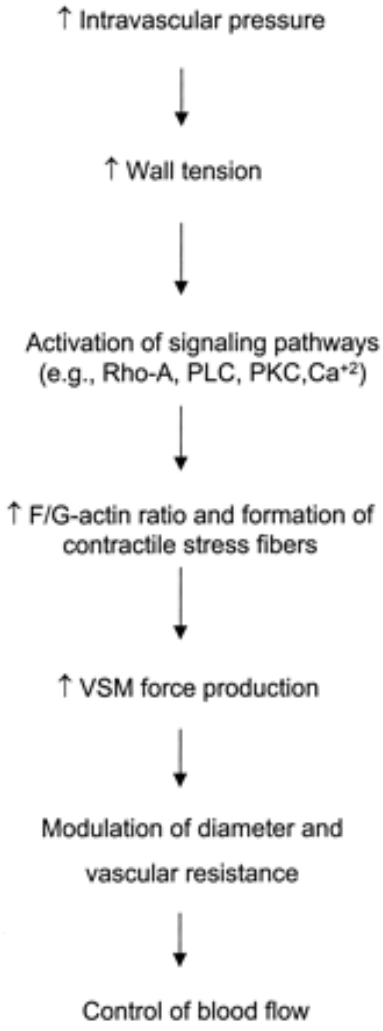

Figure 1.8. Increased intravascular pressure leads to activation of numerous cross-talking signaling pathways, along with an increased F/G-actin ration, formation of stress fibers, and greater force production. Figure from Cipolla, et al. (2002)[52].

Platelet derived growth factors (PDGF) are homo- or heterodimers of A and B polypeptide chains that can combine to form form three different dimers, PDGF-AA, BB, and AB. Thus far, two distinct PDGF receptors have been described, PDGF receptor-α, which binds all PDGF forms, and PDGF receptor-β, which binds PDGF-BB and AB [54]. It has been shown that PDGF receptor-MAPK signaling pathways can be directly activated by mechanical forces [55], suggesting a role in modulation of VSMCs. Vascular endothelial growth factor (VEGF) is also upregulated by VSMCs in response to mechanical stress. It is possible that normal physiological levels of stress are necessary to produce sufficient levels of VEGF, and therefore maintain a healthy endothelium [4].

Another significant phenomenon observed with regard to VSMC response to mechanical force is the opening of mechanically gaited ion channels, which leads to a transient influx of calcium and sodium. This cause depolarization of the membrane and a subsequent myogenic response [56]. It is likely that this calcium influx, along with increased levels of angiotensin leads to increased MAPK activation in cases of hypertension. Mechanical stress has also been shown to increase protein kinase C (PKC) activity in VSMCs, leading to formation of PKC particulates and subsequent VSMC proliferation in the case of cyclic strain [57]. It is likely that PKC is involved in a number of signaling pathways, due to the many signaling molecules that it can activate. Mitogen-activated protein kinases (MAPKs), including extracellular signal-regulated kinases (ERKs), p38, and c-Jun N-terminal kinases (JNKs), are also activated in response to mechanical stress. This is significant because MAPKs regulate such important cellular processes is DNA synthesis, proliferation, mitosis, and apoptosis [4]. Some kinases, such

as MAPK phosphatase-1 and PKA (cyclic AMP-dependent protein kinase), may actually serve as negative feedback regulators by blocking mechanical signal transduction [58, 59].

Smooth muscle cell apoptosis often occurs in atherosclerotic lesions, and is in part affected by mechanical stresses. In restenosis, VSMC apoptosis is an acute event that occurs in response to vascular injury induced by balloon-catheter or angioplasty. This medial VSMC cell death has been demonstrated *in vivo* using animal models [60]. Apoptosis after cell injury is governed by activation of MAPK signaling pathway and expression level of antiapoptotic genes. Among the factors relating SMC apoptosis in response to mechanical stress are endothelin receptor expression, p38, p53, and DNA oxidation [61-63]. Mechanical stresses play a significant role in the mediation of the VSMC inflammatory response during atherosclerosis. Increased mechanical stresses lead to increased production of leukocyte adhesion molecules and promote VSMCs to produce proteglycans. These proteoglycans bind and retain LDL particles, leading to their oxidative modification which promotes inflammatory responses within atherosclerotic lesions [64]. Production of ICAM-1 by VSMCs has also been shown to be induced by mechanical stresses in animal models [65].

Atherosclerosis Summary

It can be seen that atherosclerosis and the abnormal physiologic behavior of VSMCs associated with it, are affected by numerous stimuli working in conjunction with one another. This complexity makes understanding and treating vascular disease all the more formidable of a task. However, at its core, it is now beginning to be understood that

atherosclerosis is essentially a chronic inflammatory disease, which is greatly affected by the mechanical state of the cells and tissues involved. Therefore a better understanding of the link between atherosclerosis as an inflammatory disease and a biomechanical disorder, may yield important information to aid in the development of novel treatments.

Treatment of Atherosclerosis

Stents and Restenosis

In recent years, stenting has become the preferred method for percutaneous treatment of coronary artery disease, due to its advantages of preventing elastic recoil of the artery, preventing acute vessel closure, and improving long-term patency [66]. In the year 2000, over one million percutaneous coronary procedures were performed in the US, almost half of which included placement of intracoronary stents [66]. One of the most frequent difficulties encountered following stent implantation is that of restenosis, which is a re-occlusion of the treated vessel region. Restenosis is generally caused by vascular elastic recoil and negative remodeling of the vessel wall (Figure 1.9) [67]. Stents reduce the level of recoil, but also stimulate the formation of neointimal tissue, especially in smaller caliber arteries [67].

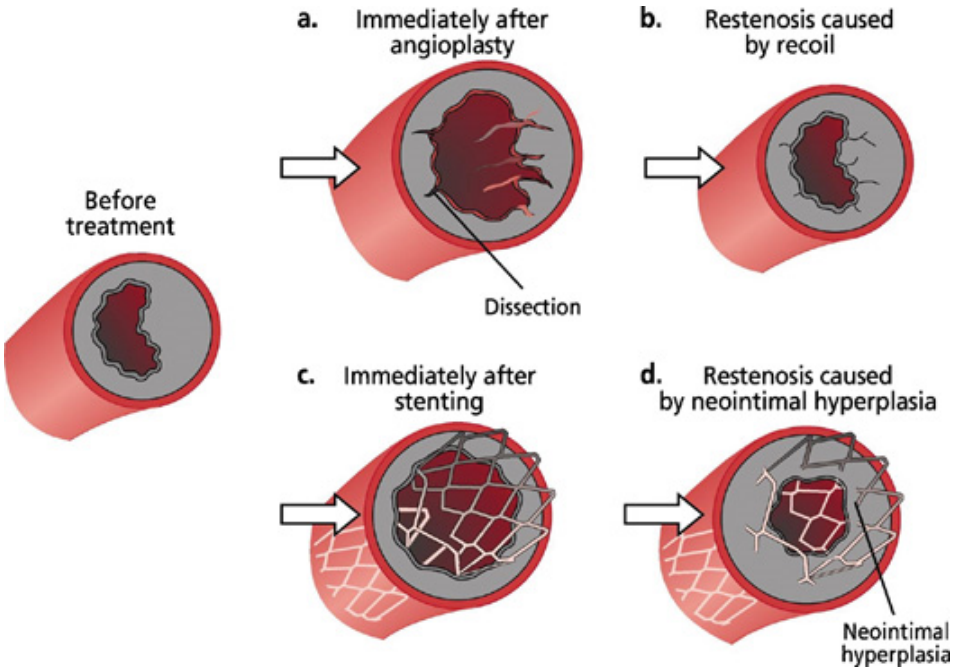

Figure 1.9. Restenosis after angioplasty (a-b) and after stenting (c-d). Figure from Kivela, et al. (2006)[68].

Stent deployment is a traumatic event that can alter local vessel conditions in a number of ways. Stainless steel stents are placed via balloon-driven expansion, often requiring a second dilation, leading to overexpansion of the vessel [69]. This initial injury caused by balloon inflation and the stent itself, leads to the migration of macrophages and polymorphonuclear neutrophils to the damaged region [70-72]. These immune cells then release chemokines, increasing the amount matrix metalloproteinase (MMP), and subsequently leading to remodeling of the ECM and SMC migration.[73, 74]. Mitogenic SMC genes are stimulated as well [75]. Furthermore, stenting has been shown to raise systemic levels of inflammatory markers such as IL-6 and C-reactive protein (Figure 1.10) [76].

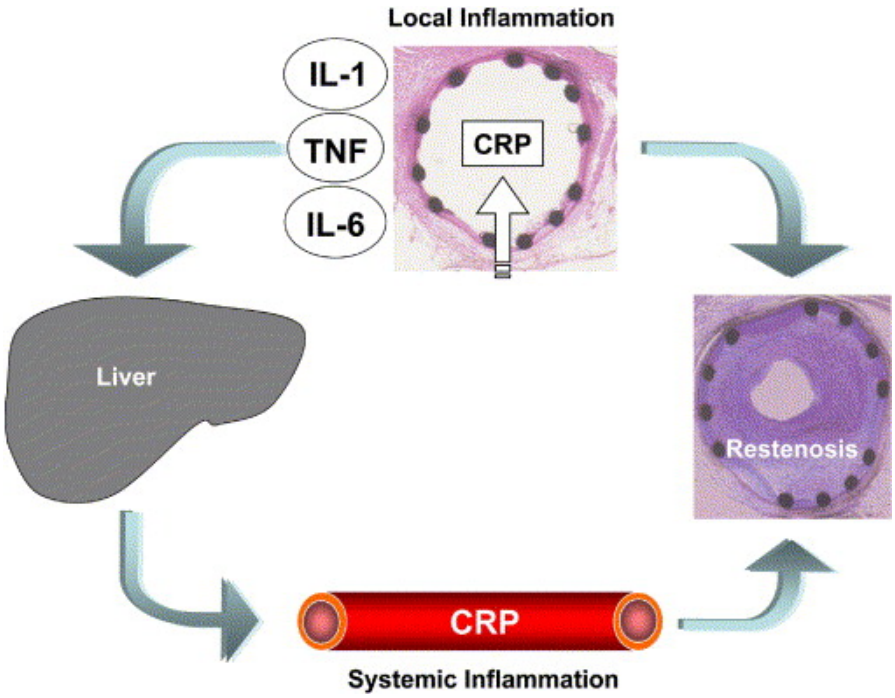

Figure 1.10. Interaction of local (cytokine release) and systemic (CRP production) inflammatory responses in the onset of restenosis. Figure from Gaspardone, et al. (2005)[77].

Improper stent deployment can alter the normally athero-protective local blood flow conditions, leading to a greater risk of restenosis [78]. The presence of the stent itself can lead to an overexpansion of the artery, as well as decreased compliance and extendibility, all of which increase stresses on the vessel wall [67, 79]. These stresses, in turn, lead to proliferation of SMCs and the formation of neointimal tissue [80]. Formation of the neointima following stent placement is associated with the action of numerous leukocytes, as well as platelets and growth factors (Figure 1.11) [68]. Taking all of these factors into account, it is the expansion of the stent which is one of the most important factors contributing to restenosis, as the stent not only causes tissue damage,

but is itself a foreign body which will itself illicit an immune response and impair healing [67].

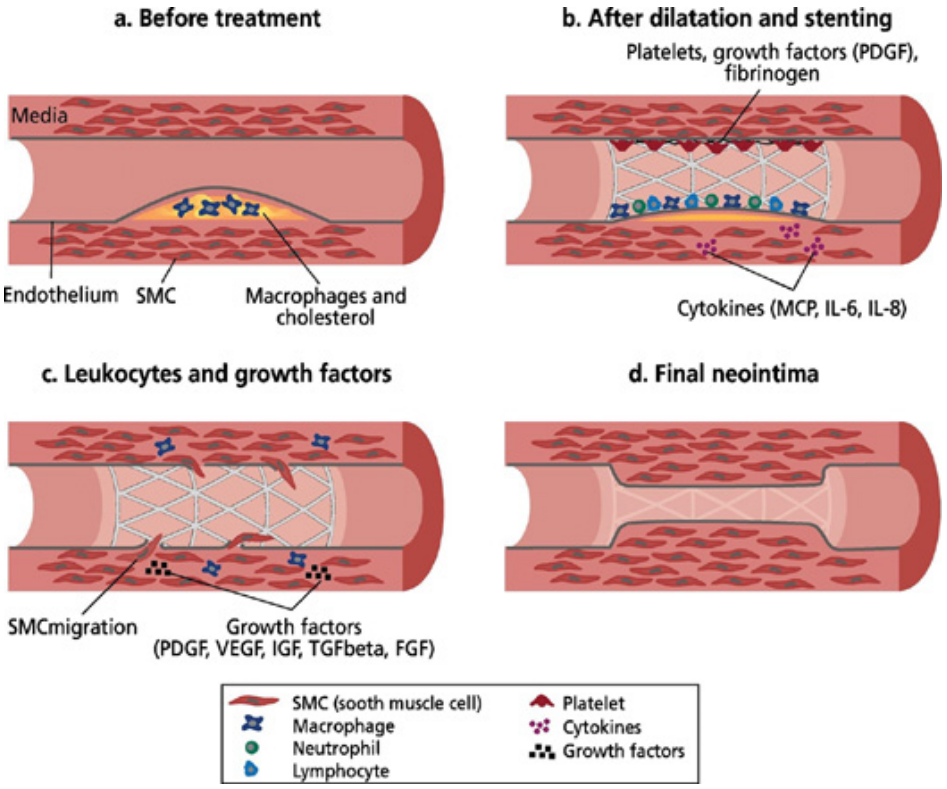

Figure 1.11. Role of cytokines, leukocytes, platelets, and growth factors in the development of restenosis. Figure from Kivela, et al. (2006)[68] .

Histological analyses have revealed that the degree of penetration of stent struts is directly related to the thickness of neointimal tissue [81]. When strut penetration is less severe, there is only a moderate layer of new SMC-rich tissue. In the first days following stent implantation, stent struts are typically surrounded by fibrin and neutrophils. Within two to three weeks however, these are replaced by the presence of macrophages and SMCs [81]. After 3-18 months post-implantation, there is typically a restenotic tissue

extremely rich with proteoglycans (including versican and hyaluronan) that is infiltrated with α-actin positive SMCs. Towards the end of the first 18 months post-implantation, type I collagen begins to prevail. After 18 months, SMC density and stent stenosis are reduced [82, 83]. These observed patterns of ECM constituents and phenomena are typical of a tissue that is incompletely healed.

The intial clotting response following stent implantation may play a significant role in restenosis, as platelet derived growth factor (PDGF) is one of the most potent stimulators of SMCs and macrophages [84]. However, at later stages following stent placement, there is little or no sign of markers suggesting an active inflammatory response or of replication SMCs [85, 86]. Star-shaped SMCs dispersed in a loose proteoglycan-based ECM is the most frequent finding in studies of later stage tissue, with the cellularity of the neointima decreasing with time after stenting. Furthermore, SMCs in late stage neointimal tissue are typically not in a synthetic state. This has led some authors to suggest that it is primarily the ECM which the main culprit in restenosis, rather than the cells themselves [85, 86]. The pattern that is emerging suggests that neointimal tissue changes from inflammatory, to proliferative, to secreting as time passes [67]. From this progression, one can divide the process of restenosis into two main phases. The first is the wound healing process, including clotting, followed by inflammation, and infiltration by myofibroblasts derived from SMCs, macrophages, and other progenitor cells. The second phase is that of neointimal hyperplasia, where myofibroblasts reduce their proliferation rate and enter a synthetic phenotype which secretes abundant ECM [67]. Mechanical and chemical stimuli working in conjunction are likely responsible for

the phenotypic changes in VSMCs during restenosis. Numerous studies have been conducted examining the effects of mechanical stresses on SMCs [67], with no clear consensus. It is speculated that in cases with greater intimal penetration of struts, a higher mechanical forces may be applied to the VSMCSs, resulting in the phenotypic shift to a proliferative state [67]. The shift to a synthetic phenotype may explain an early triggering of SMCs to participate in neointimal formation, but it does not explain the lack of proliferative cells in later stages [67].

A number of strategies have been employed to reduced restenosis rates and improve the overall performance of stents. Initial attempts to reduce restenosis rates involved the use of various systemic anti-platelet and anti-thrombus drugs. On the whole however, these efforts have not been very successful [87]. Some researchers have taken the approach of decreasing the stresses applied to the vessel wall with different stent designs, including using self-expandable stents [88], low-pressure deployment [89], and varying strut thickness [90]. There are data indicating that increased strut thickness cause excessive damage and thereby lead to higher restenosis rates [91]. A number of factors relating to the stent material itself play a significant role in host tissue response. Stainless steel, for instance, has excellent mechanical performance but possesses significant disadvantages relating to its biocompatibility[92, 93]. The corrosion resistance of stainless steel has been improved by adding more chromium to the alloy, but there is still the problem that nickel is one of the ions that can potentially be released [94]. Nitinol is currently the main alternative stent material to stainless steel. Its largest advantage is that deployment does not require balloon, due to its shape memory properties. Unfortunately,

analyses have demonstrated that nitinol has not brought any significant advantage in reducing restenosis rates thus far [67]. Improvements in nitinol biocompatibility can be achieved by inducing a titanium oxide surface, which can increase clotting time, reduce fibrinogen absorption and platelet activation, and allow for SMCs to retain their contractile phenotype, therefore reducing SMC proliferation when compared to stainless steel [95, 96].

Various coatings have been applied to stents in order to improve performance as well. Initially, researchers applied carbon or gold to alter material surface properties. Carbon coating does appear to have some beneficial attributes, most likely due to reduced thromobgenicity, although the studies were not randomized or controlled [97]. Gold coatings on the other hand have yielded discouraging results on the whole, actually resulting in increased neointimal tissue proliferation compared to bare metal stents [98]. Silicone-carbide [99], phosphorylcholine [100], and heparin coatings [101], have also exhibited little or no beneficial effects with regard to restenosis. The most success thus far has come from anti-proliferative agents, which are usually contained within polymeric stent coatings. Two of these, rapamycin and paclitaxel, have reduced restenosis rates to single digits since their introduction [102, 103]. Rapamycin (trade name Sirolimus) is an antibiotic discovered in a microbe on Easter island. It acts as an anti-proliferative agent on SMCs by inhibiting growth factor and cytokine-induced cell division and migration [104, 105]. Paclitaxel (trade name TAXUS) is a derivative of Taxol with anti-mitotic properties. It works by inhibiting microtubule depolymerization, therefore arresting the cell cycle, and halting cell proliferation [66]. Despite the success of these anti-

proliferative agents, there are still a number of concerns relating to the long term success of drug-eluting stents. For example, some evidence suggests that localized drug delivery may lead to hypersensitivity reactions and SMC drug resistance [106, 107]. Other complications from drug-eluting stents include inflammation at the stent extremities, delayed endothelialization, and a relatively high cost to the healthcare system [106-108]. Furthermore, several meta-analyses have thus far failed to yield any strong evidence that drug-eluting stents significantly reduce the risk of mortality or myocardial infarction (MI) [108]. In fact, there have actually been non-statistically significant increases in these two endpoints (mortality and MI) with drug eluting stents [109]. Currently, more than 85% of all coronary interventions in the U.S. are performed with drug eluting stents, many of which are cases for which they are not approved [109]. The major clinical trials which are often touted as evidence for the superiority of drug eluting stents have several methodological flaws, including the use of inferior thick-strutted stents as controls, biased protocol-mandated angiography, questionable clinical relevance of angiographic outcomes such as binary restenosis, and a lack of data from high risk patients [109]. These trials may have also relied too heavily on "soft outcomes" such as restenosis and revascularization, as opposed to "hard outcomes" such as MI or death. In addition there is recent evidence suggesting the drug eluting stents may result in higher levels of thrombosis, especially in cases where anti-platelet therapy is discontinued prematurely [109]. Lastly, relative costs associated with drug eluting stents may have been underestimated [109]. Some general goals with regard to stent implantation and design that should be considered are reducing excessive dilation of the stent (possible through

better self-expandable stents), and gaining a better understanding of the host response [67]. Despite all the knowledge that has been gathered, and the technological advances that have been made, there is still much to be discovered regarding the underlying causes of restenosis in terms of an immune response, and the effects of mechanical stresses on underlying tissue. It is clear that restenosis exhibits histological features distinct from those of atherosclerosis, yet increasing evidence shows that both result from inflammatory responses. Essentially, restenosis is an incomplete healing process resulting from an inflammatory response, and the presence of the implant is clearly associated with its formation, as the stent challenges vessel wall tissue by threatening its integrity, subjecting it to elevated mechanical forces, and exposing it to a foreign surface.

Cell Mechanics

The mechanical properties of cells reflect cytoskeletal state and health. Any deviation in cellular structural and mechanical properties can result in the breakdown of physiological functions [110]. Furthermore, the structural integrity of individual cells can affect overall tissue mechanics, due to cell-ECM interactions [110]. Most soft materials will exhibit a combination of solid- and fluid-like mechanical characteristics, and cells are no exception [111]. The cytoplasmic fluid component of a cell is distinct, as it depends on the rate at which force is applied as opposed to the magnitude. The viscoelasticity of cytoplasm is about 10-100 times that of water, reflecting high concentration of proteins in the fluid [111]. Overall however, a cell's behavior is that of a solid, as it will not flow without limit as a true liquid does [111]. A cell's mechanical

properties are largely determined by its cytoskeleton, which is an interconnected structure composed of three main types of filamentous biopolymers [112]. The first type is actin filaments, which carry tensile forces that are actively generated by the cell's contractile apparatus and passively through attachments to its substrate [112]. The diameter of these filaments is typically in the range of 5-10 nm, with elastic moduli on the order of GPa. Actin filaments can also be found in bundles known as actin stress fibers, which carry both tensile and compressive forces. Actin filaments are crosslinked by specific proteins such as alpha-actinin and filamin [111]. Due to their small size, actin filaments undergo thermal fluctuations, which are overcome when force is applied, after which the intrinsic elastic modulus dominates mechanical behavior. The magnitude of this elastic response is determined by the concentration of actin and the concentration of crosslinks [111]. The second major type of cytoskeletal element is the microtubule. Microtubules are tubule biopolymers (o.d. ~ 24 nm, ~ i.d. 12 nm) that carry compressive forces in order to resist contraction of the cytoskeletal network. It has been proposed that the contribution of microtubules to balancing prestress depends inversely on the extent of cell spreading [113]. The third type of cytoskeletal filament is the intermediate filament, which have a diameter of ~ 10 nm. Their role in cytoskeletal mechanics is less well understood than actin or microtubules, but it is believed that they carry tension at large strains of greater than 20% [112]. Microtubules tend to have the highest bending stiffness, while actin filaments have greater tensile strength at short extensions, although a shorter elongation to break (Figure 1.12) [114].

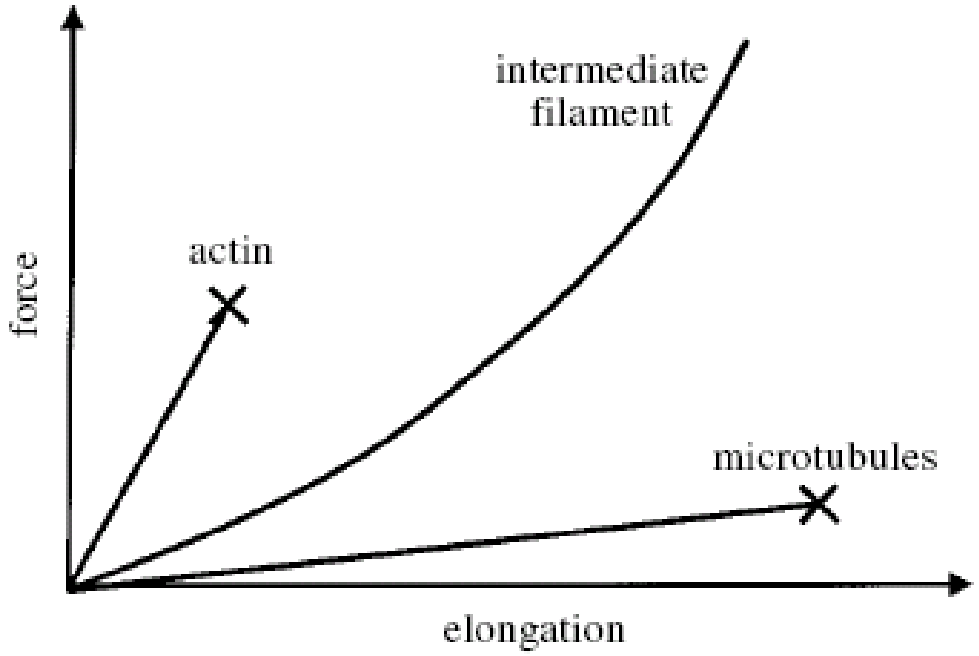

Figure 1.12. Tensile properties of the three main cytoskeletal constituents; actin, microtubules, and intermediate filaments. Figure from Humphrey (2002)[114].

An increase in contractile stress from this cytoskeletal network corresponds to an increase in cell stiffness. Adherent cells also exhibit several distinct mechanical features, including viscoelasticity, creep, stress relaxation, strain hardening, and hysteresis [112].

Mechanotransduction

In recent years, it has become recognized that mechanical factors are equally important as chemical events in terms of physiological regulation and response [115]. Mechanical forces can influence both chemical equilibria and molecular polymerization events [116]. Cellular mechanotransduction is the process by which mechanical stimuli

are converted into biochemical signals. This process is mediated by numerous elements, including cell-cell-adhesion, cytoskeletal properties, and the cell membrane, among others (Figure 1.13).

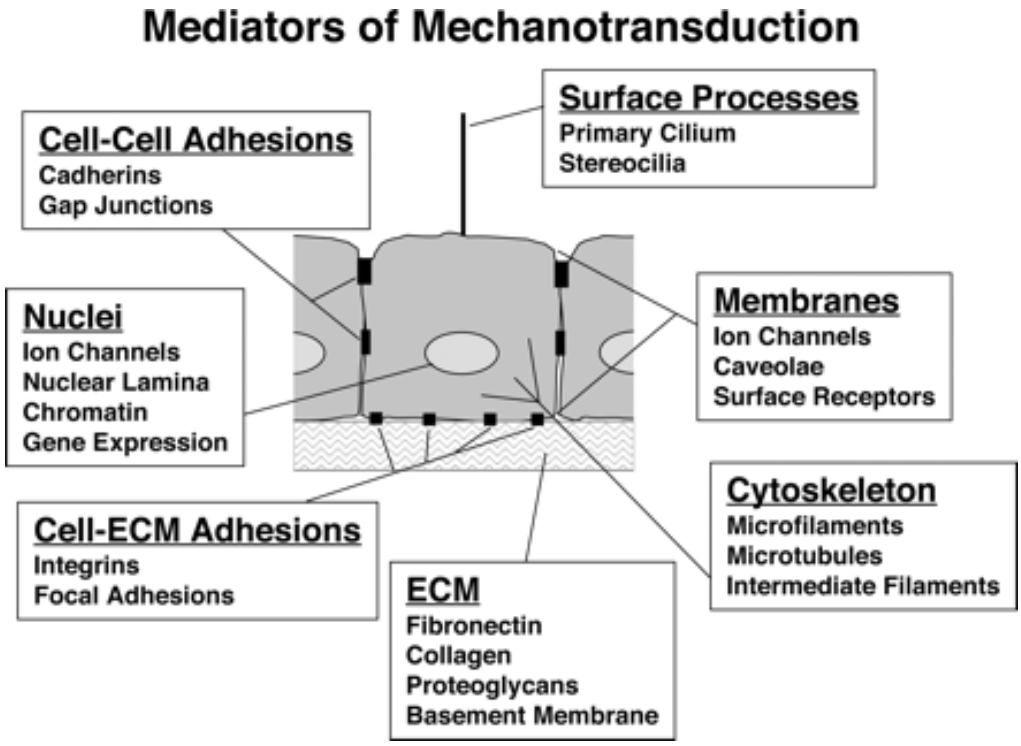

Figure 1.13. The various mediators of cellular mechanotransduction. Figure from Ingber (2006)[116].

It is believed that mechanotransduction involves structural hierarchies that span several size scales from whole organs and tissues, down to individual molecules within cells [116]. Therefore, the mechanical properties and level of prestress that exist at each level along this pathway can have significant effects on the eventual response [116].

Processes as varied as cell growth, differentiation, polarity, motility, contractility, ECM synthesis, and apoptosis are all influenced by physical deformation of cells of all types [115, 117, 118]. When a whole tissue is deformed, the forces are transmitted to cells via adhesions to the ECM [115]. Furthermore, the mechanical properties of the ECM itself also contribute significantly to the cellular mechanotransduction response. Different cell types respond to different force magnitudes. Chondrocytes and osteocytes, for example, show a biological response to forces of ~20 MPa, while endothelial cells respond to small force of < 1 Pa [111]. And within single phenotypes, it is likely that different structures are responsible for different forms of mechanical sensing. Cellular response to mechanical stimulation requires both an element that is directly altered by the applied force, and second element that transmits this information to the desired target. Currently however, knowledge regarding these mechanosensors is scarce. The most well characterized and probably most important class of receptor in terms of force transmission are integrins, as they have been shown to provide greater mechanical force transmission than other types of receptors [119]. Integrins are clustered at focal adhesion sites [120] containing multiple actin-associated proteins such as talin, vinculin, paxillin, and zyxin [116], and act to distribute externally applied stresses through the cytoskeleton. The mechanical coupling that exists between integrin and cell nucleus is largely mediated by intermediate filaments, but also to a lesser extent by actin filaments, and the efficiency of this intracellular mechanotransduction is greatly affected by cytoskeletal prestress [116]. Applying mechanical stress to integrins results in recruitment of proteins to the site in order to strengthen itself [119]. Application of mechanical forces to bound

integrins promotes focal adhesion assembly by activating small GTPase Rho and stimulating its downstream targets mDia1 and ROCK, which promote actin filament polymerization and cytoskeletal contraction respectively [121, 122]. Other transmembrane molecules such as cadherins and selectins can transmit mechanical forces across the cell membrane, but in a much less significant manner [116]. Another type of membrane protein involved in mechanotransduction are G proteins, which are localized at focal adhesion sites. Application of mechanical force causes a conformational change to G proteins, initiating a signal cascade, generation of second messengers, and eventual cell growth [118]. Receptor tyrosine kinases (RTKs) also play a significant role in integrin-mediate mechanical signal transduction, as do mitogen-activated protein kinases (MAPKs), which transduce mechanical forces into gene expression and protein synthesis through their complex pathways [118]. Because only certain molecular and structural channels within a cell transmit mechanotransductive signals, other intracellular molecules are left unaffected by mechanical stimulation [116]. In addition to protein-mediated signal transduction, the lipid bilayer may also play a role, although this hypothesis is more controversial [111].

The importance of a cell's intrinsic mechanical properties (prestress) in regulating response to stimuli has also been demonstrated in several studies [123]. Hence it is important to understand how cellular mechanical properties are altered under different conditions. Biological responses of cells to mechanical loading vary greatly, and are largely dependent on the strength and type of loading (i.e. cyclic, static, biaxial, uniaxial, etc.), the time of exposure to the mechanical forces, cell type, and the ECM or substrate

constituents [118]. When mechanical stresses are applied to a cell, the cytoskeletal filaments will distort, thus altering the shape of some the molecules that make up the filaments. Changing the shape of a molecule can alter its biophysical and biochemical properties. As many signaling molecules are located on the cytoskeleton near focal adhesion sites, this provides a mechanism for the alteration of signal transduction through the application of mechanical force [115]. In addition, all cells contain mechanically gaited ion channels that can increase or decrease the level of ion flux through a membrane upon the application of mechanical stresses [124]. Abnormal stress states and abnormal responses to mechanical forces may both contribute to the development of a very large number of diseases.

Vascular Smooth Muscle Cell Mechanics

A handful of studies have been performed examining the tensile properties of vascular smooth cells [125-127]. All of these studies have examined non-adherent vascular smooth muscle cells which were stretched using a custom-built dual micro-pipette system. Consistently, it has been observed that synthetic VSMCs have a lower tensile modulus than contractile VSMCs. For example, Nagayama and co-workers [127] found that freshly isolated contractile VSMCs had an average tensile modulus of 11 kPa, while cultured synthetic VSMCs had an average modulus of 2.6 kPa. Another study found that the tensile elastic moduli of cultured bovine VSMCs were about 1/5 that of freshly isolated rat VSMCs [125]. Miyazaki and co-workers found that both VSMC phenotypes showed almost the same load-elongation relations in small elongation ranges,

however tensile load was higher in contractile VSMCs at elongations greater than 20 um, and there were significant differences at 25 and 30 um elongation [126]. One major cytoskeletal difference that has been noted is that actin filaments in cultured cells were less abundant and almost uniform in direction, while actin content in fresh SMC was so abundant as to look uniformly stained [127]. Actin bundles much thicker in contractile cells than synthetic ones. The tensile modulus of cultured SMCs was also reduced by approximately 50% upon disruption with cytochalasin D, and it was observed that the cellular tensile properties were affected not only by the amount of actin filaments, but also by their organization and distribution [127]. Furthermore, SM-MHC are SM-α-actin are typically observed in contractile, but not synthetic VSMCs [4, 126]. Smooth muscle α-actin is found in the contractile apparatus of the cell, while β- and γ-actin are found in the cytoskeleton [126] . During phenotypic modulation, smooth muscle α-actin is downregulated by, while β- and γ-actin are upregulated, and non-muscle β-actin is found heavily in synthetic SMCs [126]. Intact arterial medial sections, which are largely composed of smooth muscle cells, have also been examined using atomic force microscopy[128]. In that study, Engler and co-workers found a medial apparent elastic modulus of 5.7 ± 0.3 kPa.

Cellular Mechanical Models

Measurements of cellular mechanical properties have now advanced to the point where forces smaller than a piconewton and displacements smaller than a nanometer can be induced and/or measured [129]. Cellular deformation can be studied in any number

of ways, including uniaxial and biaxial tension or compression, pure shear, hydrostatic pressure, bending, twisting, or a combination of these methods (Figure 1.14).

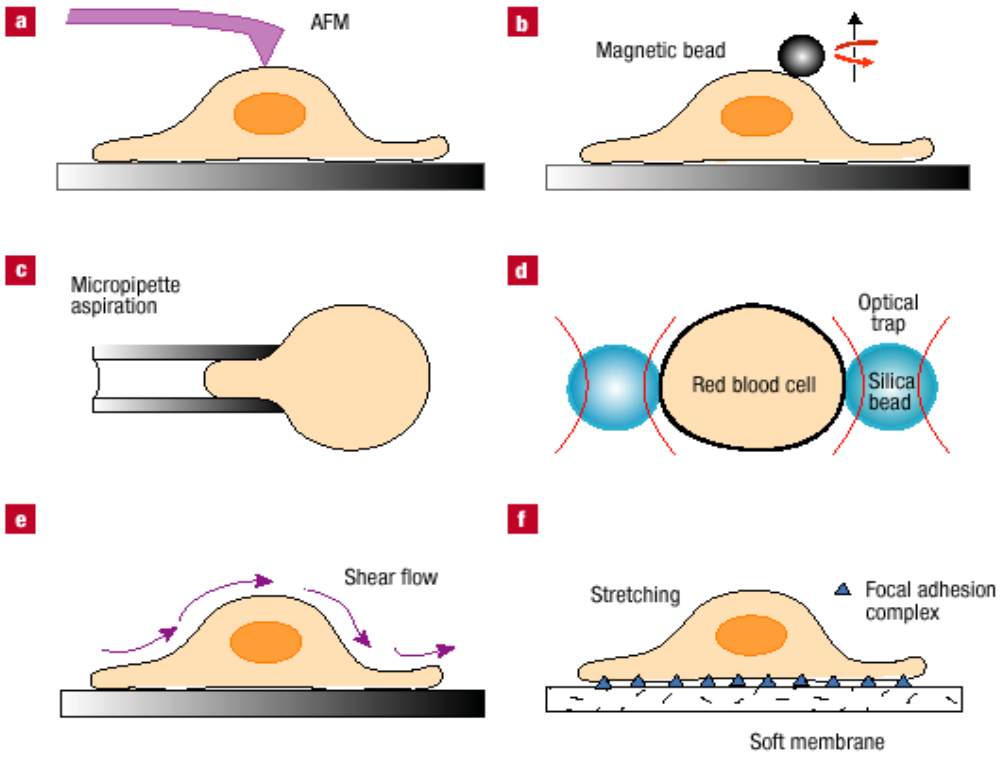

Figure 1.14. The various methods of studying cellular deformation: a) AFM b) magnetic beads c) micropipette aspiration d) optical trap e) shear flow f) membrane stretching. Figure from Bao and Suresh (2003)[129].

One can study cellular mechanical behavior with local probes deforming the cell, whole cell loading, or simultaneous stressing of a larger population of cells. Measurements of cellular apparent elastic modulus have yielded values between 10^2 and 10^5 Pa, with much of the deformability being determined by the cytoskeleton [129]. However, an important concept to take into account is that cellular mechanical properties are dynamic in nature.

That is, cells alter their cytoskeletal structures actively in response to applied forces, and during physiologic processes including cell division, crawling, spreading, rounding, and actin-based motility [129].

Given the advancements made in cellular mechanical measurement technologies, it has become necessary to develop appropriate mechanical models. Mechanical models for cells can be broadly categorized as either continuum models or micro/nanostructural models [110]. Micro/nanostructural models consider the cytoskeleton to be the prevailing structural component. The prevailing micro/nanostructural model for adherent cell mechanical behavior is that of a tensed cable network, or more specifically, the tensegrity model (Figure 1.15) [115, 130].

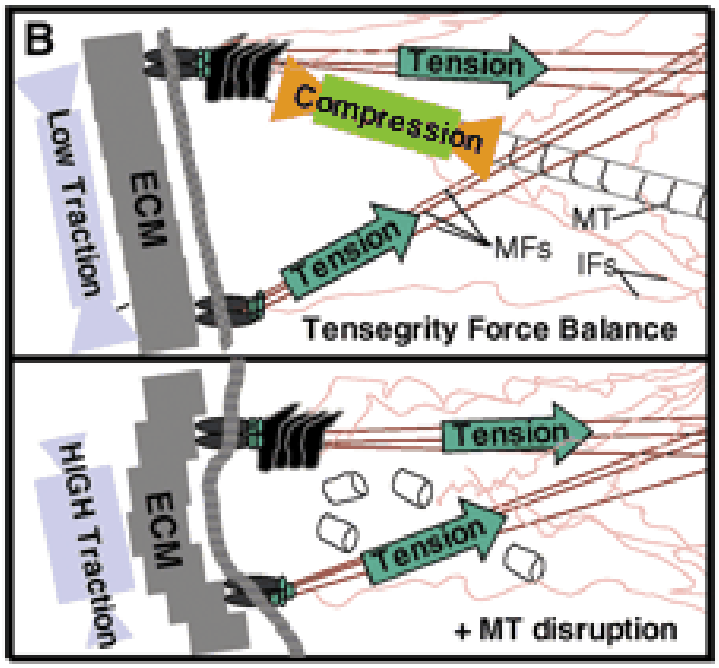

Figure 1.15. Illustration of the tensegrity model, showing the force balance achieved through actin microfilament (MF) and intermediate filament (IF) tension and compressed microtubules (MT).

The tensegrity model suggests that the cytoskeleton is composed of tensile elements (actin and intermediate filaments) that are balanced by compressive elements or struts (microtubules and actin bundles). The ECM also balances some of this tension through integrin-ECM connections. When compression reaches a critical level, the microtubules will buckle, allowing cellular deformation. The actin network carries "prestress", giving the cell shape stability. The strain hardening phenomenon observed in cells is explained by the tensegrity model to be a result of reorientation and change in spacing of cytoskeletal components in the direction of applied load. The tensegrity model is the best current model of cellular mechanical behavior in a 3D *in vivo* environment. One significant drawback however, is that structurally based models such as the tensegrity model are static and therefore not sufficient in describing the dynamic properties of a cell. For example, it has been observed that elastic and frictional moduli of cells increase with frequency according to a weak power law, and that at a given frequency these moduli increase linearly with increasing cytoskeletal prestress. All of this information underscores the complex and dynamic behavior of living cells, and the difficulty in characterization of this behavior.

The continuum approach to cellular mechanical modeling treats cells as being comprised of materials with certain continuum material properties. Appropriate constitutive material models and parameters are derived through experimental observations [110]. This method gives less detail into specific molecular events that take place, but is easier for interpreting mechanical responses at the whole-cell level. Continuum models can be further divided into liquid drop models and solid models [110].

Liquid drop models can be yet again divided into Newtonian, compound Newtonian, shear thinning, and Maxwell sub-categories. Liquid models such as these are most suitable certain mechanical characteristics of non-adherent cells, such as erythrocytes and neutrophils. Solid models generally assume the cell to be homogeneous, modeling it as either an incompressible elastic solid or a viscoelastic solid [110]. Assumption of homogeneity allows for simplification of analysis and fewer parameters. The experimental basis for such models is that an equilibrium state can be achieved after a certain amount of loading [110]. The linear elastic and viscoelastic models differ in neglect and use of a time factor, respectively. With linear elastic solid models, the apparent elastic modulus that is found does however depend on loading rate and history. Cells must maintain sufficient structural integrity to behave like a solid under mechanical stresses, but most also exhibit more fluid-like behavior for processes such as crawling and spreading [131]. The linear elastic and viscoelastic models are suitable for transient loading conditions, including the understanding of creep and stress relaxation. However, for dynamic loading, power law structural damping models have been developed. Cellular power law behavior suggests that under an applied stress, cells deform continuously and that this process is timescale invariant (does not depend on loading frequency) [131]. Often, this is accomplished through oscillatory indentation with an AFM, through which a storage modulus (G') and a loss modulus (G") are found. The loss modulus is dependent on a weak power-law with an exponent $0 < \alpha < 1$ below ~ 10 Hz, but viscous components become more significant at higher frequencies. Dynamic rheological properties of adherent cells are related to contractile stress, with larger

stresses corresponding with high dynamic moduli. The power law exponent α decreases with increasing prestress (α is an index of deformability, with 0 corresponding to elastic solid, and 1 corresponding to flowing liquids). So, fact that alpha changes with prestress suggests that this regulates the transition between solid and fluid-like behavior [131]. Power-law structural damping has been said to suggest behavior like that of a soft-glassy material (such as slurries of foams) close to its glass transition temperature [110]. On the macroscale, this results in slow cell deformation over a wide range of timescales [131].

Whole tissues have often been modeled using Fung's theory of quasilinear viscoelasticity (QLV) [132], in which it is assumed that the reduced relaxation function G(t) is independent of initial strain [133]. Stress is normalized by the peak stress at the completion of a step strain. Strain independence is an essential feature necessary for QLV modeling. While the QLV model has been applied to numerous soft tissues, it has to data never been used for describing the viscoelastic behavior of individual cells.

Mechanical Measurements Using Atomic Force Microscopy

As discussed above, there are many physiologic processes and disease states that can alter cellular mechanical properties, and such differences have been detected in cells including myocytes, chondrocytes, and hepatocytes, among others. Establishing both the normal and abnormal properties of the cells affected by disease could aid in the in vitro identification of effective treatments [134]. Information including detailed knowledge of stress/strain relationships, viscoelasticity, and hysteresis, could all be of benefit [134]. It

is theoretically possible that any disease altering the composition, organization, kinetics, or crosslinking of the cytoskeleton may be detectable using cell mechanics measuring techniques [134]. Cytoskeletal properties, particularly those relating to actin, have been found to have the greatest effect on measured cell stiffness [135] . Cell morphology, height, and degree of attachment also play significant roles [135]. Viscous properties and/or elastic properties may be altered in diseased cells, so it is important to take both into account when performing cellular mechanical measurements [134, 136] . In addition to soft tissue, mechanics of mineralized tissues have also been investigated using nano-indentation [137]. At present however, there is a lack of information regarding tissue mechanics in disease progression, tissue repair, and remodeling mechanisms associated with medical treatments [137].

There are a number of techniques for measuring cellular mechanics, including magnetic twisting cytometry, magnetic tweezers, optical stretching, and atomic force microscopy (AFM), among others [134]. Among these, the AFM has emerged as one of the most effective and useful tools in the field of mechanobiology [134, 138, 139]. The AFM is a member of the scanning probe microscope family, and was originally developed to overcome the limitations of the scanning tunneling microscope (STM) in imaging non-conducting materials [140]. In terms of cell biology, AFM usage can be divided into several categories, including imaging, micromanipulation, material property investigation, and binding force investigation [140]. Several advantages that the AFM possesses over other mechanical measurement techniques are the ability to combine high-resolution scanning with nano-indentation, the direct mechanical interaction between

probe and sample, high sensitivity, high spatial resolution, the capability of being used for real-time measurements in a physiologic aqueous environment, and commercial availability [134]. An aqueous environment has also been found to be important due to the fact that sample drying increases elastic modulus [137]. The small probe size of an AFM allows for testing of smaller samples, such as biopsy specimens or tissue samples from small animal models [137]. Other emerging capabilities of the AFM for biological research include the ability to monitor dynamic processes, study molecular and adhesion forces (such as between RGD and integrins), and elucidate intracellular force transduction [140].

The basic operating principles of the AFM are as follows. The deflection of a silicon-nitride cantilever probe, usually 100 to 300 microns long and approximately 0.5 micron thick, is measured by reflecting a laser off the probe's topside onto a photodiode (Figure 1.16).

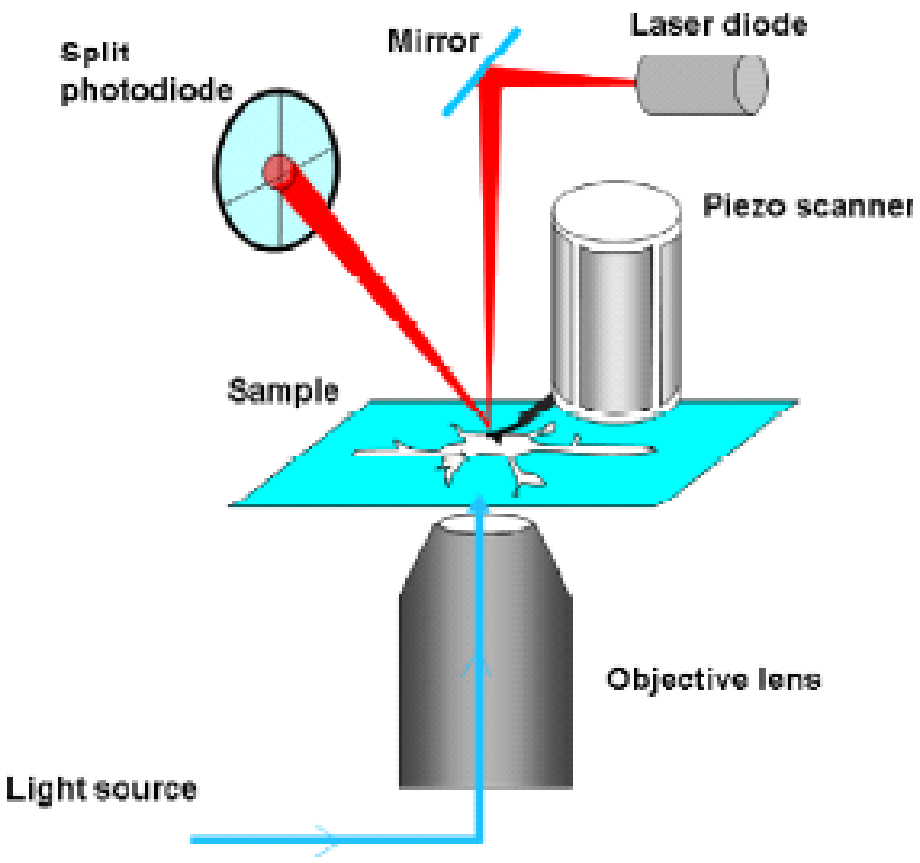

Figure 1.16. Schematic representation of the basic operating components of the atomic force microscope. Adapted from Alessandrini and Facci (2005)[140].

The photodiode can detect movements on the order of 0.1 nm. A cantilever spring constant, k, (N/m, either the nominal value or experimentally determined) is used to convert deflection into force. Cantilever deflection leads to a shift of the reflected laser spot, and thus a reduced signal on one segment of the photodiode, and an increased signal on the other. The size and shape of this spot size can also influence sensitivity [141]. Typically values for k range from 0.01 N/m to 1.0 N/m. The cantilever's mechanical properties have a significant effect on the AFM's performance [141]. Methods of

experimentally determining the cantilever spring constant include using cantilever geometrical factors, measurement of static deflection applying known force to cantilever, measuring dynamic properties with different masses on cantilever, and thermal noise (the most common method, cantilever is treated as a simple harmonic oscillator excited by thermal noise, 15-20% accuracy) [140]. Cantilevers with higher resonant frequencies, a property related to thickness, length, density, and modulus, are less subject to disturbances from external vibrations [141]. Contact mode cantilevers are usually V-shaped, in order to increase lateral stiffness and prevent fracture [141]. On the underside of the cantilever is the tip, which is usually pyramid-shaped with a blunted point of radius of 50-100 nanometers. For biological applications, the probe is typically moved relative to a stationary sample, which can be heated to the desired temperature and kept in an aqueous environment. Movement in the z-direction is accomplished using a piezoelectric actuator and has a range on the order of 6 microns, while maximum x-y movement is usually 100 x 100 microns [134]. The piezoelectric crystal itself is subject to both hysteresis and creep behavior, which can affect measurement accuracy [141]. Sample cells are typically adhered to a hard underlying substrate via an ECM component protein, such as collagen or fibronectin, or through the use of a positively charged material such as poly-l-lysine [135]. Glass or polymer microspheres can be attached to the underside of the cantilever, for the purposes of creating an easier to characterize contact geometry, increasing contact area, or attaching any number of biologically relevant molecules [134]. AFM tips can also be functionalized, for what is commonly referred to as chemical force spectroscopy. The most commonly used method, and the one with the best reliability, is

the attachment of thiol groups (-SH) to gold coated AFM tips [141]. Thiols will form a close-packed monolayer on the gold, simply by immersing the AFM probe into a thiol solution (with ethanol or dichloromethane) [141]. Other functional groups, such as carboxyl, hydroxyl, methyl, or amine, can then be added as needed.

There are two primary modes of AFM imaging, tapping and contact mode. Tapping mode involves oscillating the probe near its resonant frequency, and maintaining the height baseline, frequency, and amplitude of oscillation as the probe encounter different sample features [134, 139]. This mode is best for use with fragile samples that would be damaged with direct contact. Contact mode on the other hand, involves scanning the tip over the sample and using a feedback system to maintain constant cantilever deflection, and is best suited for obtaining mechanical properties of the sample. Both height and deflection images can be yielded using the AFM in imaging mode (Figure 1.17). The height image represents the z-distance between the substrate surface and each point on the sample, while the deflection image represents a more detailed topographical view of the sample.

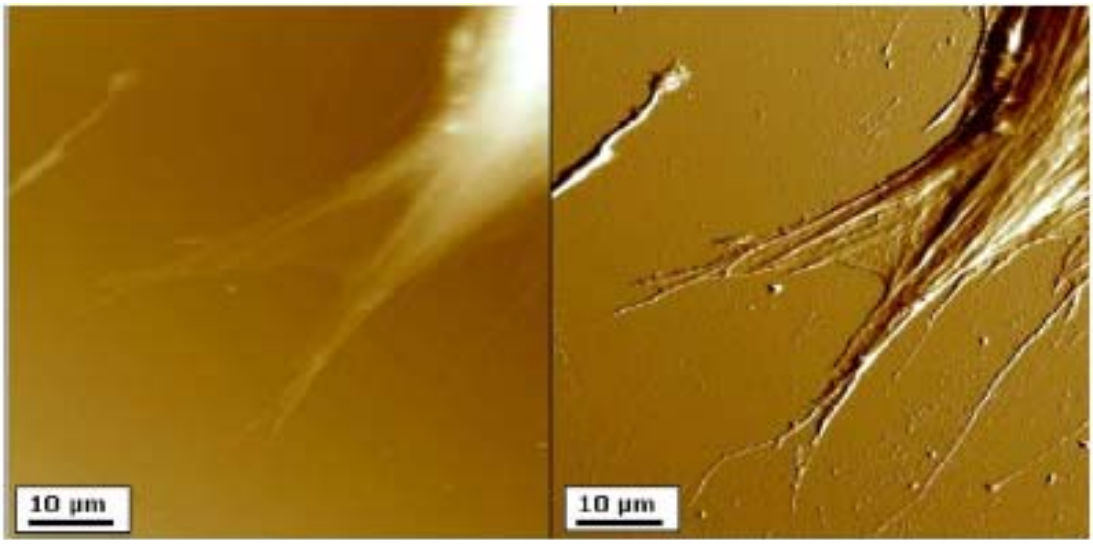

Figure 1.17. Height (left) and deflection (right) images of a human fibroblast. Figure from Alessandrini and Facci (2005)[140].

The amount of indentation into a sample is calculated using the equation D=(Z-Zo)-h, where D is sample indentation, Zo is the contact point between probe and sample, (Z-Zo) is the extension of the probe from the contact point, and h is probe deflection [134]. Varying the rate of indentation can also be used to measure viscoelastic properties, as the level of hysteresis has been shown to vary with different probe speeds [142]. Measurements such as these can be taken in separately, or in combination with imaging, which is known as force mapping. This allows for determining intracellular variation in mechanical properties. When a sample is probed, both and indentation and a retraction curve are curve, with the difference in area between the two representing the level of hysteresis [143] . Adherence of the probe to the sample can lead to negative deflections,

which is useful for measuring such things as receptor-ligand and cell-cell interactions [134, 140].

Once the force curves have been obtained, the AFM data must be analyzed, which is typically done using the Hertz model of contact between two elastic bodies [142-144] . The Hertz model is based on a number of simplifying material assumptions, including homogeneity, isotropicity, linear elasticity, axisymmetry, infinitesimal deformation, infinite sample thickness and dimensions, and a smooth sample surface. The equations relating force and depth for AFM probe indentation are: $F = (2/\pi)(E/1-\upsilon^2) \tan(\alpha)D^2$ and $F = (4/3)(E/1-\upsilon^2)(RD^3)^{1/2}$ for a cone and sphere respectively [134]. In the preceding equations, α is the semi-included angle of the cone tip, R is the sphere radius, and υ is the Poisson's ratio, which is typically taken to be 0.5 for cells due to their high water content. Correlation between micro- and macroscale properties using the Hertz model is largely dependent on the satisfaction of key assumptions listed earlier. Several recent studies have examined alternative methods of AFM force curve analysis [145, 146]. Among the other important procedures in AFM force curve analysis are the accurate identification of the contact point (which is particularly difficult with soft samples), calibration of the probe spring constant, and representation of tip geometry. Furthermore, mechanical properties of cells are substrate dependent, and have been shown to vary with difference ECM constituents [147]. Cells are also known to exert greater forces on stiffer surfaces, although the mechanism by which they do so is unknown [111]. All of these variables can have significant effects on the final data.

Several methods have been developed to directly measure and account for the viscoelastic properties of cells using the AFM. Among them are the "force modulation method" whereby sinusoidal loading is applied on the cell surface via AFM indentation and the phase and amplitude of the tip response is measured for probing the cell viscoelasticity, and the "force mapping method" in which the AFM tip touches and dwells over a period of time on the cell surfaces, and then indents slowly into the cell body [148]. Others have used closed-loop feedback to apply constant deflection and measure stress relaxation [149]. Standard viscoelastic testing methods such as creep and stress relaxation have recently become more feasible with advances in AFM technology [149]. The most easily observed viscoelastic material behavior is creep (sinking of indenter into material under constant load). When loading is followed by unloading without a hold at peak load, displacement increases slightly in the initial portion of the unloading phase, because creep rate is initially higher than the imposed unloading rate. A hold period can be used prior to unloading to allow the material to reach equilibrium. Appropriate hold time selected based on creep and unloading rates used in experiments vary from ~ 3 to 120 seconds [137] . Darling and coworkers recently developed a mathematical model for AFM stress relaxation experiments based off of the commonly used Hertz models, by employing LaPlace transformations [149].

The effect of drugs and naturally occurring soluble biomolecules on cell mechanics is another area of study possible using AFM force measurements. This can lead to information such as cell morphology and mechanical compliance, furthering our knowledge of how cells move, generate, and respond to force, as well as how drugs affect

cell behavior at the functional level [150]. Receptor-ligand binding at the cell surface can be visualized and quantified, yielding a binding force F_R (Figure 1.18) [151].

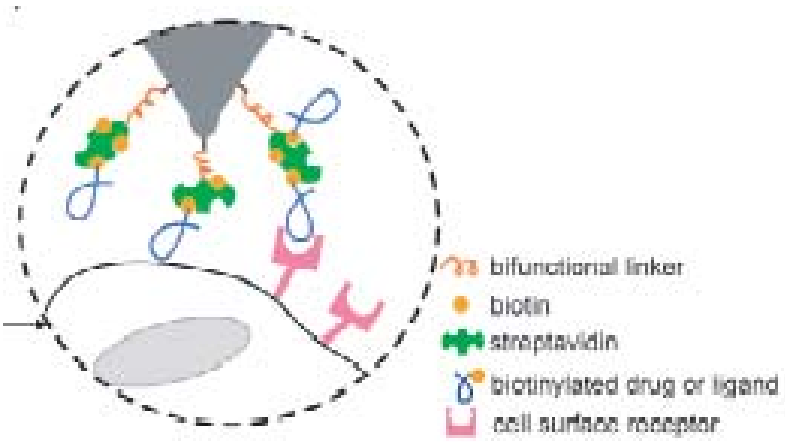

Figure 1.18. Illustration of receptor-ligand interaction measured using biomolecues bound to an AFM tip via a biofunctional linker. Figure from Van Vliet and Hinterdorfer (2006) [150].

Receptor distribution can be mapped with nanometer spatial resolution superior to that afforded by immunocytochemical staining, and can be directly correlated with structural and mechanical subcellular features such as cytoskeletal filament association [150, 151]. Unbinding or rupture force F_R (on order of 50 to 1000 pN for cells on rigid substrates) is measured directly through bending of the cantilever and can be related to binding affinities that characterize ligand-binding kinetics [151]. This allows comparisons of binding affinities among different ligands and possibly indentification of previously unknown receptors. This approach is well suited for ligands that are not compatible with conventional methods (fluorophore or radioactive isotope labeling) and receptors with

low spatial density and mobility. Typically, one or more ligand molecules are permanently tethered to the AFM tip, usually by covalent linking with a flexible linker molecule [151]. Use of a linker allows the ligand to freely move over the volume area allowed by the linker's length. The dissociation process of the receptor-ligand process is followed over time. Force-time profiles allow the monitoring of conformational changes during receptor-ligand dissociation. It is possible to detect energy barriers that are difficult to detect by conventional, near-equilibrium assays and also to probe the free energy surface of proteins and molecular complexes [151]. Rates of lateral diffusion and internalization of receptors within the cell membrane must be considered with respect to experimentally attainable scanning rates and resolutions [150]. Validation of probe functionalization is necessary, in order to ensure that molecule is tethered and oriented so that it can bind to its receptor. Accurate characterization of the cantilever spring constant, as well as demonstration of binding specificity through competitive binding that eliminates measurable F_R with the soluble ligand or ion-dependent disruption of receptor binding are also necessary [150] . Quantification of ligand-receptor rupture force has been demonstrated for a large number of proteins, with one tethered to probe, and other to rigid substrate. Ligand-receptor interactions were initially required "blindly", meaning many ligand receptor force responses were gathered at individual, randomly selected or topographically interesting sites, or by acquisition of single force responses at each of many pixels comprising an image. The drawback of this approach is that it does not allow mapping of ligand-receptor interactions with molecular-scale spatial resolution. The direct binding approach (termed recognition imaging) provides the potential to image

receptor distribution and gather ligand-receptor force distributions of cell surfaces. Cantilever deflection during oscillation of a ligand or anti-body functionalized probe can be deconvolved into a recognition image (image contrast is a function of probe-surface binding), and a topography image. By adhering whole cells to AFM cantilevers, the ligand-receptor interactions governing adhesion can be explored at the single-cell level. Such experiments are technically complex, and do not quantify receptor distribution or binding kinetics between individual ligand-receptor pairs, but this can be useful in the study of cell adhesion [150].

Contact Mechanics for Biological Problems

The origins of forces between colloid particles and surfaces can be distinguished between surface and bulk properties [148]. Surface forces result from Van der Waals forces (forces which arise from the polarization of molecules into dipoles) and electrostatic forces, and can vary significantly with surface topography, bulk viscoelastic properties, and conductivity [148]. Bulk properties are determined by such characteristics as elastic modulus and Poisson's ratio [148]. In actuality, contact between the two bodies occurs over many small areas, each a single asperity [152]. At smaller deformations, adhesive forces may potentially play a significant role in deformation, while at large deformations mechanical forces are the main determinants of deformation behavior. A spherical indenter geometry will minimize stress concentrations in soft polymers and tissues [137]. The Hertz model described above has been shown to be experimentally valid for small deformations by a non-adhesive elastic sphere against planes and other particles [148]. Solutions for Hertz contact remain valid until applied

load is sufficiently large so as to initiate plastic deformation, at which point yielding will initiate in the material with the lower yield strength [152]. For adhesive spherical solid particles, the influence of the surface forces, which was not incorporated in the original Hertz theory, must be taken into account. Johnson-Kendall-Roberts (JKR) and Derjaguin-Muller-Toporov (DMT) contact theories have been widely used to correct behavior of Hertzian contact in presence of surface forces. JKR assumes that adhesive forces are confined to the contact area, while DMT assumes adhesive forces act outside the contact area [152]. They modify Hertz theory for two adhering smooth, elastic spheres by including thermodynamic work of adhesion, $\Delta\gamma$. Simulated results indicate that JKR theory is generally applicable to systems with large, soft bodies and high surface energies, while DMT provides a better description of small, hard solid particles with low surface energies [148]. JKR method may be more applicable in cases where there is significant adhesion, and an obvious "snap to contact" point is visible between the AFM probe and sample [137]. It should be +also noted that both JKR and DMT are limited to cases of small contact area (contact radius is generally less than 10% of particle's radius) [148].

CHAPTER TWO

RESEARCH AIMS

Aim 1: Characterization of VSMC Mechanical Changes Associated With Phenotypic Shifts

The phenotypic state of VSMCs can be affected by numerous different stimuli, including humoral factors, cell-cell interactions, and mechanical forces [4]. Smooth muscle cells are unique among the three major types of muscle cells (skeletal, cardiac, smooth) in their retention of phenotypic plasticity, where as both skeletal and cardiac muscle cells are terminally differentiated [4, 29] . Although present as a reparative mechanism, this plasticity can often give rise to the development of atherosclerotic lesions. In certain cases, such as during vascular development, and in disease states such as atherosclerosis and restenosis, a shift from a contractile to a synthetic phenotypic takes place. This shift from the normal contractile state to a synthetic state, known as modulation, is associated with a decrease in contractile protein content, as well as increased rates of proliferation, migration, and matrix production [29]. Changes to intrinsic VSMC mechanical properties could alter the cell's response to mechanical stimuli, thereby disrupting vital signaling pathways and contributing to the positive feedback phenomenon that is characteristic of atherosclerotic lesion development [153].

By inducing phenotypic changes *in vitro* via serum deprivation, we are able to create a model system for studying the cellular mechanical consequences of such changes. Employing AFM indentation, along with data analysis using the Hertz model,

we have the ability to determine what, if any, mechanical differences emerge from VSMC phenotypic shifts.

Aim 2: Measurement and Modeling of VSMC Stress Relaxation

Until recently, the majority of AFM cell mechanics research has focused on simple indentation curves, whereby cantilever deflection (force) is related to indentation depth, and an apparent elastic modulus is calculated, often employing Hertzian contact equations. While this technique has been useful for comparative purposes, linear elastic models greatly oversimplify the true mechanical behavior of a living cell. More recently, researchers have begun to explore the technique of using the AFM to measure stress relaxation behavior [149, 154, 155]. In doing so, the power of the AFM to extract cellular viscoelastic properties has been greatly enhanced. However, In order to maximize the potential of this technique, appropriate mechanical models need to be employed.

The theory of quasilinear viscoelasticity (QLV) was originally developed by Fung in order to model the viscoelastic behavior of biological tissues[132]. While it has been extensively utilized in that capacity, it has yet to be applied to cells. As such, QLV modeling is a candidate for potential improvement over existing AFM relaxation models. Additionally, while the role of various cytoskeletal constituents (e.g. actin & microtubules) has been investigated in regards to AFM indentation experiments and various forms of dynamic mechanical measurements, their role in governing relaxation behavior is not as well understood. Numerous cytoskeletal agents, causing assembly,

disassembly, or stabilization of cytoskeletal components, are commercially available for studies of this nature. In the present study, we attempt to determine the roles of both actin and microtubules in governing vascular smooth muscle cell relaxation behavior, and in the process, identify a suitable model for representing that behavior. This is accomplished by developing novel methods and protocols for AFM relaxation experiments.

Aim 3: Measurement and Characterization of VSMC Frictional Properties

While significant steps have been made towards understanding the bulk mechanical properties of living cells, very little is known about their frictional or surface shear properties. Understanding surface shear properties is of interest from a basic science viewpoint. For example, cellular frictional properties are of interest for the study of physiological phenomena including red blood cell flow [156] , cartilaginous tissues subject to articulation [157], and cell migration [158]. Cells lining the vascular lumen are subject to shear forces from blood flow, and it is believed that these forces play a significant role in the regulation of vascular health [159]. In regards to the study of endovascular surgical procedures, increased knowledge of these properties could also be of great clinical value. Deployment of endovascular devices results in significant shear forces on underlying vascular cells [160]. Complex lesions are of particular interest, as reduction of friction has been shown to ease delivery of endovascular devices in such cases [161]. Stent struts remain in constant contact with underlying vascular smooth muscle cells following stent deployment. Any stent migration or micro-motion that

occurs will therefore result in shear forces at stent strut/cell interfaces. Along these same lines, a better understanding of the frictional properties of vascular cells would allow more accurate computer modeling of *in vivo* stent behavior [160, 162] . Finite element models of AFM cell mechanics experiments have thus far relied on assumptions of slip or no-slip conditions, due to the lack of much hard data in support of either scenario [163, 164]. Atomic force microscopy has been utilized extensively to measure frictional properties of various materials [141]. However, no such measurements have performed using intact living cells. By functionalized the AFM probe with self-assembled monolayers (SAMs) of various known properties (e.g. hydrophobic or hydrophilic) we will be able to quantify surface shear forces between the cell and probe, and in doing so, develop a new method with further potential biological applications. Our working hypothesis is that the primary friction-reducing component at the cell surface is the glycocalyx, a layer of glycoproteins and proteoglycans, which in VSMCs, is composed mostly of chondroitin sulfate and heparin sulfate, and is believed to play a role in mechanotransduction.[165] In vascular endothelial cells, the glycocalyx is believed to play a major role in lubrication [156], raising the possibility that the same function is served in VSMCs.

Aim 4: Effects of OxLDL on VSMC Viscoelastic and Frictional Properties

The links between oxidized low-density lipoprotein (oxLDL) and atherosclerosis have been well-documented by numerous researchers [166, 167] . Oxidized LDL is

believed to be one of the most significant factors in vascular disease development **[168]**. Among the numerous observed effects of oxLDL, has been the alteration of cytoskeletal structure in both endothelial [169] and vascular smooth muscle cells (VSMCs) [170, 171]. In the case of endothelial cells, cytoskeletal have been shown to result in cellular mechanical changes as well [169]. To date, no such investigation of oxLD- associated VSMC mechanical changes has been performed. Changes in cytoskeletal structure can have considerable effects on cellular function, particularly in terms of mechanotransduction [116]. Given that the cytoskeleton plays a dominant role in governing mechanical properties in most cell types, alterations to cytoskeletal composition can result in changes to cellular deformation in response to mechanical loading. As a result, the subsequent mechanotransduced biochemical response can be altered as well. Vascular smooth muscle cells can be subjected to mechanical loading from several sources, including blood pressure and endovascular devices such as stents and angioplasty balloons. For these reasons, a better understanding of VSMC mechanical changes caused by clinically relevant stimuli, such as oxLDL, is important not only in terms of gaining a basic understanding of the underlying phenomena, but in understanding vascular disease progression as well.

The atomic force microscope (AFM) is an extremely useful tool in the measurement of cellular mechanical properties [147, 172, 173]. Recently, techniques have been developed to measure stress relaxation behavior of living cells using an AFM [154, 155]. As cells typically exhibit viscoelastic behavior, the use of AFM stress

relaxation techniques can serve as a useful compliment to more widely used techniques such as cell indentation, which is commonly analyzed using Hertzian elastic models.

In the current study, it was hypothesized that oxLDL alters the viscoelastic properties of VSMCs through cytoskeletal and morphological changes. To test this hypothesis, we examined the effects of oxLDL on cellular morphology, actin and microtubule distribution, and cellular viscoelasticity.

CHAPTER THREE

EFFECTS OF SERUM DEPRIVATION ON THE MECHANICAL PROPERTIES OF VASCULAR SMOOTH MUSCLE CELLS

Abstract: Vascular smooth muscle cell (VSMC) function plays a key role in regulating the development and progression of vascular lesions. Among the more significant phenomena that occur during the development of these lesions is the phenotypic switching of VSMCs from a contractile to a synthetic state. A better understanding of the concurrent changes to VSMC mechanical properties that occur with phenotypic shifts can help elucidate the role of VSMC mechanics in the development of vascular diseases. In the current study, the mechanical properties of adherent cultured rat aortic VSMCs were assessed by atomic force microscopy (AFM). Serum starvation was used to induce a phenotypic shift *in vitro*. It was concluded that serum starvation led to a statistically significant increase in apparent elastic modulus after 5 days, as well a statistically significant decrease in hysteresis after 3 days in culture. If this trend of VSMC mechanical properties changing concurrently with phenotypic shifts were to hold true *in vivo*, such changes could affect the processes of mechanotransduction and/or arterial mechanical properties, thereby contributing to the progression of vascular disease.

Introduction

Vascular smooth muscle cells (VSMCs) are one of the main constituents of the arterial medial layer and therefore are continuously exposed to mechanical stresses from arterial blood pressure. It is known that alterations in a cell's mechanical properties can have profound effects on the response to such external mechanical forces [115]. For this reason, the study of single cell mechanical properties has become an increasingly valuable research area in recent years [146, 174] as investigators have begun uncovering the importance of mechanical cues in numerous disease pathologies [115, 134, 175]. Any disease that affects the cytoskeleton may, in turn, affect cellular mechanical properties. Furthermore, the mechanical behavior of individual cells often shares many characteristics with macroscopic tissues [134]. Given the relationship between vascular disease and mechanical stimuli, a better understanding of VSMC mechanical properties would provide valuable data to our knowledge of the complex atherosclerotic and restenotic disease processes.

Vascular SMCs typically take on a synthetic phenotype after a short time in culture, but a shift towards a contractile phenotype has been shown to be possible *in vitro* through serum starvation and reversible through the subsequent re-addition of serum [176]. Serum starvation can have numerous affects on VSMCs in culture, including upregulation of cytoskeletal and contractile proteins [176-179], alterations in growth factor receptor expression [180], changes in integrin binding characteristics [181], altered Ca^{2+} response and chemotaxic behavior [179], decreased attachment and proliferation [182], decreased cell volume [183], and increased collagen expression [184]. It has been

demonstrated that *in vitro* VSMC serum starvation for 3 or more days results in restoration of contractility and significant upregulation of intracellular proteins characteristic of the contractile phenotype [176, 177]. Although serum starvation has not always been shown to induce complete restoration of the contractile phenotype [185], it has consistently been found to upregulate expression of the cytoskeletal and contractile proteins, which would contribute to cellular mechanical properties [176-179]. It is unlikely that VSMCs in culture would ever precisely mimic the mechanical behavior of VSMCs *in vivo* due to factors such as a lack of exposure to an *in vivo* physiological mechanical environment, differences in ECM composition, and the effects of a 2-D rather than a 3-D environment. However, serum deprivation has consistently been shown to result in a shift along the phenotypic continuum [32]. This makes this system a suitable model for the purpose of this study, which addresses mechanical properties of different phenotypes of VSMCs.

Previous studies have been performed examining the tensile elastic properties of VSMCs using a custom-designed micro-pipette system, with the data indicating that synthetic VSMCs have a lower tensile elastic modulus than contractile VSMCs [125-127]. Nagayama and collaborators also reported that tensile properties of VSMCs were affected by the quantity, organization, and distribution of α-actin filaments [127]. These previous studies however, were performed using trypsinized non-adherent VSMCs, and only elastic properties were measured, despite cellular mechanical behavior being viscoelastic in nature [112]. Nonetheless, this previous research has provided some insight into the mechanical properties of VSMCs, which could be expanded upon by

additional characterization of the mechanical properties of adherent VSMC utilizing nanoindentation with an atomic force microscope (AFM).

The major objective of the present study was to assess the differences in mechanical properties between serum-fed and serum-starved VSMCs using AFM nanoindentation. As measures of elastic and viscous properties, VSMC apparent elastic modulus was quantified, along with the degree of hysteresis between indentation and retraction curves at different indentation speeds. It was hypothesized that serum-starved VSMCs would exhibit greater elastic moduli due to their increased cytoskeletal and contractile protein content. A secondary objective was to quantify intracellular variations in VSMC elastic modulus.

Materials and Methods

Cell Culture

Rat aortic VSMCs (Vectechnologies, Rensselaer, NY) from an established cell line were cultured in Dulbecco's Modified Eagle's Medium (DMEM) (Mediatech, Herndon, VA) with fetal bovine serum (FBS) (10%) (Sigma, St. Louis, MO) and antibiotic/antimycotic solution (1%) (Sigma). Cells were maintained in T-75 polystyrene flasks in an incubator at 37ºC with 5% CO_2, and fresh media was exchanged every 48 hours. Cells were utilized between passages 5 and 8. For all AFM force measurements, cells were allowed to grow to ~80% confluency in the flasks then trypsinized with 0.25% trypsin (Mediatech) / 0.02% EDTA (Sigma) and seeded in a sub-confluent layer onto 22 x 22 mm glass coverslips (VWR, West Chester, PA). Coverslips had each been coated

with 40 μl of 50 μg/ml monomeric type I collagen (Vitrogen 100, Cohesion Technologies, Palo Alto, CA) 24 hours prior to cell seeding. Cells were seeded sub-confluently in order to minimize overlapping and to control for the mechanical stiffening effects known to be imparted upon cells once they reach confluency in culture [174]. For each experiment, the seeded cells were divided into two groups, serum-starved and serum-fed. Seeded coverslips in the serum-starved groups were maintained in serum-free (0% FBS) DMEM for 3 or 5-days, while the serum-fed groups were concurrently maintained in DMEM with 10% FBS. Serum-starved cells were washed with phosphate buffered saline (PBS) (Mediatech) prior to switching to serum-free media. All of the cell-seeded coverslips were maintained in 6-well plates at 37ºC with 5% CO_2, and media was exchanged every 48 hours prior to AFM experimentation.

AFM Indentation

Atomic force microscopy (AFM) experiments were performed 3 or 5 days after the cells were seeded onto the coverslips, depending upon the designated number of days of serum starvation for each group. For all AFM experiments, a Digital Instruments Dimension 3000 AFM with a Nanoscope IV controller (Veeco Metrology, Santa Barbara, CA) was operated in contact mode with a fluid cell. During AFM experiments, cells were kept on the coverslips in their respective culture media, which was exchanged approximately every 30 minutes with warm 37ºC media throughout the course of the AFM experiments, each lasting for approximately 2 h in total. For each experiment, representative cells (n=15) were chosen based on their appearance as being either “spread” for the serum-fed

group, or "spindle-shaped" for the serum-starved group. This was based on previous reports of morphological changes of serum-starved VSMCs [176, 177] and ensured that only cells that had responded to serum starvation were chosen for analysis. The AFM probe was positioned over the central region of each cell body, avoiding the thin cell edges, and the cell was indented 5 times consecutively at each of 3 different approach speeds (0.095 Hz (0.50 μm/s), 0.498 Hz (2.62 μm/s), 1.94 Hz (10 μm/s)) for a total of 15 indentations per cell. Approach speeds were randomized for some samples in order to control for any mechanical changes that may be caused by repeated indentation. The approximate depth of each indentation was 500 to 600 nm, although the Hertz model was only applied at 150 to 200 nm of each force curve, as described below. Indentation depth was regulated by adjusting the triggering force (~ 20 nN) as necessary. A single 5 μm diameter borosilicate spherical-tipped AFM probe (BioForce Nanosciences, Ames, IA) on a silicon-nitride cantilever with a nominal spring constant of 0.58 N/m, was utilized throughout the study. Prior to each experiment, deflection sensitivity (nm/V) was determined by indenting onto a clean glass coverslip in DMEM.

Several cells were also imaged in contact mode using a 0.58 N/m pyramidal AFM probe (Veeco Metrology). These images were then used to determine cell height and to construct 40 × 40 point force-curve maps — covering a total area of approximately 1600 μm^2 — by using the "point and shoot" function in the NanoScope v6.13R1 software (Veeco Metrology) for the purpose of quantifying spatial variations in intracellular elastic modulus. In order to determine intracellular variations in elastic modulus, the indentation depth at 20 nN for each point in the force-curve matrices was calculated and mapped.

Additionally, the coefficient of variation (COV) for elastic modulus in the central region (~ 25 μm^2 area) of the cell was calculated. Intracellular modulus measurements were conducted as a means to gauge the intracellular variability of elastic modulus values and therefore the validity of reported measurements from single-point AFM indentation throughout the current study.

Force Curve Analysis

Following the AFM experiments, a MATLAB (MATLAB 7.0, The MathWorks, Inc., Natick, MA) script was used to normalize the force curves and shift them as needed to a common zero point. Contact points were determined by visually identifying the region at which the slope of each curve shifted upwards. In addition, and as a comparison, other methods for determining the contact point were also employed. The first method calculates the contact as the point where the force increases above the level of noise [186]. In the second method, the contact point is calculated as the point where the slope of the curve changes by fitting the curve to a 2-region model [146]. These methods gave a contact point similar to the visual inspection of the curve and did not significantly affect the calculated moduli or trends observed.

To obtain a measure of individual cell stiffness, the apparent elastic moduli of the cells were calculated using the Hertz model for a spherical indenter [173]:

$$F = \frac{4}{3}\frac{E}{(1-\upsilon^2)}R^{\frac{1}{2}}\delta^{\frac{3}{2}}$$

where F is the measured force (N), δ is indentation depth (m), E is apparent elastic modulus (Pa), υ is Poisson's ratio (0.5) [187], and R is the spherical indenter radius (2.5 μm). A "normalized indentation depth" was calculated for both serum-fed and serum-starved VSMCs. This was chosen to be approximately 10% of the cell height, as this is the depth at which the Hertz model remains accurate [188]. As average cell height was measured using contact mode AFM imaging as ~ 1.5 μm for serum-fed cells and ~ 2.0 μm for serum-starved cells (Figure 3.1), the corresponding depths at which the Hertz model was applied were 150 and 200 nm respectively. The "pointwise modulus" method of cellular mechanical analysis developed by Costa, et al.[145] was utilized in addition to, and as support usage of the Hertzian method described above. This method illustrates variations in elastic modulus as a function of indenter depth and geometry. Indentation force F_i is related to the pointwise apparent elastic modulus $\hat{E}_i$ by the equation:

$$F_i = 2\pi\Phi(D_i)\,\hat{E}_i$$

where $\Phi(D)$ is a function relating the contribution of indenter geometry to depth dependence of the indentation response [145]. In essence, this is a rearrangement of the Hertz model that allows for the determination of elastic modulus variations as a function of indentation depth. Performing this calculation allows one to determine whether significant variations in elastic modulus values would be obtained should the Hertz model be applied at different depths.

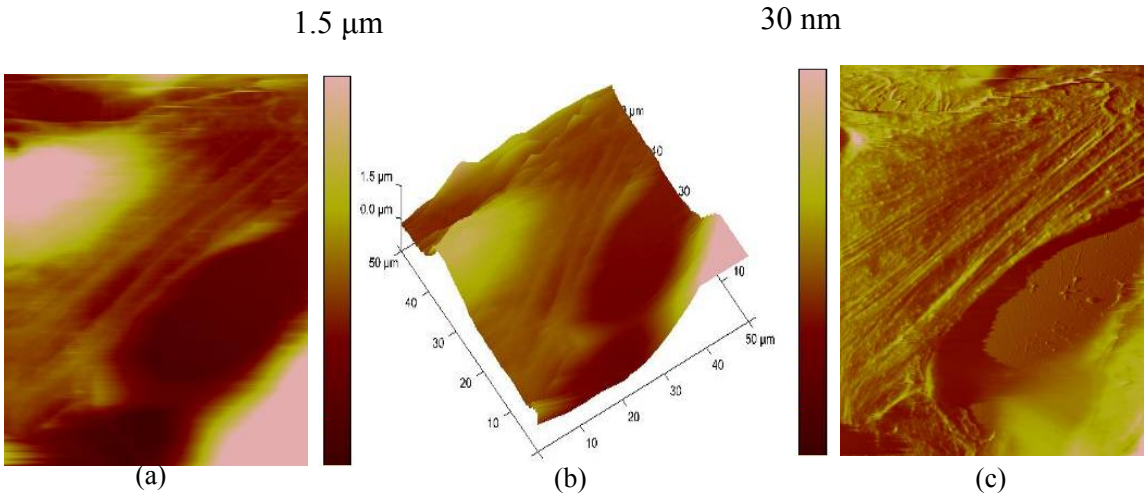

Figure 3.1. Serum-fed VSMC imaged in contact mode; (a) Height image illustrating variations in cell height in reference to underlying substrate, (b) 3D height image, (c) Deflection image illustrating cell surface details.

In addition to the elastic modulus calculations, the degree of hysteresis exhibited by each cell was calculated by subtracting the area under the entirety of each retraction curve from the area under the entirety of its corresponding indentation curve and then normalizing by the area under the indentation curve in order to account for variations in indentation depth (Figure 3.2) [143]. This calculation of hysteresis, combined with the changes in modulus with indentation speed, provided a measurement of non-elastic behavior and viscous energy dissipation [189]. Calculating hysteresis in the force curves provided a measure of viscous contributions that is independent of any concerns that would arise regarding the validity of various existing viscoelastic models.

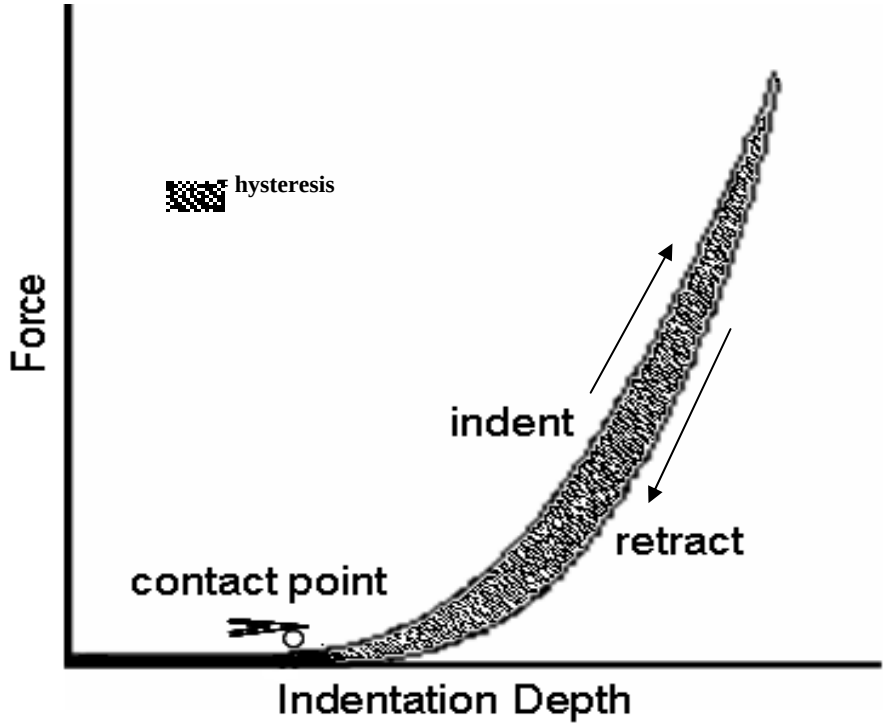

Figure 3.2. A force curve obtained using an AFM is comprised of both an indent and a retract curve. The contact point was determined by visually identifying the region at which the slope of the indent curve turned upward. Hysteresis can be calculated by finding the area between the two curves and normalizing by the indent curve in order to account for variations in indentation depth.

Immunofluorescence

Immunofluorescence staining of SM-α-actin, which is one of the most abundant proteins in VSMCs and is known to be downregulated during phenotypic modulation [176, 190], was used as a means of visualizing any changes in α-actin distribution or expression level. Cells designated for immunofluorescence were fixed in 100% ethanol at room temperature for 30 minutes at the same time points as the cells for the corresponding AFM experiments. The cells were then incubated with blocking solution consisting of PBS (90%) (Sigma), bovine serum albumin (3.8%) (Sigma), donkey serum

(3.0%) (Sigma), and Triton-X (0.2%) (Sigma) for 30 minutes, followed by incubation with rat SM-α-actin monoclonal primary antibody (Abcam, Inc., Cambridge, MA) overnight. A FITC-conjugated secondary antibody (Invitrogen, Inc., Carlsbad, CA) was added the following day for 2 hours, followed by incubation with DAPI for 5 minutes (Invitrogen, Carlsbad, CA). Immunostained cells were visualized on glass slides using a Nikon Eclipse TE2000-S fluorescence microscope (Nikon USA, Melville, NY) with a FITC-filter, and digital images were captured using QCapture 2.68 imaging software (QImaging, Inc., Burnaby, BC).

Statistics

Repeated measures ANOVA was used to determine any statistically significant differences in apparent elastic modulus or hysteresis within experimental groups at different probe speeds, while Student's t-tests were used to determine any statistically significant differences in apparent elastic modulus or hysteresis between experimental groups at a given speed. In cases where normality tests failed ($P < 0.05$), Friedman repeated measures ANOVA on ranks and Mann-Whitney rank sum tests were used in place of repeated measures ANOVA and Student's t-tests respectively, due to their greater stringency. All statistical analyses were performed using SigmaStat 3.1 software (Systat Software, Inc., Richmond, CA). An alpha level of 0.05 was used for all performed tests. Coefficients of variation (standard deviation / mean) were calculated within each experimental group as a measure of cell-to-cell variations in modulus, within each cell loading session as a measure of data repeatability on a single point of

indentation, and within the force-curve matrices to determine intracellular modulus variation.

Results

Hertzian Apparent Elastic Modulus

Statistically significant increases in hysteresis were observed with the increase of approach speeds in all VSMC groups ($p < 0.05$). Furthermore, increased approach speeds resulted in greater measured apparent elastic modulus values in all experimental groups, as is commonly observed in viscous materials including cells [189]. Accordingly, the lowest AFM approach speed used in this study (0.5 um/s) was used for all calculations of apparent elastic modulus in order to minimize any viscous effects on the calculated estimate of the elastic modulus. Approach speed randomization revealed no temporal changes in modulus measurements throughout indentation cycles. Serum starvation for 5 days resulted in a statistically significant increase in apparent elastic modulus. All 3-day serum-starved groups exhibited non-significant increases in apparent elastic modulus. The mean apparent elastic for VSMCs was 13.5 ± 2.8 and 15.1 ± 6.2 kPa for the serum-fed and 3-day serum-starved groups respectively ($p = 0.842$, Fig 3). For VSMCs serum-starved for 5-days, the mean apparent elastic modulus was 15.3 ± 4.3 kPa, compared to 11.1 ± 4.1 kPa for serum-fed cells ($p = 0.010$, Figure 3.3).

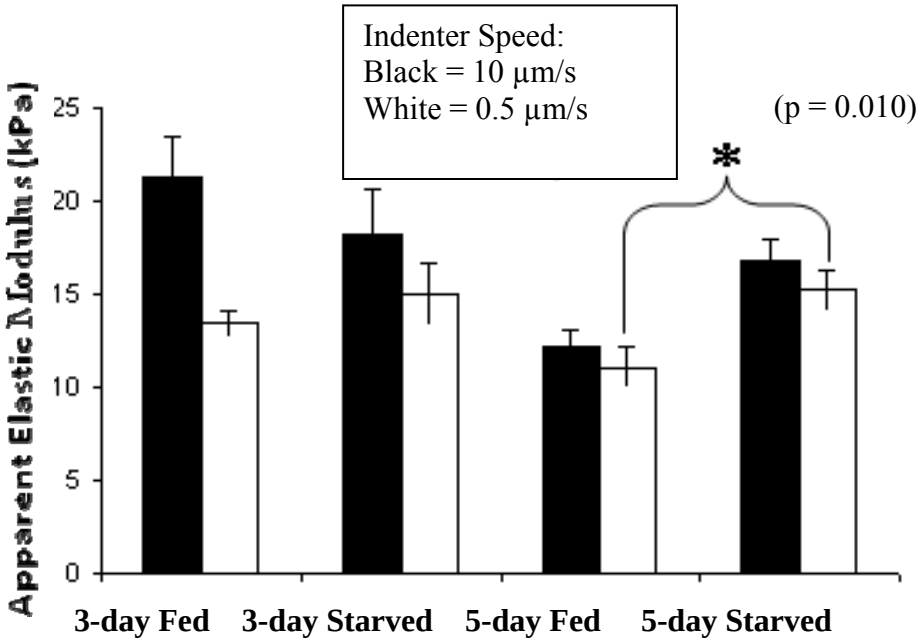

Figure 3. 3. Apparent elastic moduli of serum-fed and serum-starved (3 and 5-days) rat aortic VSMCs measured with a 5 μm diameter borosilicate spherical AFM probe at approach speeds of 0.5 (white) and 10.0 μm/s (black), with 10% indentation depths approximated at 150 and 200 nm for serum-fed and serum-starved groups respectively (n = 15 cells per group). At greater indenter speeds, artificially inflated elastic modulus values are commonly observed in materials exhibiting significant **hysteresis.** Therefore, data from 0.5 μm/s measurements were used for statistical comparisons of elastic modulus. Data are presented as mean ± SE.

Histograms were plotted from the 5-day group in order to more clearly illustrate the differences in elastic modulus distribution between treated and control groups (Figure 3. 4).

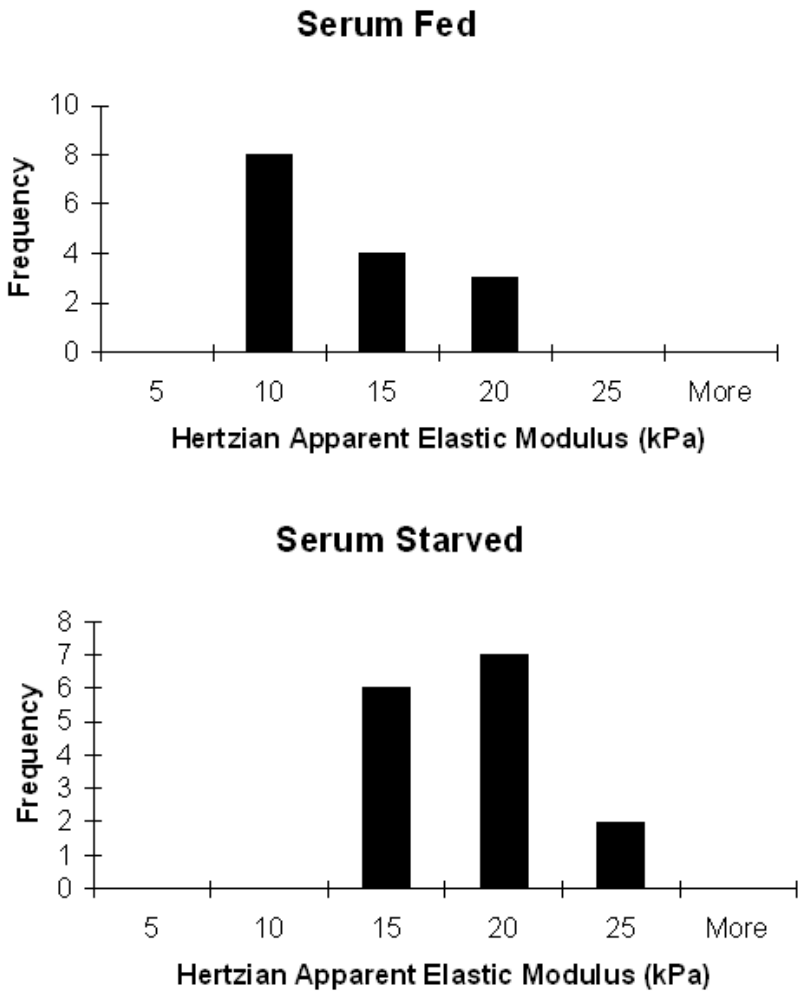

Figure 3.4. Histograms illustrate the distribution of apparent elastic modulus values for 5-day serum-starved VSMCs and controls. As is commonly found with cell mechanics measurements, there is a relatively high degree of deviation in mechanical properties. However, the serum-starved group clearly exhibits a greater proportion of high modulus samples as compared to the serum-fed group.

Averaged indentation curves (Figure 3.5a) with the standard deviation, noted at the depth of Hertz model application, illustrate the observed difference between treated and control groups. Additionally, representative force curves from both a serum-fed and a serum-

starved sample (Figure 3.5b&c) with the Hertz model overlaid at the fitted region visually represent the fit of the model.

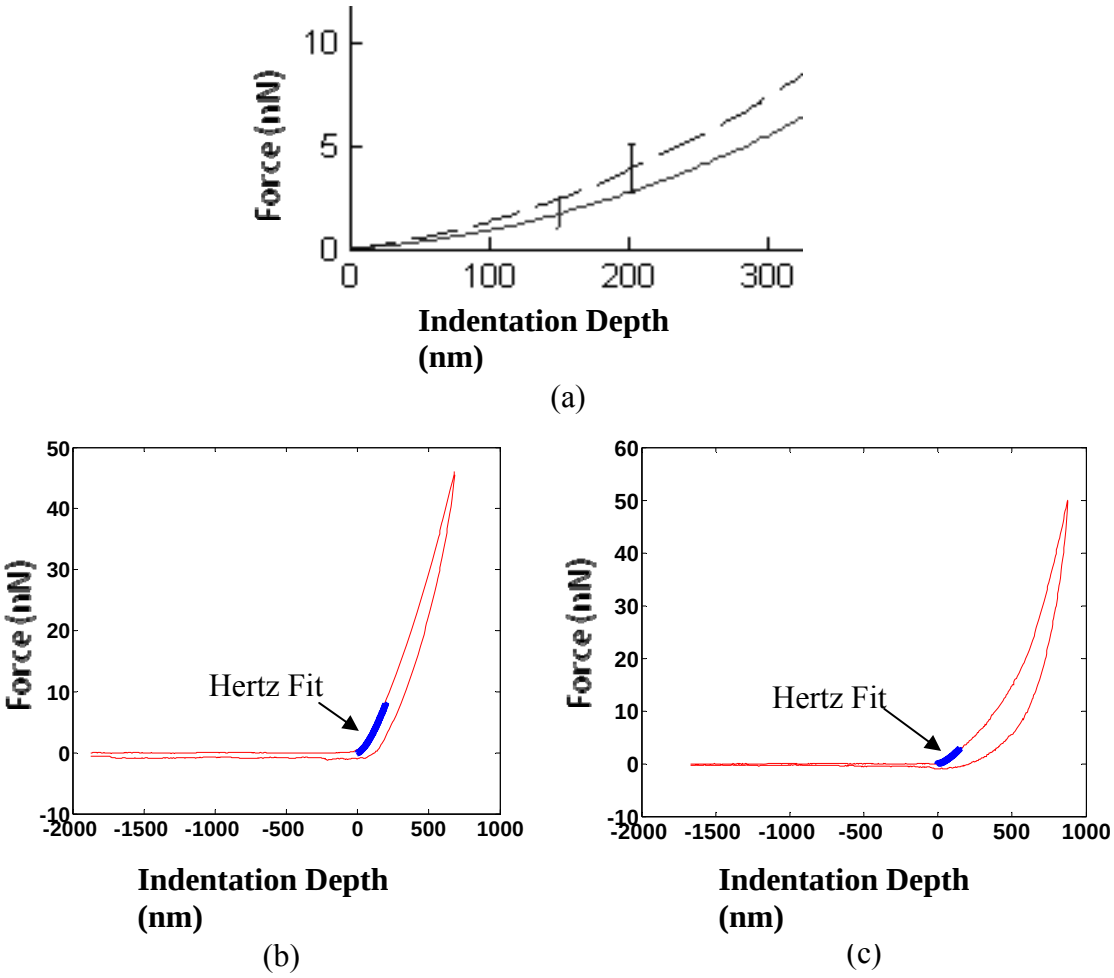

Figure 3.5. Averaged force curves of serum-fed (solid) and serum-starved (hashed) VSMCs with respective points of Hertz fit (± SE) denoted by vertical bars (a). Representative force curves from 5-day serum-starved (b) and serum-fed (c) groups, overlaid by corresponding Hertz model fits.

The cell-to-cell apparent elastic modulus COV had a mean of 32.0 ± 9.5%. The mean COV for moduli measured at a single point was 6.0 ± 5.3%. Cell-to-cell apparent elastic modulus COVs and repeated indentation COVs for each experimental group are summarized in Table 3.1.

Table 3.1. Cell-to-cell and repeated point elastic modulus COVs

	Cell-to-Cell COV (%)	Repeated Point COV (%)
3- day Serum-fed	20.6	4.1
3-day Serum-starved	42.3	4.2
5-day Serum-fed	36.8	10.3
5-day Serum-starved	28.4	5.3
All (mean ± SD)	32.0 ± 9.5	6.0 ± 5.3

Pointwise Elastic Modulus

Averaged pointwise elastic modulus normalized to the Hertz model was plotted for both 5-day serum-starved cells and controls (Figure 3.6 a&b). For the relevant regions of these plots, which includes the first 200 nm of indentation, both the serum-starved and control groups appear relatively flat, providing evidence that the Hertz model is suitable in this region [145]. Beyond 200 nm, the plots do begin to exhibit increasing nonlinearity (Figure 3.6 c&d). However, these larger indentation depths were not taken into account for modulus calculations and are therefore irrelevant to the current discussion.

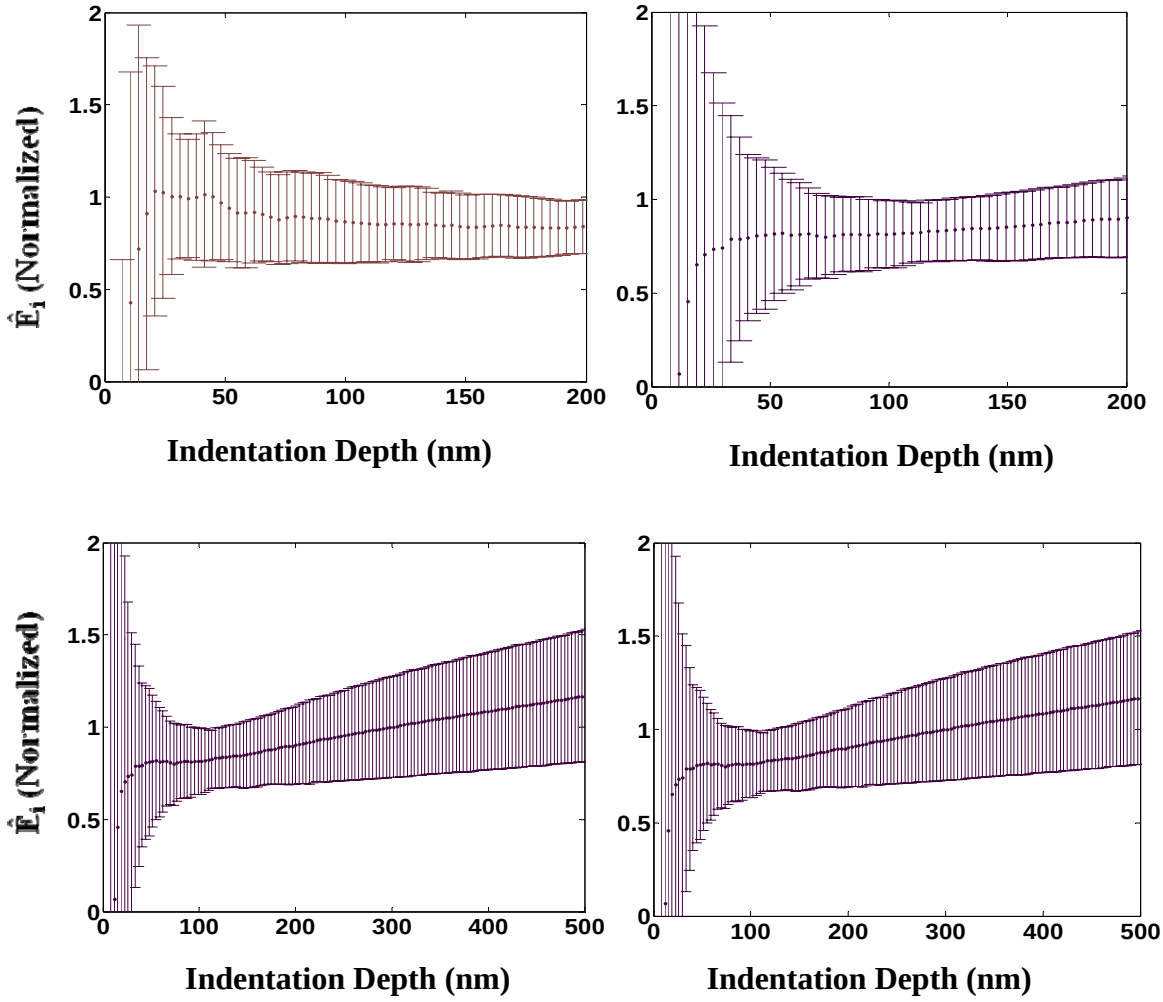

Figure 3. 6. Pointwise modulus normalized to Hertz model modulus of 5 day serum-fed (a&c) and serum-starved (b&d) groups shown to 200 nm depth (a&b) and to 500 nm depth (c&d). Up to 200 nm, the plots are relatively linear and centered around a value of 1, indicating applicability of the Hertz model. However, beyond that depth, nonlinearity increases (particularly for the serum-starved cells).

Intracellular Elastic Modulus Variation

Spatial intracellular variations in apparent elastic modulus for 3 mapped cells were found to be similar to cell-to-cell variations (COVs of ~ 35 to 40%). The indentation depth at 20nN varied from approximately 100 nm to 1 μm over the entire cell (Figure 3.7). However, in the more relevant central region, with an area of approximately 25 μm^2, which was probed for elastic modulus measurements, indentation depth at 20 nN varied only between ~ 500 to 600 nm. Since only these inner regions of the cells were targeted for indentation throughout this study, the thinner peripheral regions are of lesser relevance.

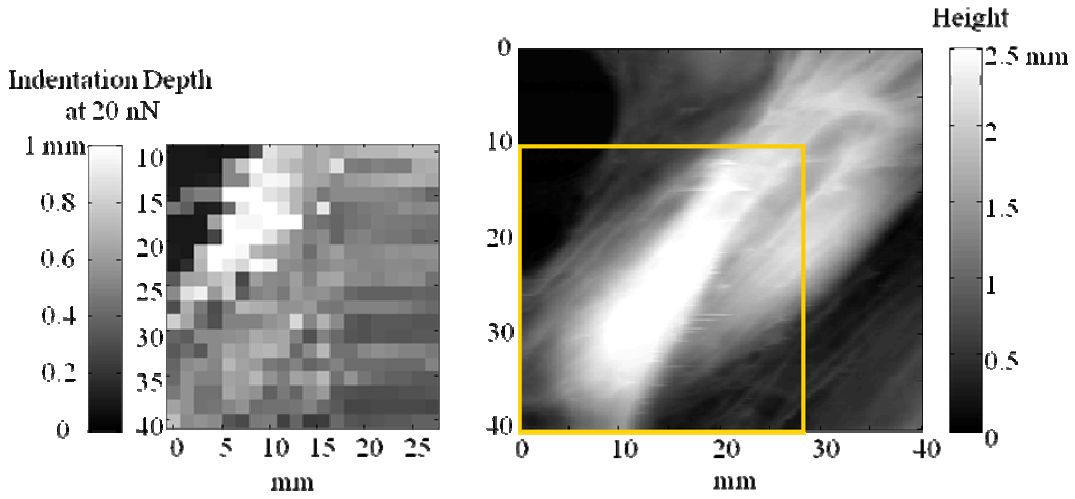

Figure 3.7. Indentation depth at 20 nN (left) and height image (right) from a representative serum-starved VSMC. Lighter pixels represent greater indentation depth (lower elastic modulus). The soft region in the upper-left quadrant of the indentation depth image is most likely due to a region of overlapping cells which was noticed during the imaging experiment.

Hysteresis

Hysteresis was statistically significantly greater at higher AFM probe approach speeds for all experimental groups in this study ($p < 0.05$). It was therefore determined that the maximum probe approach speed that was used, 10 μm/s, would be utilized for all calculations of hysteresis in order to accentuate any differences in viscous contributions between cell phenotypes. Hysteresis was statistically significantly lower for early passage 3-day serum-starved VSMCs (0.41 ± 0.08 and 0.32 ± 0.09 for serum-fed and serum-starved respectively, $p = 0.007$) (Figure 3.8). Hysteresis was also statistically significantly lower in 5-day serum-starved than in serum-fed VSMCs ($p < 0.001$) (Figure 3.8).

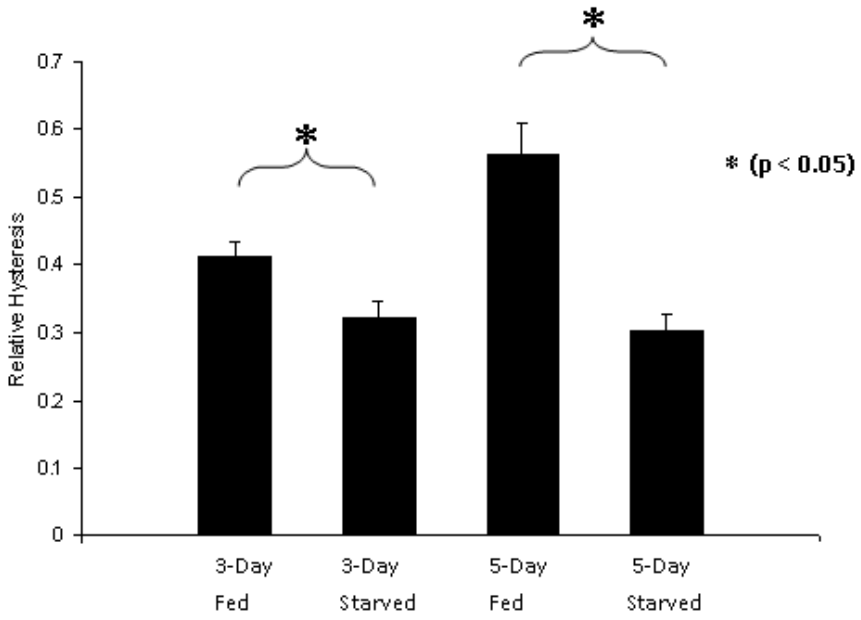

Figure 3. 8 . Hysteresis of VSMCs, serum-fed or serum-starved for three or five days, measured at an approach speed of 10.0 μm/s. Data are presented as mean ± SE.

Immunofluorescence

Serum starvation resulted in decreased cell spreading at both 3 and 5 day timepoints. Immunofluorescence staining revealed that both serum-fed and serum-starved VSMCs were positive for SM-α-actin. In the majority of serum-fed VSMCs, SM-α-actin was randomly distributed; however, many cells did appear to stain darker around the cellular periphery. Actin filaments were typically thin in appearance and were randomly oriented. Serum-starved VSMCs exhibited a more heterogeneous staining profile, as some cells appeared to be very similar to the serum-fed cells while others had become elongated, with thicker actin filaments that were more evenly distributed, and ran parallel to the major axis. Given that these elongated VSMCs were selected for indentation, the actin filament distribution within them is of greater relevance to the current study. No obvious differences were noted in SM-α-actin content between 3 and 5-day serum-starved cells. Representative SM-α-actin images are shown in Fig. 9.

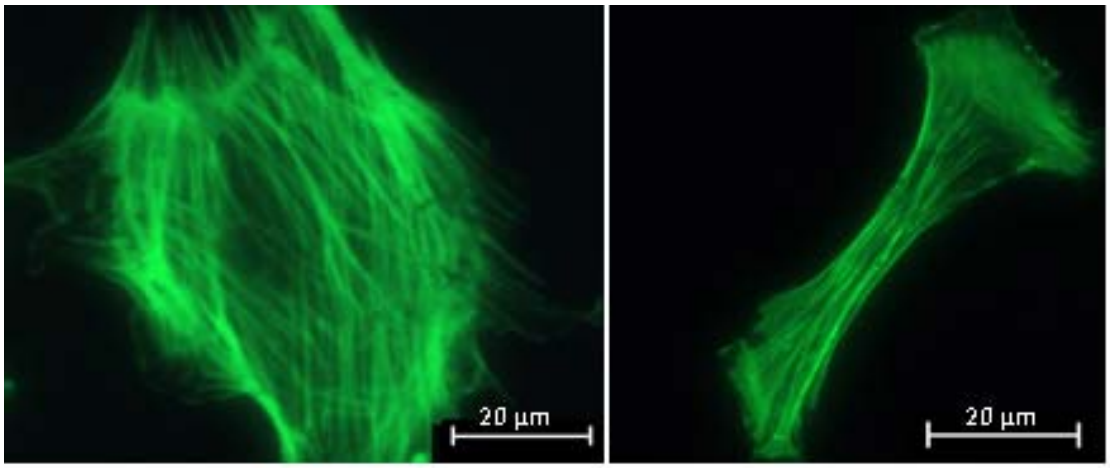

Figure 3.9. Representative smooth muscle alpha-actin immunofluorescence images of an elongated serum-starved VSMC (left) and spread serum-fed VSMC (right) at 40x.

Discussion

The present study was designed to model a phenotypic shift of VSMCs *in vitro* through the use of serum-starved and serum-fed VSMCs and to identify any trends in cellular mechanical property changes that occur during such a phenotypic shift. Differences in cell height between serum-fed and serum-starved VSMCs were accounted for by using a "normalized indentation depth" of ~10%. This parameter is closely related to other factors, namely indenter radius and layer thickness. Recent computational research suggests that modulus values are not significantly in error with a 2.5 μm radius indenter when the ratio of indentation depth to sample thickness is at or below 0.1, as in the current study [191]. Support of the Hertz model using the pointwise modulus method was also undertaken. Plots of pointwise elastic modulus were relatively flat for the first 200 nm. Therefore, as stated by Costa, et al.[145] the Hertz model is reasonably appropriate for modeling this region (~ 200 nm). Regions beyond 200 nm in depth exhibiting increasing nonlinearity were not modeled and are therefore of lesser relevance. It is well-documented that the Hertz model has significant deficiencies when it comes to cell mechanical modeling, resulting in part from the fact that cells and tissues do not meet several assumptions of the Hertz model, e.g. linearity and isotropicity. However, as a means of comparative analysis, Hertzian modeling does provide a quantitative measure relating to cellular mechanical properties, which can be useful under certain conditions. The validity of Hertzian analysis under the conditions of the current study was strengthened through the use of Costa's pointwise modulus method. This does not mean,

however, that use of the Hertz model is appropriate under all conditions and for all cell types. Indeed, as demonstrated by Costa, there are scenarios in which significant nonlinearities are evident following pointwise analysis, and it is in these cases that the Hertz model should be deemed less appropriate.

To the best of our knowledge, this is the first AFM study examining the changes in mechanical properties of VSMCs adhered to an arterial ECM constituent. In addition to the basic science motivations behind this research, it also carries clinical significance, as it is known that elastic and/or viscous properties of single cells can be altered during many different diseases states and that these cellular mechanical properties can have significant effects on the process of mechanotransduction [115, 134]. In the case of vascular lesion development, VSMC mechanical changes may indeed have detrimental effects.

In the current study, *in vitro* serum starvation of VSMCs resulted in statistically significantly increased apparent elastic modulus and statistically significantly decreased hysteresis. The observed differences in elastic modulus are likely due, in part, to changes in expression level, organization, and orientation of cytoskeletal and contractile proteins [190]. However, two factors that have not yet been taken into account to explain the differences in mechanical properties between the serum-fed and serum-starved groups are cell adhesion and cell morphology (spreading). There is evidence that increased cell adhesion [192] and increased cell spreading [193] both correlate with increased stiffness. In the present study, the serum-fed groups consistently displayed stronger adhesion and greater spreading, which may have offset cytoskeletal changes brought about through

serum starvation. One possible limitation of measuring "elongated" serum-starved cells and "spread" serum-fed cells is that in actuality one would be assessing the mechanical differences associated with these two distinct morphologies. However, it should be noted that such morphological differences are one of the key distinguishing features used to define VSMC phenotype [194]. Furthermore, under the conditions used in the current study very few (less than 5%) elongated cells were observed in serum-supplemented media. Nevertheless, a potential means to address this limitation in future studies would be the addition of a contractile agent to the media, and the subsequent mechanical measurement of responsive versus non-responsive cells.

Previous studies relating VSMC mechanical changes to phenotype utilized tensile strains of unattached, freshly isolated contractile and synthetic VSMCs, while the current study utilized indentation of attached serum-starved and serum-fed VSMCs in culture. Despite the differences in study protocols, data from the current study are in agreement in finding that a shift towards the synthetic phenotype results in a decrease in elastic modulus. In terms of cell-to-cell elastic modulus variation, the present study yielded a mean COV of $32.0 \pm 9.5\%$, which is towards the lower end of previously reported COVs from AFM cell indentations studies [174].

The relatively low spatial intracellular variations in elastic modulus exhibited by the VSMCs in the current study provide evidence that indenting a single point near the center region of the cell serves as an adequate measure of cellular elastic modulus. Although a few previous studies have found differences in stiffness in a localized center of the cell due to contributions from the nucleus [142, 189], this was not observed in our

measurements. In this study, indentations of 10% of the total cell height were used to obtain modulus values, and the full-force indentation curves themselves were typically in the range of 500-600nm. At these small indentations, it is likely that any effect on stiffness due to the underlying nucleus is negligible. Additionally, cell-to-cell elastic modulus variability was found to be in the same range as intracellular variability. Repeated indentations at a single point did not appear to affect measured modulus values, nor damage the cell in any significant manner. The mean COV for moduli measured at a single point was 6.0 ± 5.3% in the present study.

Fluorescent microscopic images of FITC-labeled SM-α-actin revealed that both serum-fed and serum-starved VSMCs were SM-α-actin positive. However, a larger percentage (~ 25%) of serum-starved cells appeared to be elongated, with SM-α-actin distributed uniformly throughout the cells, while most (~ 95%) of the serum-fed cells exhibited random orientation of thinner SM-α-actin filaments. Given the previous data regarding changes in SM-α-actin during modulation [176, 190, 195] and its relationship to mechanical properties [127], it is hypothesized that such changes, along with morphological and adhesive alterations, contributed to the altered mechanical properties reported here.

The extent to which serum starvation in culture can accurately replicate *in vivo* phenotypic changes is arguable. Nonetheless, most available evidence does suggest that serum starvation in culture serves to mimic *in vivo* phenotypic changes through altered morphology, upregulation of intracellular cytoskeletal and contractile proteins, inhibition of proliferation and migration, and restored contractility [176, 177, 196]. Furthermore,

use of the current protocol can be justified by the fact that populations of VSMCs within even a single blood vessel *in vivo* are known to be highly heterogeneous [4], and the process of phenotypic shift itself occurs along a continuum [32]. It was demonstrated that a shift along this continuum significantly affects VSMC viscoelastic properties.

Conclusions

In vitro 5-day serum-starved VSMCs exhibit statistically significantly greater apparent elastic moduli and statistically significantly lower hysteresis than serum-fed VSMCs. Further study is required to determine whether the observed *in vitro* trends accurately reflect an *in vivo* pathological scenario, and if so, how significant an impact such mechanical changes may have on mechanotransduction and vascular lesion development.

CHAPTER FOUR

ROLE OF CYTOSKELETAL COMPONENTS IN STRESS RELAXATION BEHAVIOR OF ADHERENT VASCULAR SMOOTH MUSCLE CELLS

Abstract: A number of recent studies have demonstrated the effectiveness of atomic force microscopy (AFM) for characterization of cellular stress relaxation behavior. However, this technique's recent development creates considerable need for exploration of appropriate mechanical models for analysis of the resultant data and of the roles of various cytoskeletal components responsible for governing stress relaxation behavior. The viscoelastic properties of vascular smooth muscle cells (VSMCs) are of particular interest due to their role in the development of vascular diseases, including atherosclerosis and restenosis. Various cytoskeletal agents, including cytochalasin D, jasplakinolide, paclitaxel, and nocodazole, were used to alter the cytoskeletal architecture of the VSMCs. Stress relaxation experiments were performed on the VSMCs using AFM. The quasilinear viscoelastic (QLV) reduced relaxation function, as well as a simple power-law model, and the standard linear solid (SLS) model, were fit to the resultant stress relaxation data. Actin depolymerization via cytochalasin D resulted in significant increases in both rate of relaxation and percentage of relaxation; actin stabilization via jasplakinolide did not affect stress relaxation behavior. Microtubule depolymerization via nocodazole resulted in nonsignificant increases in rate and percentage of relaxation, while microtubule stabilization via paclitaxel caused significant decreases in both rate and percentage of relaxation. Both the QLV reduced relaxation function and the power-law model provided excellent fits to the data ($R^2 = 0.98$), while

the SLS model was less adequate ($R^2 = 0.91$). Data from the current study indicate the important role of not only actin, but also microtubules, in governing VSMC viscoelastic behavior. Excellent fits to the data show potential for future use of both the QLV reduced relaxation function and power-law models in conjunction with AFM stress relaxation experiments.

Introduction

The importance of mechanotransduction in regulating numerous physiological processes has become increasingly evident in recent years [115]. Mechanical stimuli have been found to play a significant role in the cellular pathology of numerous diseases, including atherosclerosis [197], cancer [198], and arthritis [199]. Thus, the behavior of a cell in reaction to mechanical stimuli appears to affect the cell's subsequent biochemical response to those stimuli. These findings have prompted development of improved techniques to further elucidate the complex mechanical behavior of cells and tissues [129]. One commonly used tool for the study of cell mechanics is the atomic force microscope (AFM) [134]. Until recently, the majority of AFM cell-mechanics research focused on simple indentation curves, whereby cantilever deflection (force) is related to indentation depth, and an apparent elastic modulus is calculated (often employing Hertzian contact equations) [143, 200]. The AFM, however, has also been used to quantify viscoelastic properties of living, adherent cells via stress-relaxation [149, 154, 155] and cyclic-loading measurements [187]. While previous AFM stress relaxation work demonstrated the technique's potential, it did not explore cytoskeletal roles in governing stress relaxation, and it relied on linear viscoelastic models [149, 154, 155, 187]. Thus, understanding the overall process of mechanotransduction requires identification of the contributions of cytoskeletal components and development of appropriate viscoelastic models [110].

The mechanical behavior of vascular smooth muscle cells (VSMCs) is particularly important from a clinical perspective. Because these cells have been implicated in the

pathogenesis of various vascular diseases (e.g., hypertension, atherosclerosis, and restenosis) [197], elucidating their intrinsic mechanical properties is essential to understanding the role of mechanotransduction in these disease processes. The role of VSMCs in the regulation of hemodynamics and their exposure to a range of mechanical stimuli (from sources including shear blood flow, blood pressure, and endovascular devices) underscore the value of characterizing their mechanical behavior. Although stress relaxation of individual VSMCs has been measured [201, 202], the cells used in these studies were not adherent to a substrate, and custom tensile testers were used to obtain the data.

The goal of the present study was to determine the roles of both actin and microtubules in governing VSMC viscoelastic behavior. Thus, we measured the stress relaxation response of VSMCs via AFM and compared three existing models to analyze that behavior.

Materials and Methods

Smooth muscle cells isolated from adult male Sprague-Dawley rat aortal explants were cultured in Dulbecco's Modified Eagle's Medium (DMEM) (Mediatech, Herndon, VA) supplemented with fetal bovine serum (FBS) (10 %) (Sigma, St. Louis, MO) and antibiotic/antimycotic (1 %) (Sigma). Cells were maintained in a humidified, 37 ºC, 5% CO_2, 95% air environment. Prior to AFM experiments, cells were seeded onto 22 x 22 mm glass coverslips coated with type I collagen (Vitrogen 100, Cohesion Technologies, Palo Alto, CA) at a density of 150,000 cells per coverslip. Seeded coverslips were incubated in 6-well plates with DMEM (10% FBS) at 37 ºC with 5% CO_2 for 3 to 5 days prior to AFM experimentation. Cells were used in experiments between passages 5 and 8.

AFM Stress Relaxation Experiments

For all AFM experiments, a Veeco Dimension 3000 AFM with a Nanoscope IV controller (Veeco Metrology, Santa Barbara, CA) and hybrid x-y-z head was operated in contact mode with a fluid cell. A single borosilicate spherical-tipped AFM probe (5 μm diameter) (NovaScan, Ames, IA) on a silicon-nitride cantilever with a nominal spring constant of 0.12 N/m was used throughout the study. AFM experiments were performed after VSMCs had formed a confluent layer. Following the identification of a target cell, the AFM probe was positioned over the central region of the cell body. Relaxation tests were controlled using the strip-chart feature within the PicoForce mode of the NanoScope v6.13R1 software (Veeco Metrology). Channel 1 was set to record cantilever deflection, while channel 2 was set to record Z-piezo movement. Before each relaxation test was

run, the approximate separation distance between probe and cell was determined by visually inspecting a single force/displacement curve, Figure 4.1.

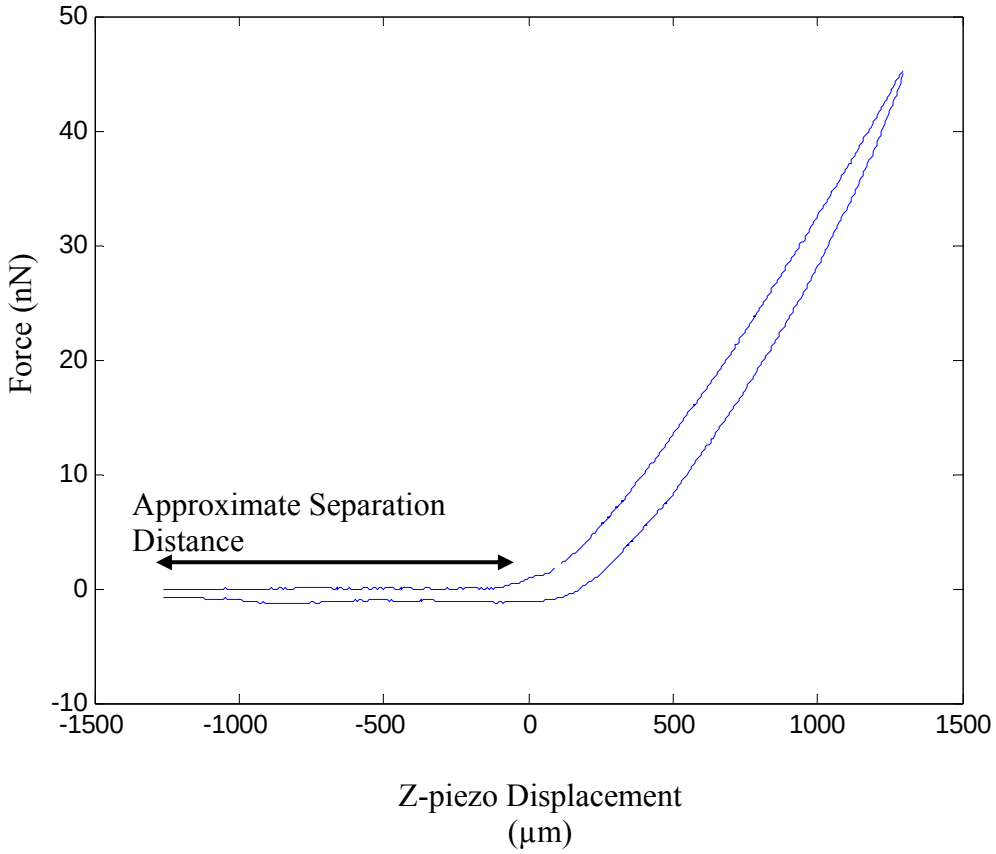

Figure 4.1. Sample indentation curve illustrating approximate probe-cell separation distance.

The estimated Z-separation gap was then minimized by lowering the probe in appropriate submicron increments using the step motor. This method provided a good approximation for starting each ramp at or near the cell surface. During AFM experiments, cell-culture media was changed approximately every 30 minutes; each experiment lasted no longer than 2 hrs in total.

For each relaxation test, a ramp speed of 50 μm/s was used during both the approach and the retract phase. This strain rate allowed for a reasonable approximation of a step strain while staying well below the Z-piezo's maximum programmable velocity (~200

μm/s) to assure accuracy of measurement and reduce the presence of fluid-related artifacts. To evaluate strain dependence, VSMCs were subjected to step indentations of 0.5, 1.0, and 1.5 μm for 120 seconds (Figure 4.2) consecutively; to allow time for mechanical recovery, approximately one minute was allowed to elapse between tests.

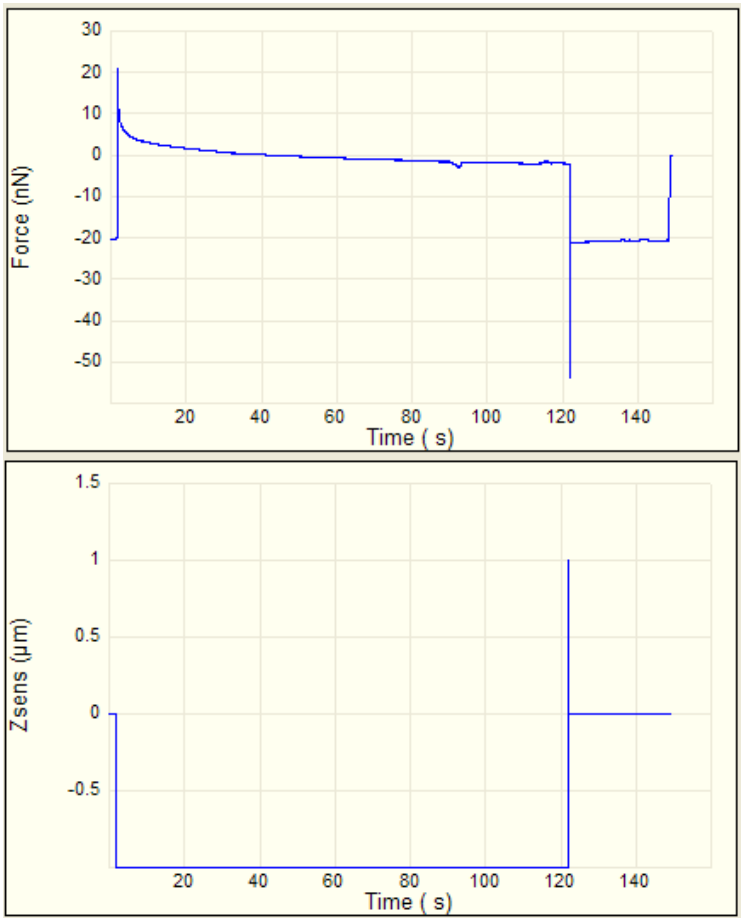

Figure 4.2. Top, cantilever deflection force vs. time; Bottom, Z-piezo movement vs. time.

The order in which the three ramp distances were used was randomized for each cell. For all experiments evaluating the effects of various cytoskeletal agents, a ramp distance of 1 μm was chosen. During the 120-second holding period, the fluctuation in strain in most cases was found to be on the order of 1% (5 to 15 nm), which was considered negligible. At the conclusion of all relaxation tests, the probe was retracted 2 μm to ensure probe/cell detachment in case any adhesion occurred during the relaxation phase. Data were collected at a sampling rate of 100 Hz for the duration of each relaxation test.

Cytoskeletal Agents

To assess the role of actin filaments in VSMC stress relaxation behavior, cells were treated with either 1 μM cytochalasin D (Sigma, St. Louis, MO) or 0.1 μm jasplakinolide (Fisher Scientific, Pittsburgh, PA) at 37 °C for 1 hour prior to tests. Cytochalasin D is an actin depolymerizing agent that caps the barbed end of F-actin, while jasplakinolide is an actin stabilizing agent that binds to both ends of actin filaments, preventing depolymerization. Likewise, to determine the role of microtubules in stress relaxation behavior, groups of cells were treated with either 20 μm nocodazole or 10 μM paclitaxel (both from Sigma) at 37 °C for 1 hour to induce microtubule depolymerization or hyperpolymerization, respectively. Both nocodazole and paclitaxel bind to β-tubulin; however, the former disrupts and the latter stabilizes microtubules. Concentrations of all cytoskeletal agents were chosen based on published research [143, 147, 203] or based on our own experience, as in the case of cytochalasin D, where we chose the maximum concentration that can be used without inducing cell detachment. Control groups for each

experiment consisted of cells treated only with the equivalent amount of vehicle (DMSO) for these cyoskeletal agent treatments.

Relaxation Data Analysis

Following data collection, all stress relaxation curves were shifted to give a baseline force value of 0 and were then normalized by their respective t=0.01 s force values to obtain a starting (maximum) force value of 1.0 for each relaxation curve. The 0.01 s time point was used for normalization due to the usage of logarithmic time spacing and the 100 Hz initial sampling rate. Following normalization, data were resampled using logarithmic spacing with 100 data points from the start to the finish of each test. The percentage of relaxation was calculated for each relaxation curve, with the parameter G(120), denoting G at t=120 s, representing 1 – % relaxation. Custom MATLAB scripts (MATLAB 7.0, The MathWorks, Inc., Natick, MA) were written to fit each curve using three different relaxation models: quasilinear viscoelastic (QLV) reduced relaxation function, Eq. (1); power-law, Eq. (2); and standard linear solid (SLS), Eq. (3). The reduced relaxation function, G(t), Eq. (1) contains 3 parameters, c, τ_1, and τ_2, with a continuous relaxation spectrum, $S(\tau) = c/\tau$, between τ_1 and τ_2, which are time constants governing short and long term relaxation behavior, respectively.

$$G(t) = \frac{1 + c\int_{\tau_1}^{\tau_2} \frac{e^{-t/\tau}}{\tau} d\tau}{1 + c\int_{\tau_1}^{\tau_2} \frac{1}{\tau} d\tau} \qquad (1)$$

The constant, c, is unitless, and represents a relative measure of viscous energy dissipation (damping).

The power law relaxation model used was of the form

$$At^{-\alpha} \quad (2)$$

where A and α are constants governing the rate of decay.

The relaxation behavior of a standard linear solid is defined by the equation:

$$G(t) = E_R\left[1-(1-\frac{\tau_\sigma}{\tau_\varepsilon})e^{-t/\tau_\varepsilon}\right] \quad (3)$$

where E_R is the reduced relaxation modulus, and τ_ε and τ_σ are the relaxation times for constant strain and constant stress, respectively [132].

Immunofluorescence

Immunofluorescence staining was used to visualize actin filaments and microtubules. Cells were fixed in 4% paraformaldedyde at room temperature for 30 minutes following cytoskeletal-agent treatments at the same time points as the cells for the corresponding AFM experiments. The cells were then incubated with blocking solution consisting of PBS (90%) (Sigma), bovine serum albumin (3.8%) (Sigma), donkey serum (3.0%) (Sigma), and Triton-X (0.2%) (Sigma) for 30 minutes. This was followed by incubation with either alexa fluor 488 conjugated phalloidin (Sigma) at room temperature for 15 minutes for actin staining or alpha- and beta-tubulin primary antibodies (Hybridoma Bank, U. of Iowa) at 4°C overnight for microtubule staining. The microtubule-stained cells were further incubated with a TRITC-conjugated secondary

antibody (Invitrogen, Inc., Carlsbad, CA) the following day for 2 hours and then with DAPI for 5 minutes (Invitrogen, Carlsbad, CA). All samples were viewed using an Olympus IX71 inverted microscope (Olympus, Tokyo, Japan); images were subsequently collected and processed using HCImage software (Hamamatsu Corp., Bridgewater, NJ).

Statistical Analyses

Coefficients of determination (R^2) were determined for each individual curve fit for all 3 models. Constants derived from each model are presented as a mean ± standard deviation. Values of G(120) and α for respective treatment and control groups were compared using Student's t-tests. The effect of indentation depth (strain dependence) was evaluated using a Repeated Measures one-way ANOVA (on ranks when normality tests failed), followed by Tukey tests for pairwise comparison. P-values < 0.05 were considered statistically significant for all tests.

Results

Vascular smooth muscle cells pretreated with cytochalasin D exhibited significantly ($p=0.033$) greater relaxation percentage, G(120) , and relaxation rate, α, ($p = 0.002$) than controls (Table 4.1). In contrast, similar stress relaxation was observed between jasplakinolide-treated cells and controls, G(120) and α ($p=0.931$ and 0.436, respectively) (Table 4.1). Paclitaxel-treated cells exhibited significantly lower relaxation percentage ($p=0.008$) and relaxation rate ($p=0.011$) compared to controls (Table 4.1). Nocodazole-treated cells exhibited nonsignificant decreases in relaxation percentage ($p=0.220$) and

relaxation rate ($p=0.091$) compared to controls (Table 4.1). Averaged relaxation curves for each cytoskeletal agent were plotted vs. respective control groups on a logarithmic time scale, Figure 4.3.

Table 4.1. G(120) values for each cell treatment and corresponding control group. (* Denotes $p < 0.05$).

	G(120)	α
Cytochalasin D (n=9)	0.11±0.12*	-0.29±0.06*
Control (n=5)	0.29±0.09	-0.16±0.06
Jasplakinolide (n=12)	0.41±0.09	-0.09±0.02
Control (n=12)	0.41±0.08	-0.09±0.02
Paclitaxel (n=12)	0.44±0.08*	-0.08±0.02*
Control (n=12)	0.32±0.11	-0.11±0.03
Nocodazole (n=23)	0.44±0.13	-0.09±0.03
Control (n=15)	0.38±0.14	-0.11±0.03

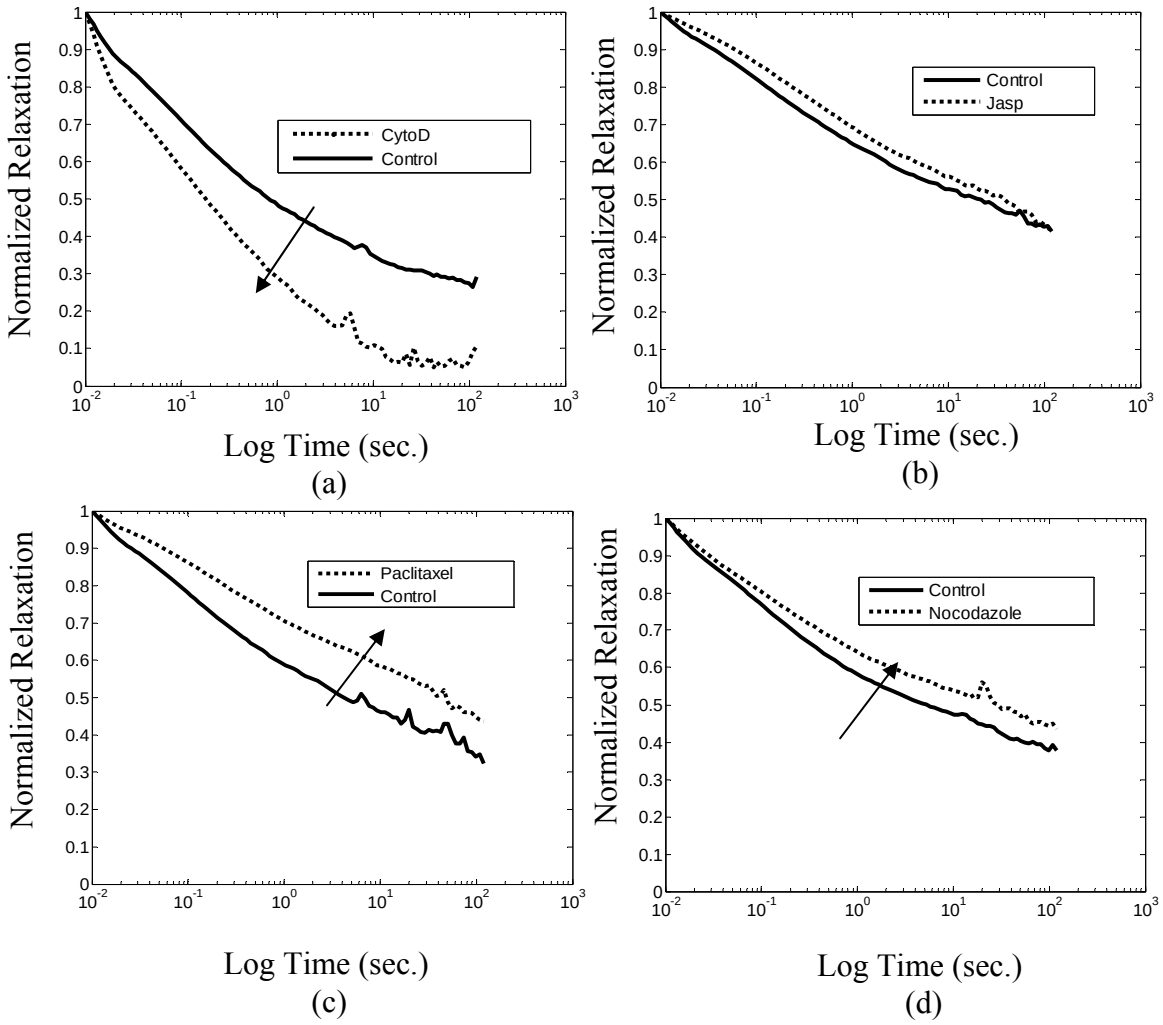

Figure 4.3. Averaged normalized VSMC relaxation curves plotted vs. logarithmic time from (a) Cytochalasin D, (b) Jasplakinolide, (c) Paclitaxel, (d) Nocodazole. Arrows indicate the direction that curves of treated cells are shifted relative to controls. Due to the usage of logarithmic spacing and the 100 Hz initial sampling rate, the initial time point of each curve is 0.01 seconds.

The power-law exponent, α, and the normalized percentage of relaxation at the conclusion of each test , G(120), were used as statistical measures of strain dependence to examine the validity of the reduced relaxation function under current study conditions. Mean power-law exponents were similar for 0.5, 1.0 and 1.5 μm indentations (p=0.499)

(Table 4.2). Repeated measures ANOVA indicated that the mean G(120) values also did not statistically vary with strain level (p=0.062) (Table 4.2). Consecutive relaxation tests at 1 um depth revealed no statistically significant changes with each successive trial (data not shown).

Table 4.2. Mean G(120) and power-law exponent (α) vs. indentation depth for untreated VSMCs. (n=24 cells ± SD).

Indentation Depth (μm)	G(120)	α
0.5	0.39 ± 0.14	-0.10 ± 0.03
1	0.42 ± 0.11	-0.10 ± 0.03
1.5	0.44 ± 0.12	-0.10 ± 0.03

The effects of the cytoskeletal agents used in this study are also reflected in the constants derived from the QLV reduced relaxation function. In general, increased relaxation percentage and rate were observed to correspond to greater C values, lower τ_2, and greater α values, while the short-term time constant, τ_1, appeared to be unaffected (Table 4.3). Due to the relatively poor fit of the SLS model, these parameters were not included in any further analysis.

Table 4.3. QLV parameters from VSMCs treated with cytoskeletal agents and respective controls. C is a unitless measure of damping; τ_1 and τ_2, short and long-term QLV time constants, respectively, serve as the bounds for the continuous spectrum of relaxation.

	C	τ1 (s)	τ2 (s)
Cytochalasin D (n=9)	3.4±3.7	0.06±0.02	76±130
Control (n=5)	0.34±0.17	0.07±0.02	96±50
Jasplakinolide (n=12)	0.17 ± 0.06	0.09 ± 0.04	240 ± 310
Control (n=12)	0.15 ± 0.03	0.08 ± 0.05	270 ± 290
Paclitaxel (n=12)	0.16±0.06	0.09±0.04	400±310
Control (n=12)	0.23±0.17	0.08±0.02	190±200
Nocodazole (n=23)	0.14±0.06	0.08±0.03	230±250
Control (n=15)	0.20±0.08	0.08±0.04	320±320

Relaxation curves were fit very well by both the QLV reduced relaxation function, (R^2 = 0.98 +/- 0.02, n=120), Figure 4.4(a), and the power-law relaxation model, (R^2 = 0.98 +/- 0.03, n=125), Figure 4.4(b). The standard linear solid model, however, provided a less adequate fit, (R^2 = 0.91 +/- 0.03, n=117), Figure 4.4(c).

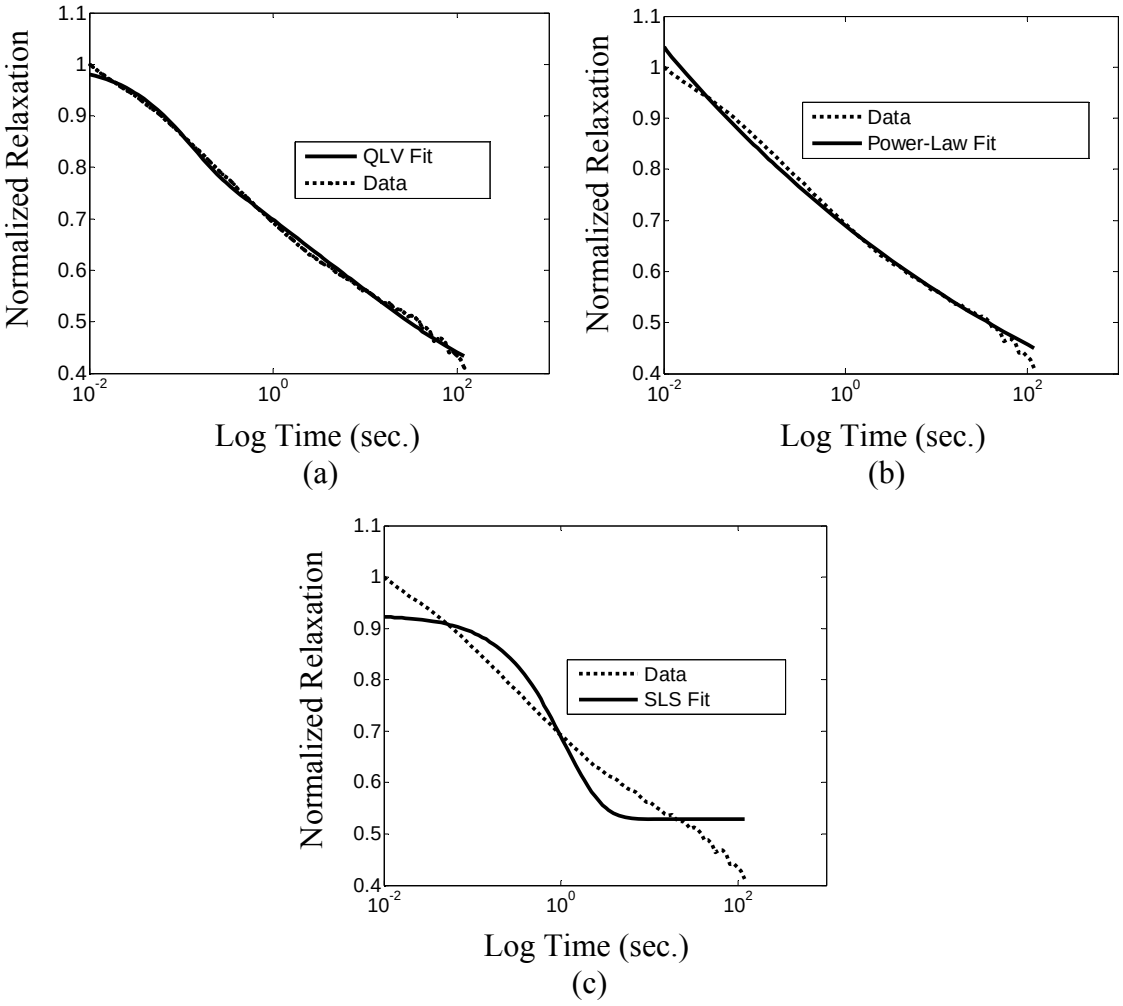

Figure 4.4. Representative examples of normalized VSMC relaxation curves plotted vs. logarithmic time with curve fits of (a) QLV reduced relaxation, (b) power-law, and (c) SLS models. Due to the usage of logarithmic spacing and the 100 Hz initial sampling rate, the initial time point of each curve is 0.01 seconds.

Untreated VSMCs exhibited normal actin (Figure 4.5(a)) and microtubule structure (Figure 4.5(b)). Immunofluorescence imaging of actin (Figure 4.5(c)) and microtubules (Figure 4.5(d)) in cytochalasin D-treated VSMCs revealed significant disruption of actin stress fibers and no identifiable changes to microtubule structure. Nocodazole-treated

VSMCs showed significant microtubule disruption (Figure 4.5(f)) without any changes to actin structure (Figure 4.5(e)). No consistent visual differences were observed with actin or microtubule structure in paclitaxel-treated VSMCs (Figure 4.5(g) and 4.5(h)), although some cells did appear to exhibit denser microtubule content with less free tubulin. No visual differences were observed in actin or microtubules (Figure 4.5(i) and 4.5(j)) of jasplakinolide-treated VSMCs.

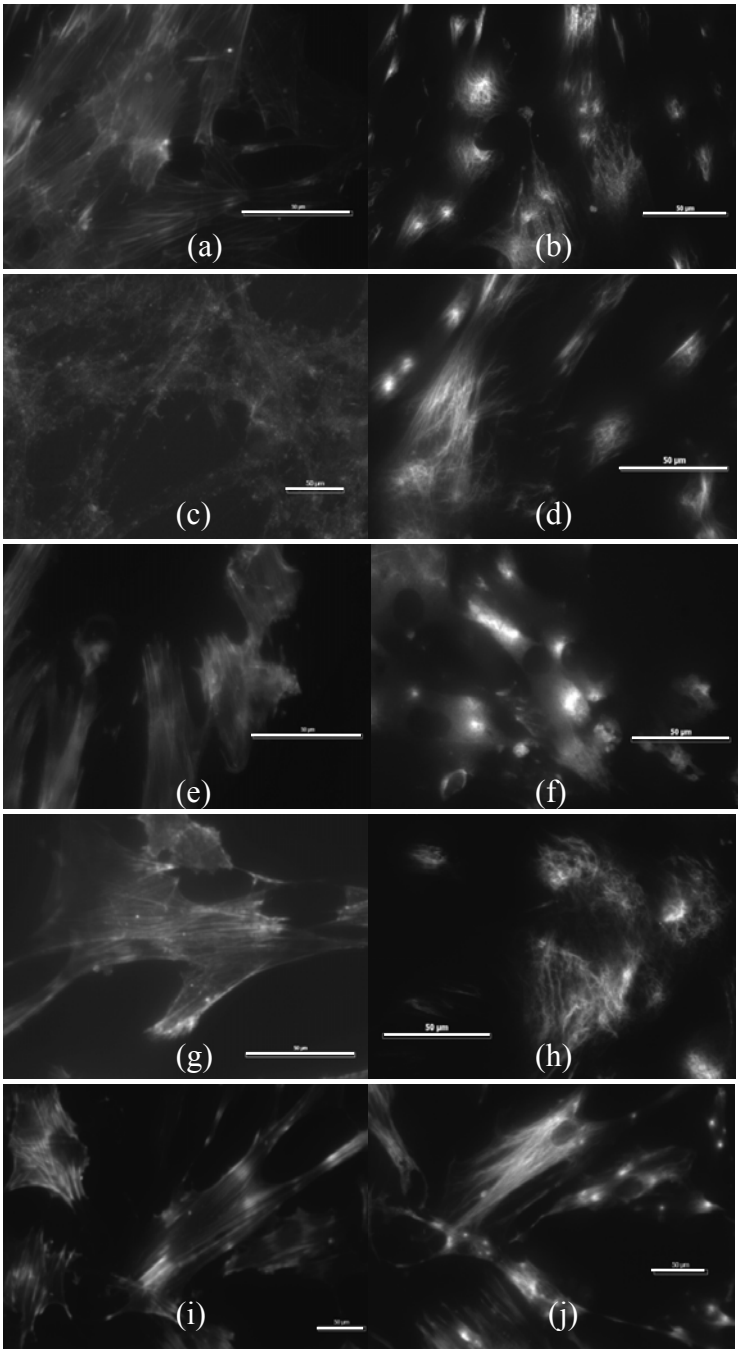

Figure 4.5. Immunofluorescence images of untreated VSMC (a) actin and (b) microtubules; cytochalasin D-treated VSMC (c) actin and (d) microtubules; nocodazole-treated VSMC (e) actin and (f) microtubules; paclitaxel-treated VSMC (g) actin and (h) microtubules; jasplakinolide-treated VSMC (i) actin and (j) microtubules. Scalebars represent 50 μm.

Discussion

Mechanotransduction, the process by which mechanical stimuli are converted into physiological responses, is important in regulating a wide array of biological processes. Major human diseases, including atherosclerosis [197], cancer [198], and arthritis [199], are affected by mechanobiological phenomena. At the cellular level, mechanical stimuli and resultant deformations are converted into physiological responses that affect growth, migration, differentiation, and protein processing. Detailed knowledge of the role cytoskeletal components play in governing cellular mechanics is necessary for comprehensive understanding of mechanotransduction in disease development. Acquiring this knowledge requires development of techniques to better quantify cellular viscoelastic behavior using commercially available equipment and identification of simple yet accurate models for the description of the resultant data. In this study, the effects of four cytoskeletal agents on the viscoelastic properties of VSMCs were evaluated. Subsequently, three distinct viscoelastic models were applied to the collected AFM stress relaxation data, and the strengths and weaknesses of each were evaluated.

Data from this study provided evidence that actin disruption with cytochalasin D greatly altered the viscoelastic behavior of cultured vascular smooth muscle cells. In agreement with previous cellular viscoelastic research [187], actin disruption increased damping behavior and decreased viscosity. With the actin cytoskeleton largely disassembled, the more fluid-like cytoplasm dominates viscoelastic behavior, so the observed increases in relaxation and damping are unsurprising. In contrast to cytochalasin D, 0.1 μM jasplakinolide had no significant effects on relaxation behavior. Jasplakinolide has been shown to have little effect on the relaxation

behavior of protoplasts at 10 μM [204]; in another study, however, it increased storage and loss moduli of airway smooth muscle cells as measured via magnetic twisting cytometry at 0.07 μM [205]. In the current study, pretreatment with 1 μM concentrations of jasplakinolide resulted in cell death and detachment from the cover slip within approximately 30 minutes. It has been suggested that stabilizing actin (and thereby inhibiting the dynamic nature of actin filaments) disturbs the actin cytoskeleton in a manner similar to that observed in actin depolymerization [206] with cytochalasin D. This effect may be what was observed when the VSMCs treated with 1μM jasplakinolide detached from the substrate. Given the complex effects of jasplakinolide that were seen when it was used under other conditions [203, 207] and the lack of reported use due to its relatively recent discovery, differences in the reported data are not surprising. The variety of results among studies pertaining to effects of jasplakinolide on cellular viscoelasticity may warrant further investigation.

The role of microtubules in cellular mechanical behavior is more controversial than that of actin and can depend greatly on factors such as the degree of cell spreading [113]. For example, previous studies have demonstrated an increase in cellular stiffness from microtubule disruption [123, 208], while others have found the opposite effect [209]. In the present study, microtubule disruption via nocodazole resulted in statistically nonsignificant decreases in the percentage and rate of relaxation. A possible explanation for these observations is that microtubule disrupting agents, including nocodazole, have been found to induce the formation of actin stress fibers via a Rho signaling mechanism [210]. In the present study, evidence of increased actin stress fiber content was not observed from immunofluorescence images (Fig. 6), and further analysis of gene expression or actin protein content was not conducted. An alternative explanation for the

effects of nocodazole observed here is that microtubule disruption resulted in a decrease in the level of prestress balanced by the microtubules [113]. Although elastic shear modulus (normally associated with prestress) is a parameter that is distinct from the stress relaxation data obtained in the current study, a comparison between the two might provide a framework for understanding the effects of cytoskeletal treatments on stress relaxation behavior. This is because cellular prestress has been found to positively correlate with both storage and loss moduli [211]. The precise physical mechanisms behind this correlation are not yet known.

Given that microtubule disruption with nocodazole resulted in decreased relaxation rate and percentage in the current study, it would seem counterintuitive that microtubule stabilization with paclitaxel resulted in statistically significant decreases in both parameters. However, previous researchers have also observed increased viscosity as a result of paclitaxel treatment in cardiomyocytes [212, 213], endothelial cells [209], and isolated sections of cardiac muscle [214]. In addition to stabilizing microtubules, paclitaxel has been found to decrease microtubule flexural rigidity [215, 216], induce microtubule bundling [217], cause internal protofilament sliding [218], and increase microtubule relaxation time [216]. Each of these secondary effects resulting from paclitaxel treatment could conceivably affect whole-cell viscoelastic properties. Although the exact mechanisms involved in these changes are not well understood, the viscoelastic effects observed in the current and in past studies may be due to one or a combination of several factors: internal microtubule friction (i.e., viscous sliding of protofilaments); frictional interactions among microtubule bundles; frictional interactions

between microtubules and cytoplasmic constituents; and intrinsically altered relaxation behavior of the microtubule filaments. In the context of the mechanical-testing protocol used in the current study, a proposed hypothetical scenario could involve rapid displacement of flexible paclitaxel-stabilized microtubules and cytoplasm caused by the high-velocity impact of the AFM probe. The high-viscosity flow of microtubules caused by these displacements could cause friction that could then lead to decreased rate of relaxation and relaxation percentage. Therefore, the apparently similar viscoelastic effects of nocodazole and paclitaxel on VSMCs may be the result of two distinct phenomena. The findings related to paclitaxel reported here are particularly interesting from a clinical perspective because paclitaxel is used in some drug-eluting stents to prevent VSMC hyperplasia.

The theory of quasilinear viscoelasticity (QLV) was originally developed by Fung to model the viscoelastic behavior of biological tissues [132]. The QLV model contains the reduced relaxation function, G(t), describing stress relaxation behavior. Although numerous studies have dealt with the successful application of the QLV model to whole tissues, including blood vessels [219], heart valves [220], and ligaments [221], the model has yet to be applied to isolated cells. For the QLV reduced relaxation function to be valid for the cells used in the current study, strain independence had to be demonstrated; i.e., relaxation should be a function of time only. To test this relationship between strain and relaxation, we compared both the rate of relaxation, α, and the total percentage of relaxation, G(120), at varying strains. Both rate of relaxation and total percentage of relaxation were found to be independent of initial strain, a finding that could be viewed as

supportive of the validity of the reduced relaxation function under the conditions of the current study [222]. The reduced relaxation function exhibited an excellent fit (R^2 = 0.98) for AFM stress relaxation data of VSMCs. When applied to cellular viscoelastic research, the reduced relaxation function provides the ability to compare data to previous studies on whole tissues. Tanaka and Fung found C parameter values an order of magnitude lower for circumferential and longitudinal mechanical testing of intact aortas [219]. Cytochalasin D-treated VSMCs were the lone exception to this trend: Their significantly increased damping behavior was reflected in C values two orders of magnitude greater than those of intact aortas. Short-term time constants (τ_1) in the current study did not vary significantly with the various cytoskeletal treatments. However, they were found to be on the same order as those of the abdominal aorta and lower than those of the thoracic aorta [219]. A possible explanation for this finding could be the higher collagen and elastin content of the thoracic aorta compared to the abdominal aorta [223], which result in larger contributions of those ECM components to viscoelastic behavior. The long-term time constant (τ_2) values in the current study were of the same order as intact aortas [219], although standard deviations were exceptionally large, and many values were greater than the 120-second duration of the stress relaxation tests. However, long-term QLV time constants vary widely in the literature and within given test protocols [224]. Future AFM stress relaxation studies utilizing the QLV reduced relaxation function could perhaps specify longer relaxation protocols; these would more accurately capture long-term relaxation behavior. The viscoelastic differences between whole aortas and isolated VSMCs are unsurprising since the

comparatively stiffer and less viscous ECM plays a large role in governing mechanical behavior of whole tissues.

The attention that power-law behavior of cells has lately received is in part due to recent experiments examining the behavior of cells under cyclic loading conditions [225]. Creep behavior of cells has also been modeled using a power-law function, $J(t) = At^{\alpha}$ [226]. In the present study, stress relaxation data of VSMCs were fit very well (R^2 = 0.98) using the power-law model. It has been suggested that power-law behavior is an intrinsic cellular feature that is independent of measuring technique [226]. This issue, to which the current data may be relevant, warrants continued investigation. Power-law fitting comple**m**ents the QLV model, as it can be used to validate or invalidate use of the latter, as it was in this study. A simple power-law stress relaxation fit provides a numerical gauge of the rate of decay, but no other information is provided, i.e. there are no time constants, etc**.** Nonetheless, the data reported here add to a growing body of literature pertaining to power-law behavior of cells mainly from dynamic mechanical analyses, but also from creep measurement [226, 227], and now AFM stress relaxation. Future AFM stress relaxation studies may employ the power-law equation used herein or perhaps variations thereof.

The SLS model has previously been applied to cells [228] and tissues [229]. Previous indentation tests and analyses of the intimal vessel wall of healthy human arteries using an AFM-based technique and the SLS model [229] found SLS parameters τ_ε & τ_σ with values of 16.9 and 29.3, respectively. These SLS parameters are an order of magnitude greater than typical SLS parameter values measured in the current study for untreated

attached VSMCs, though the SLS model fit was unsatisfactory for VSMCs. Additional elements (springs and dashpots) could possibly be added to the SLS model to improve the fit; however this would require extra fitting parameters and more complex analyses. Extracellular matrix contributions to whole tissue mechanics possibly explain the differences in SLS parameters between whole tissues and the current VSMCs. In summary, although the SLS model has been used to successfully for tissue relaxation data in the past, it did not provide an adequate fit to the current VSMC data.

Conclusions

To our knowledge, the data presented herein are the first describing the role of actin and microtubules in governing stress relaxation behavior of adherent VSMCs. This information adds to previous work pertaining to the role of cytoskeletal components in governing the viscoelastic behavior of cells under dynamic conditions [123, 187]. While it is generally agreed that actin stress fibers play the primary role in governing cellular viscoelastic properties, these data indicate the relevance of the contributions of microtubules. This relevance underscores a major limitation of relying solely upon elastic modulus measurements to describe the mechanical properties of viscoelastic materials such as cells.

In the current study, the QLV reduced relaxation function was applied to isolated cells rather than to whole tissues. Validity of the QLV reduced relaxation function under the current conditions was checked by testing the strain dependence of both rate and percentage of relaxation [222]. It must be recognized that applicability here does not indicate that the QLV reduced relaxation function will be universally valid for cell mechanics studies. For AFM stress relaxation studies, the use of the QLV reduced relaxation function in combination with a power-law model may serve as a simple method of describing the viscoelastic behavior of cells under various treatment conditions. The reduced relaxation function will permit comparisons to data from whole tissue. With the power-law model, comparisons of AFM stress relaxation data with power-law data collected using other techniques will be possible. As previous studies

have suggested, when modeling whole tissues, it may be desirable to model the viscoelastic contributions of the cellular and ECM components separately [230]. Thus, data from the current study may aid future AFM-based analyses of arterial mechanics.

CHAPTER FIVE

FRICTIONAL PROPERTY MEASUREMENT OF INDIVIDUAL VASCULAR SMOOTH MUSCLE CELLS

Abstract: With the advancement of the field of biotribology, considerable interest has arisen in the study of cell and tissue frictional properties. From the perspective of medical device development, the frictional properties between a rigid surface and underlying cells and tissues is of a particular clinical interest. As with many bearing surfaces, it is likely that contact asperities exist at the size scale of single cells and below. Thus, a technique to measure cellular frictional properties would be beneficial from both a clinical and a basic science perspective. In the current study, an atomic force microscope with a 5 μm diameter borosilicate spherical probe was used to measure the surface frictional properties of vascular smooth muscle cells (VSMCs). Various treatments were used to alter cell structure, in order to better understand the cellular components and mechanisms responsible for governing frictional properties. It was found that untreated VSMCs had a frictional coefficient of approximately 0.06. The friction coefficient has been shown to be greatly affected by cellular rigidity.

Introduction

While significant steps have been made towards understanding the bulk mechanical properties of living cells, comparatively little is known about their surface frictional properties. The study of cellular frictional properties is of interest for a variety of reasons. For example, numerous physiological processes including blood flow [156] , articulating cartilaginous tissues [157], respiration [231], cell adhesion [232], and cell migration [158], are all affected in some manner by cellular and tissue frictional properties. In regards to endovascular surgical procedures, increased knowledge of cellular frictional properties could also be of a significant clinical value. The deployment of endovascular devices results in the exertion of mechanical shear forces on underlying vascular endothelial and vascular smooth muscle cells (VSMCs) [160]. In cases of complex or tortuous vascular lesions, a reduction of friction has been shown to ease delivery of endovascular devices [161]. The process of stent placement typically results in endothelial denudation [233]. As a result, stent struts are in direct contact with underlying VSMCs. More accurate computer modeling of *in vivo* stent behavior could be accomplished if the frictional properties of vascular cells were elucidated [160, 162]. Similarly, finite element models of atomic force microscope (AFM) cell mechanics experiments have thus far relied on assumptions of frictional conditions, due to a lack of experimental data [163, 164].

Numerous cellular constituents may play a role in governing frictional properties. The glycocalyx, an extracellular matrix of proteglycans and glycoproteins is believed to play a role in the lubrication of red blood cells [156] and endothelial cells [234].

Additionally, the glycocalyx is involved in mechanical signal transduction in both endothelial cells and VSMCs [165]. In the case of VSMCs, the glycocalyx is composed primarily of chondroitin sulphate and heparan sulphate [235]. Located beneath the glycocalyx, the cell membrane is composed of a lipid bilayer containing a wide array of transmembrane proteins. Lipid bilayers alone have complex frictional and viscous properties [236], and in the case of intact living cells, these properties are likely made even more complex by the presence of transmembrane molecules and surface charge distribution. Finite element research on the frictional properties of soft biological tissues has shown a positive correlation between the friction coefficient and the modulus of elasticity [231]. It is quite possible that this same relationship would exist for individual cells, in which case the cytoskeleton, the main determinant of cellular elastic modulus, would also play a significant role in governing cellular frictional properties. In many cell types, actin and microtubules are the cytoskeletal components primarily responsible for determining cellular mechanical properties [237]. All of these cellular constituents (glycocalyx, cell membrane, cytoskeleton) are of course physically linked with one another, making it rather difficult to fully separate the effects of each on whole-cell frictional properties.

The atomic force microscope (AFM) is a useful tool for the measurement of frictional forces at the nano- and micro- scales [141], a technique often referred to as lateral force microscopy. Numerous studies have examined frictional properties on a range of materials, including various polymers, films, and lipid bilayers [141]. Currently however, very little data exist relating to the frictional properties of living cells or tissues

at the micro-scale. However, recent studies have examined macro-scale frictional properties of vascular endothelial cells [160] and corneal epithelial cells [238, 239]. The AFM technique described herein is capable of providing microscale frictional data to complement the available macroscale data. A significant advantage of AFM-based cellular friction measurements is the use of considerably lower normal loading forces as compared to macro-scale, reducing the chances of any cell damage occurring during the experimental procedure.

The main goal of the current study was the development of an AFM-based technique for micro-scale measurement of individual cell surface frictional properties, as well as elucidation of the cellular physical constituents responsible for governing frictional behavior. Vascular smooth muscle cells were chosen for this research due to the clinical relevance of their frictional properties with respect to endovascular surgical procedures.

Materials and Methods

Cell Culture

Rat aortic VSMCs were isolated from adult male Sprague-Dawley rats and cultured in Dulbecco's Modified Eagle's Medium (DMEM) (Mediatech, Herndon, VA) with fetal bovine serum (FBS) (10 %) (Sigma, St. Louis, MO) and antibiotic/antimycotic solution (1 %) (Sigma). Cells were maintained in T-75 polystyrene flasks in an incubator at 37 ºC, with 5% CO_2, and fresh media was exchanged every 48 hours. Cells were allowed to grow to ~80% confluency in the flasks, then trypsinized with 0.25% trypsin (Mediatech) / 0.02% EDTA (Sigma) and seeded onto 22 x 22 mm glass coverslips (VWR, West Chester, PA) at a density of 150,000 cells per coverslip Seeded coverslips were incubated in 6-well plates with DMEM (10% FBS) at 37 ºC with 5% CO_2, and media was exchanged every 48 hours prior to AFM experimentation. Cells were utilized between passages 5 and 8.

AFM Friction Experiments

Atomic force microscopy (AFM) experiments were performed once cells had formed a confluent monolayer on coverslips, typically between 5 to 6 days. For all AFM experiments, a Veeco Dimension 3000 AFM with a Nanoscope IV controller (Veeco Metrology, Santa Barbara, CA) was operated in contact scanning mode. A borosilicate spherical-tipped AFM probe (5 μm diameter) (NovaScan, Ames, IA) on a silicon-nitride cantilever with a nominal spring constant of 0.12 N/m, was used throughout the study. A 5 μm AFM probe was chosen, in part, due to its proximity in size to that of asperities

previously observed on the surface of endovascular stents in our laboratory, Fig 1. During AFM experiments, cells were kept on the coverslips in their culture media (DMEM w/ 10% FBS), which was exchanged approximately every 30 minutes with warm 37 ºC media throughout the course of the AFM experiments, each lasting for approximately 1 hr in total.

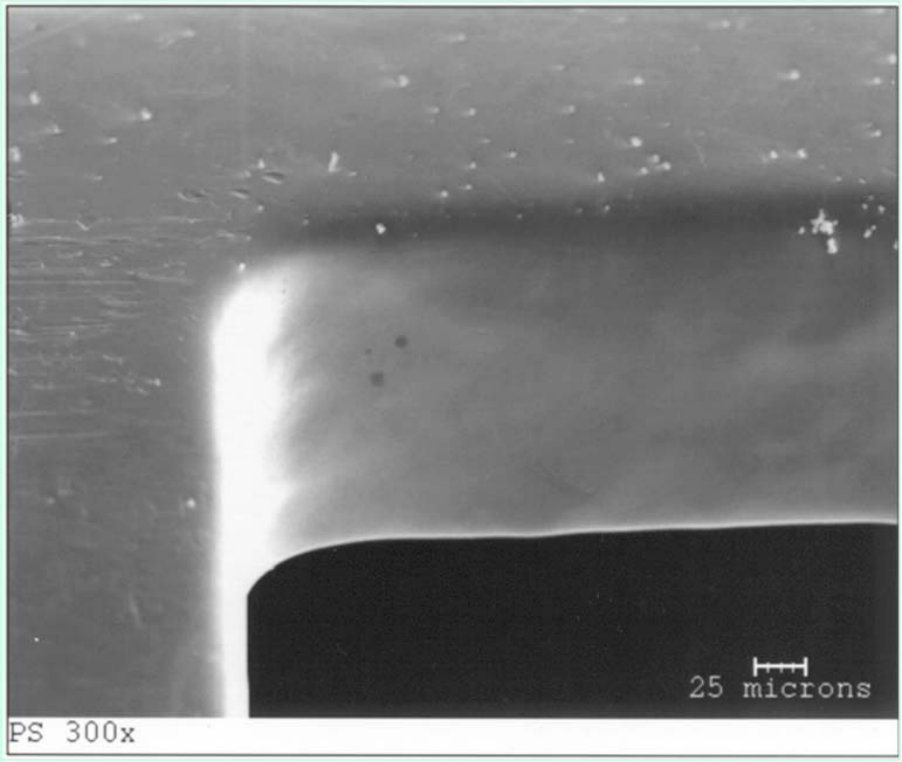

Figure 5.1. Scanning electron micrograph of a stainless steel stent, illustrating size and prevalence of surface asperities.

Cells received one of the following treatments prior to AFM friction experiments; fixation with 3% glutaraldehyde overnight at room temperature, incubation with 0.2 U/ml

of chondroitinase ABC and 0.2 U/ml heparinase III (Sigma, St. Louis, MO) for 30 min. at 37 °C, incubation with 5μM cytochalasin D (Sigma) for 30 min. at 37 °C. Each of these agents was chosen due to their known effects on cellular structure. Glutaraldehyde is a commonly used fixative for cells and tissues that induces significant crosslinking. Cytochalasin D is an agent known to disrupt the actin network of living cells. Chondroitinase ABC and heparinase III are responsible for the enzymatic degradation of the glycocalyx constituents chondroitin sulphate and heparan sulphate, respectively. Untreated VSMCs were used as controls.

Following the identification of a target cell, the AFM probe was positioned over the central region of the cell body. Elongated cells were chosen for friction testing, with the AFM probe reciprocating along the major axis of each test cell as in Figure 5.2, thus preventing the probe from coming into contact with adjacent cells or substrate. Friction measurements were performed at a 90° scan angle with a scan size (reciprocating cutoff length) of 10 μm.

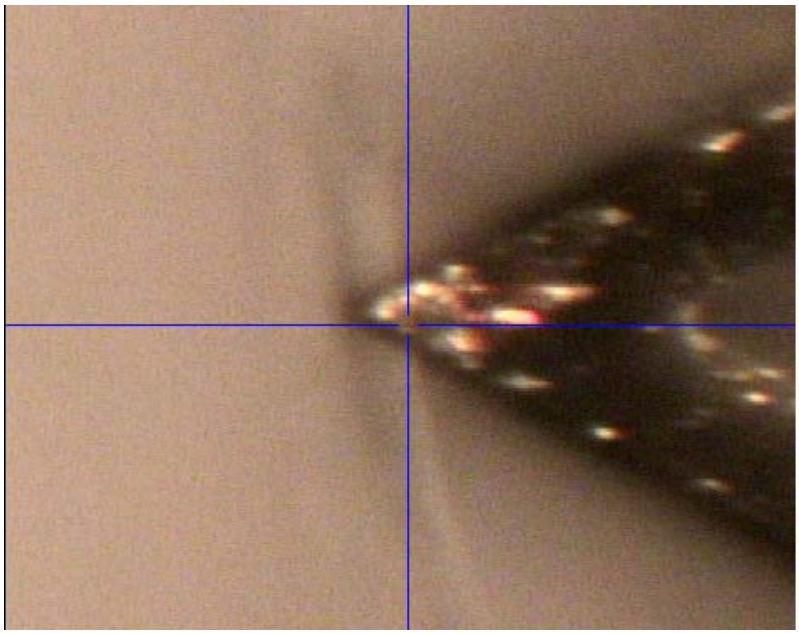

Figure 5.2. Screen capture of AFM probe positioned over an elongated VSMC, with reciprocation along the major axis of the cell.

Most measurements were performed at tip velocity of 20 μm/s, however for some experiments a velocity of 2 μm/s was used in order to evaluate velocity-dependence. Normal forces were incrementally increased by adjusting the deflection setpoint from -2 to +8 volts, or approximately 0 to 100 nN, in 0.25 to 0.5 volt increments. For each deflection setpoint on a given cell, 16 lines of trace and retrace frictional data were recorded, with 512 data points recorded per line (Figure 5.3).

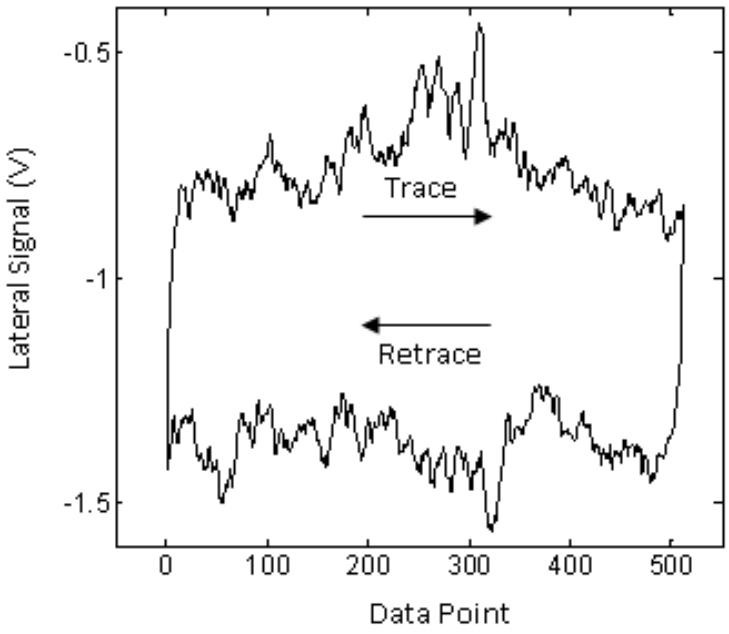

Figure 5.3. Representative raw trace and retrace curves from a VSMC. 512 data points were collected on each line. Recording trace and retrace data allows one to distinguish frictional from topographical effects on the lateral signal.

The maximum normal force exerted on each cell was in the range of 100 nN, with the exact value dependent upon deflection sensitivity and cantilever spring constant. At the start and finish of each experiment, frictional force data were also collected on a clean glass coverslip in media. The resulting friction coefficients could then be compared to existing data on the coefficient of friction between 2 glass surfaces under lubricated conditions, revealing whether the values determined for cells were reasonably accurate.

The lateral sensitivity of the cantilever was determined using the previously published "modified wedge method" for calibration of micro-sized tips [240, 241].

Briefly, the probe was used to collect frictional force data on a flat mica surface, as well as a mica surface positioned at a known angle of incline. The resulting voltage vs. normal force plots are used to determine the lateral sensitivity, α, of the cantilever. This lateral sensitivity value is then used to convert all lateral deflection signals (V) into lateral force values (nN). Cell surface frictional coefficients (μ) were then calculated based on the equation:

$$F_L = \mu \times F_N,$$

where F_L is the lateral force acting on the AFM probe, and F_N is the normal force. The normal force applied at each deflection setpoint was determined by the product of the deflection setpoint (V), deflection sensitivity (nm/V), and cantilever spring constant (N/m). For untreated and glutaraldehyde-treated VSMCs, a Stribeck curve was plotted using data from 5 separate cells, with an approximation of the Sommerfeld number calculated as:

$$(\eta \times v)/F_N,$$

where η is the dynamic viscosity of DMEM (0.00078 Pa·s)[242], v is probe velocity (20 μm/s), and F_N is normal force (N),.

Data Analysis

Following each experiment, data were processed using custom MATLAB (The Mathworks,Inc., Natick, MA) scripts. Excessive noise was filtered from the data by eliminating all data points greater than 2 standard deviations away from the mean lateral signal value at a given normal force. The net lateral signal from each pair of trace and retrace lines is calculated as half of the difference between the two of them. Laser drift

that occurred during frictional measurements was accounted for by recording the lateral voltage on the photodiode at the start and finish of each cell, and correcting using a linear algebraic function. Mean lateral forces and standard deviations were plotted vs. normal forces, from which a linear fit was used to determine the slope of each line, i.e., the coefficient of friction, μ.

Statistical Analysis

Coefficients of friction between groups were compared using one-way analysis of variance (ANOVA) tests with subsequent pairwise comparison using Students t-tests. All tests were performed with an alpha of 0.05, and p-values less than 0.05 were considered statistically significant.

Results

For the AFM cantilever used in these experiments, the lateral sensitivity, α, was found to be approximately 68 nN/V, based on two separate calibration measurements. In total, 16 data points were collected at each given normal force, for each individual cell, Figure 5.4.

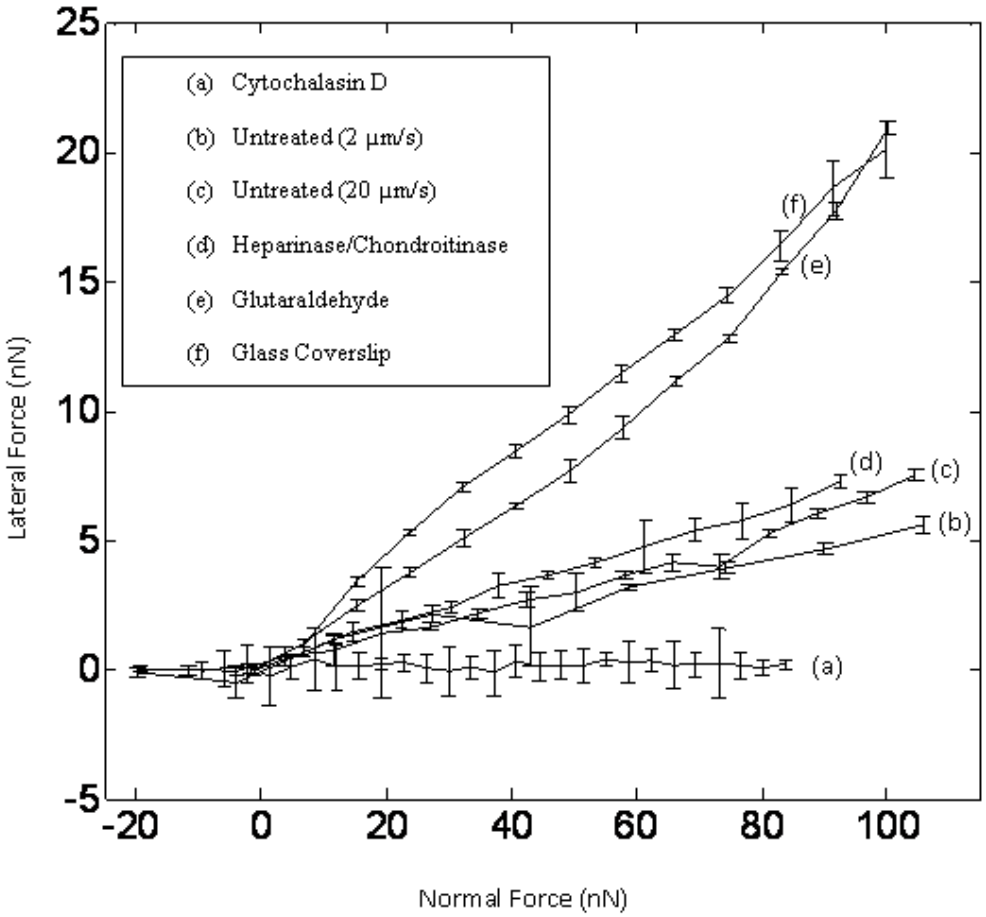

Figure 5.4. Representative frictional data (lateral force vs. normal force) from each VSMC group in the current study. Each curve corresponds to an individual cell chosen as a representative example due to its proximity to its respective VSMC group mean frictional coefficient. Each data point within a curve represents the mean ± SD for a particular normal force.

One-way ANOVA comparison of friction coefficients indicated a statistically significant difference between groups, $p<0.001$. Subsequent pairwise comparisons indicated significantly greater friction coefficients for glutaraldehyde treated VSMCs ($\mu=0.21 \pm 0.04$) vs. controls ($\mu=0.06 \pm 0.02$), $p = 7.8 \times 10^{-6}$, and significantly lower friction coefficients for cytochalasin D treated VSMCs ($\mu = 0.01 \pm 0.01$) vs. controls, $p = 3.4 \times 10^{-6}$. No significant difference was found between chondroitinase/heparinase treated VSMCs ($\mu = 0.06 \pm 0.01$) and controls ($p = 0.41$). There was no significant difference between untreated VSMCs measured at 20 or 2 μm/s ($\mu = 0.05 \pm 0.001$), $p = 0.17$. The mean coefficient of friction on glass coverslips in media was 0.18 ± 0.09, which is in the range of the coefficient of friction for glass on glass under lubricated conditions (0.1 to 0.6) [243]. Measured coefficient of friction values for all VSMC groups are compared in Figure 5.5.

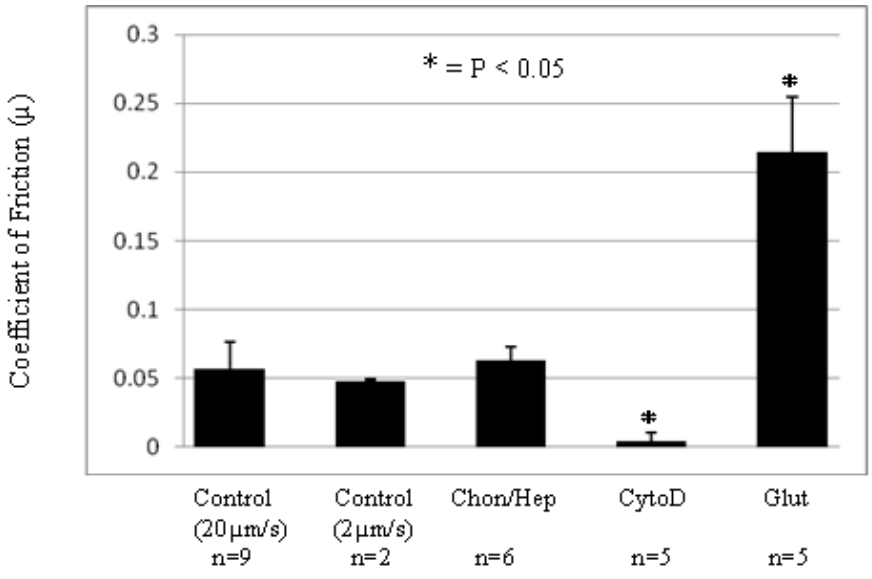

Figure 5.5. VSMC coefficients of friction. Data are presented as mean ± SD.

A linear fit to data in the approximated Stribeck curve for untreated VSMCs, revealed a positive slope with increasing $(\eta \times v)/F_N$ ratio, Figure 5.6.

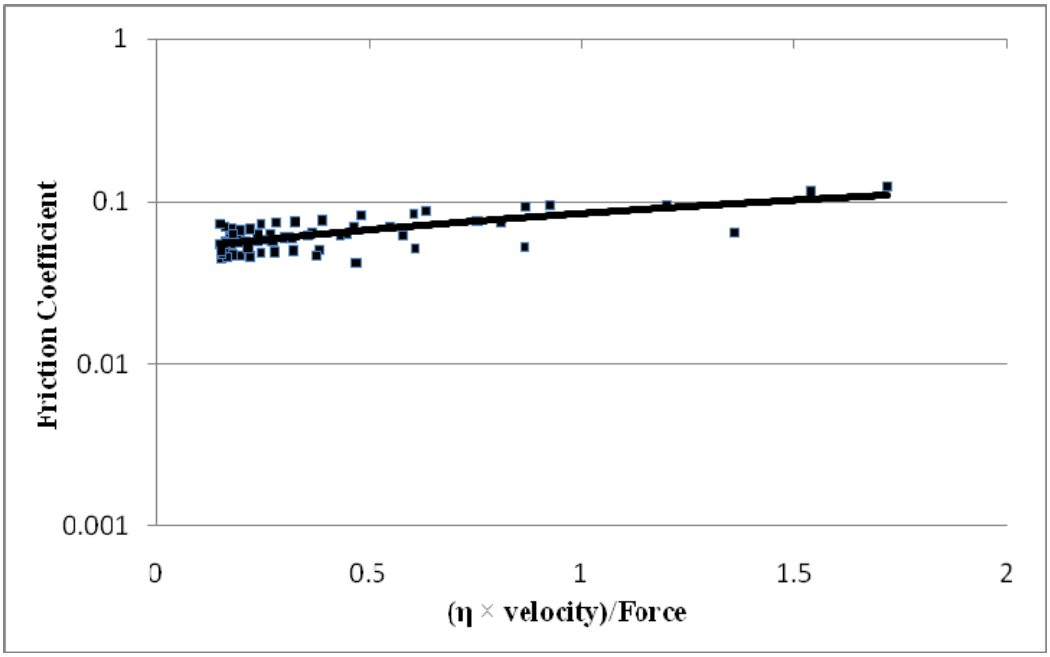

Figure 5.6. Coefficient of friction for untreated VSMCs plotted versus an approximated Sommerfeld number. The data points are from 5 separate VSMCs, and were fit with a linear trendline, $R^2 = 0.539$.

In contrast, the approximated Stribeck curve for glutaraldehyde-treated VSMCs revealed a relatively flat relationship between friction coefficient and $(\eta \times v)/F_N$, Figure 5.7.

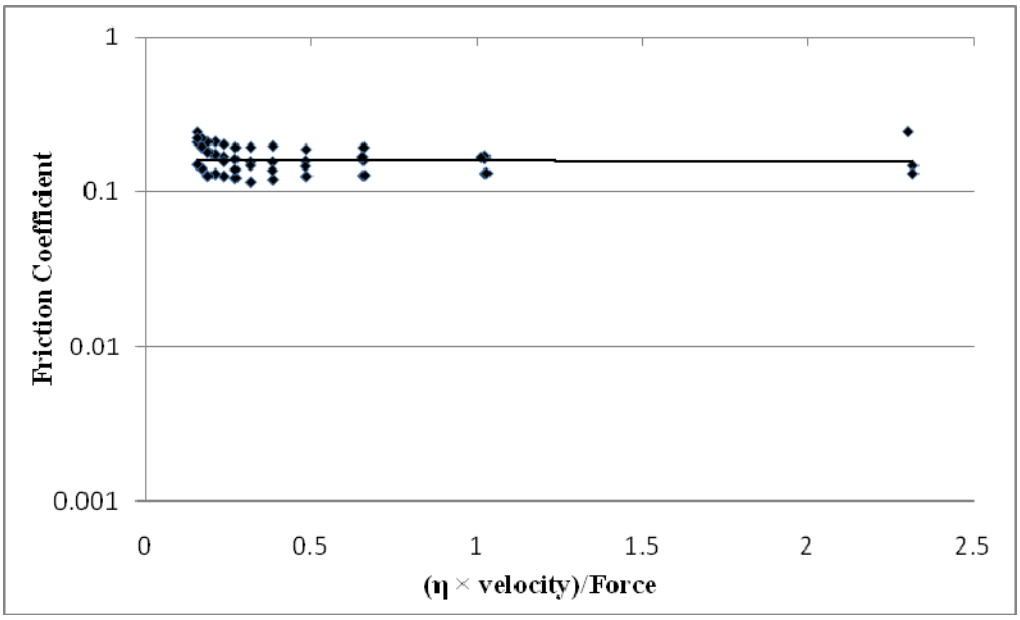

Figure 5.7. Coefficient of friction for glutaraldehyde-treated VSMCs plotted versus an approximated Sommerfeld number. The data points are from 5 separate VSMCs, and were fit with an exponential trendline, $R^2 = 0.0002$.

Discussion

The principal goal of the current study was to investigate the development of an AFM-based method for measurement of cell surface frictional properties on the micro-scale, with a specific interest in vascular smooth muscle cells. Secondly, an attempt was made to elucidate which cellular structural components are responsible for governing frictional behavior. To the best of the authors' knowledge, the current data represent the first reporting of cellular surface frictional coefficients obtained via AFM. The mean coefficient of friction for untreated VSMCs found in the current study (0.06 ± 0.02) is similar to macroscale values previously reported for endothelial cells ($\mu = 0.03–0.06$) [160] and corneal epithelial cells ($\mu = 0.05 \pm 0.02$) [239]. It should be noted that not only were these previous cellular friction studies conducted on different cell types on the macroscale, but probe speed, diameter, and velocity were all substantially different than the current study. Each of these studies was carried out in media with 10% serum, meaning there was undoubtedly significant protein adhesion to the probe. Such protein adhesion however, is precisely what one would expect from almost any implant material once it comes in contact with blood. Protein adsorption has been found to increase friction on polymer surfaces [244], and it may very well have had an effect under the current conditions, although this was not investigated. No detachment or noticeable displacement of cells was observed in any of the VSMC sample groups during friction testing, indicating that the cells were firmly adhered to the substrate. The lone exception to this was the observation that cytochalasin D treated VSMCs underwent a noticeable bulk reciprocating motion in phase with probe motion. Through microscopic

observation, cells did not appear to be physically damaged as a result of AFM probe contact. Furthermore, the use of spherical as opposed to pyramidal AFM probes, greatly reduces contact stresses at a given normal force and lessens the chances of cell damage [245].

The observation that glutaraldehdye (a crossklinking agent) and cytochalasin D (an actin depolymerizing agent) caused significant increases and decreases in frictional coefficients, respectively, serves as evidence that bulk cellular modulus does correlate positively with frictional coefficient, as it does with whole tissue [231]. Although VSMC exposure to the glycocalyx degrading enzymes for chondroitin sulphate and heparin sulphate did not significantly affect frictional coefficients in the current study, this does not mean that the glycocalyx should be ruled out as a source of VSMC lubrication. It is unlikely that the glycocalyx would be completely removed from enzymatic treatment at the concentrations used in this study [165]. Consequently, further investigation is warranted. It has been suggested that fluid film lubrication, and in particular elastohydrodynamic lubrication, is a common lubricating mechanism in biological systems [246]. Certainly, vascular smooth muscle cells such as those used in the current study are soft enough to be subject to deformation under most loading regimes. However, given that fluid film coefficients of friction are typically in the range of 0.001 to 0.01, while boundary lubrication yields friction coefficients closer to 0.1, it is also possible that the intermediate values found for untreated VSMCs are indicative of a mixed lubrication regime [247] for the contact and tribological conditions used in this study. The Stribeck curve for untreated VSMCs plotted in the current study revealed a

positive correlation between frictional coefficient and the approximated Sommerfeld number. This behavior is representative of fluid film lubrication. This is in agreement with previously a published finite element simulation of elastohydrodynamic lubrication, showing decreasing frictional coefficients with increased pressure in soft biological tissues [231]. It is possible that glutaraldehyde-fixed VSMCs exhibited a different lubrication profile either due to mechanical changes (increased stiffness) or chemical changes at the cell surface. If the former cause is true, and VSMC mechanical and frictional properties also varied *in vivo*, this could result in intrinsic variable contact stresses within the tissue, and a variable frictional profile over the surface, leading to disturbed contact stresses [248].

Future mechanistic studies examining VSMC lubrication regimes are indeed warranted, especially to further determine the effects of velocity, load, and lubricant viscosity. One potential benefit of an AFM-based cellular friction technique is the ability to modify the AFM probes with any number of different surface chemistries, for instance based on charge or hydrophilicity. In combination with treatments altering the physical chemistry and makeup of the underlying cells, such experiments could help reveal the underlying mechanisms of cellular and tissue lubrication. The technique described in the current study could be used to gather valuable information in the area of biotribology. Given the mechanical and material complexity of living cells, innovative and accurate frictional measurement techniques will be needed to determine the underlying mechanism(s) of friction and lubrication.

Conclusions

Measurement of cellular surface frictional properties via AFM is a viable, albeit complex technique. In the current study, frictional coefficients of untreated VSMCs were found to be approximately 0.06. Frictional coefficients were increased by cellular crosslinking, and decreased by cytoskeletal depolymerization. Further study using this technique is needed to determine the precise mechanisms underlying cellular lubrication.

CHAPTER SIX

THE EFFECTS OF OXLDL ON MECHANICAL PROPERTIES OF VASCULAR SMOOTH MUSCLE CELLS

Abstract: The study of single cell mechanics has gained considerable interest recently, due in part to the recognition that mechanical properties can greatly affect physiologic behavior. Vascular smooth muscle cells (VSMCs) and oxidized low density lipoprotein (oxLDL) are two of the key players in the development of vascular disorders, including atherosclerosis and restenosis. Recently, it has been observed that oxLDL can affect the cytoskeleton of vascular smooth muscle cells. In light of this evidence, it was hypothesized in the current study that oxLDL-associated cytoskeletal changes would have effects on VSMC mechanical properties. This hypothesis was tested using atomic force microsopy based elastic and viscoelastic measuring techniques. It was found that *in vitro*, oxLDL at a concentration of 50 μg/ml induced cytoskeletal and morphological changes in VSMCs similar to those associated with a transition towards a synthetic phenotype. After 5 days of exposure, oxLDL caused significant reductions in apparent elastic modulus, and significantly increased rate and percentage of stress relaxation, when compared to controls. These findings raise the possibility that similar VSMC mechanical changes may result from oxLDL *exposure in vivo.*

Introduction

Oxidized low-density lipoprotein (oxLDL) is believed to be one of the most significant factors in vascular disease development **[168]**, and the links between oxLDL and atherosclerosis have been well-documented by numerous researchers. [166, 167] Among the observed effects of oxLDL, is the alteration of cytoskeletal structure in both endothelial [169] and vascular smooth muscle cells (VSMCs) [170, 171]. Changes in cytoskeletal structure can have considerable effects on cellular biochemical responses to mechanical loading [116], given that the cytoskeleton plays a dominant role in governing mechanical properties of most cell types. In endothelial cells, oxLDL-related cytoskeletal changes have been shown to result in cellular mechanical changes [169]. However, no such investigation of oxLDL-associated VSMC mechanical changes has yet been performed. Vascular smooth muscle cells are subjected to mechanical loading from several sources, including blood pressure, blood flow, and in some cases, endovascular devices such as stents and angioplasty balloons. For these reasons, a better understanding of VSMC mechanical changes associated with clinically relevant biochemical stimuli, such as oxLDL, is important not only in terms of gaining a basic understanding of the underlying phenomena, but in understanding vascular disease progression, and potentially developing targeted treatments.

The atomic force microscope (AFM) is an extremely useful tool in the measurement of cellular mechanical properties, allowing for experimentation on living cells in aqueous media [147, 172, 173]. Recently, techniques have been developed to

analyze stress relaxation behavior of living cells using an AFM [154, 155, 249]. As cells typically exhibit viscoelastic behavior, AFM stress relaxation techniques can serve as a useful compliment to other AFM-based mechanical techniques such as cell indentation, which assume elastic behavior.

In the current study, it was hypothesized that oxLDL alters the viscoelastic properties of VSMCs through cytoskeletal and morphological changes. To test this hypothesis, we examined the effects of oxLDL on cellular morphology, actin and microtubule distribution, as well as cellular viscoelastic and surface shear properties.

Materials and Methods

Cell Culture

Rat aortic VSMCs previously isolated from adult male Sprague-Dawley rats were cultured in Dulbecco's Modified Eagle's Medium (DMEM) (Mediatech, Herndon, VA) with fetal bovine serum (FBS) (10 %) (Sigma, St. Louis, MO) and antibiotic/antimycotic solution (1 %) (Sigma). Cells were maintained in T-75 polystyrene flasks in an incubator at 37 ºC, with 5% CO_2, and fresh media was exchanged every 48 hours. Cells were allowed to grow to no greater than ~70% confluency in the flasks, then trypsinized with 0.25% trypsin (Mediatech) / 0.02% EDTA (Sigma) and seeded onto 22 x 22 mm glass coverslips (VWR, West Chester, PA) at a density of 10,000 cells per coverslip. Seeded coverslips were incubated in 6-well plates with DMEM (10% FBS) at 37 ºC with 5% CO_2, for 24 hours. After 24 hours, FBS-supplemented DMEM was replaced with serum-free DMEM supplemented with insulin-transferrin-selenium (ITS) media supplement (Sigma, St. Louis, MO) at a concentration of 5 µg/ml insulin, 5 µg/ml transferrin, and 5 ng/ml sodium selenite. Cells were kept in ITS-supplemented serum-free media for 72 hours prior to addition of lipoproteins. All cells in the current study were used between passages 4 and 6.

Lipoprotein Supplementation

Native LDL and OxLDL were obtained from Biomedical Technologies,Inc (Stoughton, MA). The oxidation level of OxLDL was 17.7 nmoles of MDA/mg protein, as determined by the supplier. Following 72 hours in ITS-supplemented DMEM, VSMCs were exposed to either native LDL or OxLDL at a concentration of 0.05 mg/ml

for periods of 1,3, and 5 days. Control VSMCs remained in media only for the same time periods. Media was exchanged every 24 hours, along with fresh aliquots of LDL and OxLDL.

Immunofluorescence

Immunofluorescence staining was used to visualize actin filaments and microtubules. At each timepoint, VSMCs were fixed in 4% paraformaldedyde at room temperature for 30 minutes. The cells were then incubated with blocking solution consisting of PBS (90%) (Sigma), bovine serum albumin (3.8%) (Sigma), donkey serum (3.0%) (Sigma), and Triton-X (0.2%) (Sigma) for 30 minutes. This was followed by incubation with a beta-tubulin primary antibody (Invitrogen, Inc. Carlsbad, CA) at 4°C overnight for microtubule staining. The cells were then incubated the following day with a TRITC-conjugated secondary antibody (Invitrogen, Inc., Carlsbad, CA) for 2 hours, followed by alexa fluor 488 conjugated phalloidin (Sigma) at room temperature for 15 minutes for actin staining, and DAPI nuclear staining for 5 minutes (Invitrogen, Carlsbad, CA). All samples were viewed using an Olympus IX71 inverted microscope (Olympus, Tokyo, Japan); images were collected and processed using HCImage software (Hamamatsu Corp., Bridgewater, NJ). Cells from the 5 day treatment group were measured along their major and minor axes using HCImage software (Hamamatsu Corp., Bridgewater, NJ), as an approximate measure of any changes to cell size and shape that resulted from oxLDL treatment. For each group, 25 randomly selected cells were used for measurements.

Confocal Microscopy

Confocal microscopy was performed using a Zeiss LSM 510 (Carl Zeiss MicroImaging, Inc., Thornwood, NY). As with the conventional fluorescence microscopy, cells were fixed on glass coverslips with 4% paraformaldehyde, and F- actin was labeled with alexa fluor 488 conjugated phalloidin, while beta-tubulin was labeled with anti-beta tubulin and a TRITC-conjugated secondary antibody (Invitrogen). Some samples were also stained with amphipathic Cellmask™ Deep Red, a Membrane Stain (Invitrogen), both prior to and after plasma membrane permeabilization in order to visualize cell shape. Coverslips containing labeled cells were mounted on glass slides along with SlowFade Gold antifade reagent (Invitrogen). Confocal images were processed using Zeiss LSM Image Browser software (Carl Zeiss Microimaging).

AFM Mechanical Measurements

Cellular indentation and stress relaxation tests were performed on VSMCs in succession. Briefly, the AFM probe was first positioned over the center of a target cell. Three consecutive indentation curves were taken at an approach speed of 500 nm/s. The quasi-static loading was then followed by a 120 sec stress relaxation test, with an indentation distance of 1 μm at 50 μm/s approach speed, as previously described [249]. At 3 and 5 day timepoints, 11 cells were subjected to indentation and stress relaxation testing for both control and oxLDL groups, while 6 cells were tested for each group at 1 day. Lateral force microscopy measurements were also performed on some cells, during which the AFM probe was reciprocated at a 90° angle along a 10 μm path length at 20

μm/s, with incremental increases in normal force up to approximately 100 nN. For all measurements, a 5 μm diameter borosilicate probe with a spring constant of 0.12 N/m was used.

Modeling

Following AFM experiments, indentation curves were fit using the modified Hertz model for a spherical indenter [250]

$$F = \frac{4}{3}\frac{E}{(1-\upsilon^2)}R^{\frac{1}{2}}\delta^{\frac{3}{2}}$$

where F is the measured force (N), δ is indentation depth (m), E is apparent elastic modulus (Pa), υ is Poisson's ratio (0.5) [187], and R is the spherical indenter radius (2.5 μm). The Hertz model was fit to an indentation depth of 300 μm, which is approximately 10% of VSMC height on the glass substrates used in the current study. Apparent elastic moduli were calculated by averaging the three indentation curves from each cell. Hysteresis exhibited by each indentation loop was calculated by subtracting the area under the entirety of each retraction curve from the area under the entirety of its corresponding indentation curve, and then normalizing by the area under the indentation curve in order to account for variations in indentation depth. Nonspecific adhesion between VSMCs and the AFM probe was quantified by measuring the maximum separation force from each retraction curve.

Stress relaxation curves were fit using the QLV reduced relaxation function,

$$G(t) = \frac{1 + c\int_{\tau_1}^{\tau_2} \frac{e^{-t/\tau}}{\tau} d\tau}{1 + c\int_{\tau_1}^{\tau_2} \frac{1}{\tau} d\tau}$$

where τ_1 and τ_2 are time constants governing short and long term relaxation behavior, respectively, and c is a unitless constant, representing a relative measure of viscous energy dissipation (damping).

Relaxation curves were also fit with a power-law relaxation model,

$$At^{-\alpha}$$

where A and α are constants governing the rate of decay.

All stress relaxation curves were shifted to give a baseline force value of 0 and were then normalized by their respective force values at time, t=0.01 s to obtain a starting (maximum) force value of 1.0 for each relaxation curve. The 0.01 s time point was used as the initial time point for normalization due to the usage of logarithmic time spacing and the 100 Hz initial sampling rate. Following normalization, data were resampled using logarithmic spacing with 100 data points from the start to the finish of each test. The degree of relaxation was quantified for each relaxation curve using the parameter G(120), denoting G at t=120 s. Nonspecific adhesion during relaxation tests was quantified using the breakaway force during tip retraction.

For lateral force data, excessive noise was first filtered from the data by eliminating any data points greater than 2 standard deviations away from the mean lateral signal value at a given normal force. The net lateral signal from each pair of trace and retrace lines was calculated as half of the difference between the two lines. Laser drift that occurred during lateral force measurements was accounted for by recording the lateral voltage on the photodiode at the start and finish of each cell, and correcting using a linear algebraic function. Mean lateral voltage and standard deviations were plotted against normal forces, and a linear fit was used to determine the slope of each line, μ, which represents the magnitude of lateral probe deflection from shear forces at the cell surface. All numerical data were processed using custom MATLAB (The Mathworks, Natick, MA) scripts.

Statistical Analyses

Two-way analysis of variance (ANOVA), with time and LDL treatment as factors, was used for comparison of Hertzian apparent elastic moduli, hysteresis, G(120), and the power-law exponent, α. Post-hoc pairwise analyses were performed using the Holm-Sidak method. In addition, correlations between measured variables were compared using coefficients of correlation. Coefficients of determination (R^2) were calculated for each individual curve fit for both stress relaxation models. Constants derived from each model are presented as a mean ± standard deviation. P-values < 0.05 were considered statistically significant for all tests.

Results

Immunostaining and fluorescence imaging revealed no changes to cell morphology, actin, or microtubule structure, for native LDL-treated VSMCs at any timepoint in the current study, Figure 6.1. However, treatment with oxLDL led to changes in VSMC morphology and cytoskeletal structure were noted at both 3 and 5 days. More specifically, at 3 days oxLDL-treated VSMCs exhibited elongated processes extending from the cell body, and greater dispersion of microtubules when compared to untreated VSMCs, Figure 6.2.

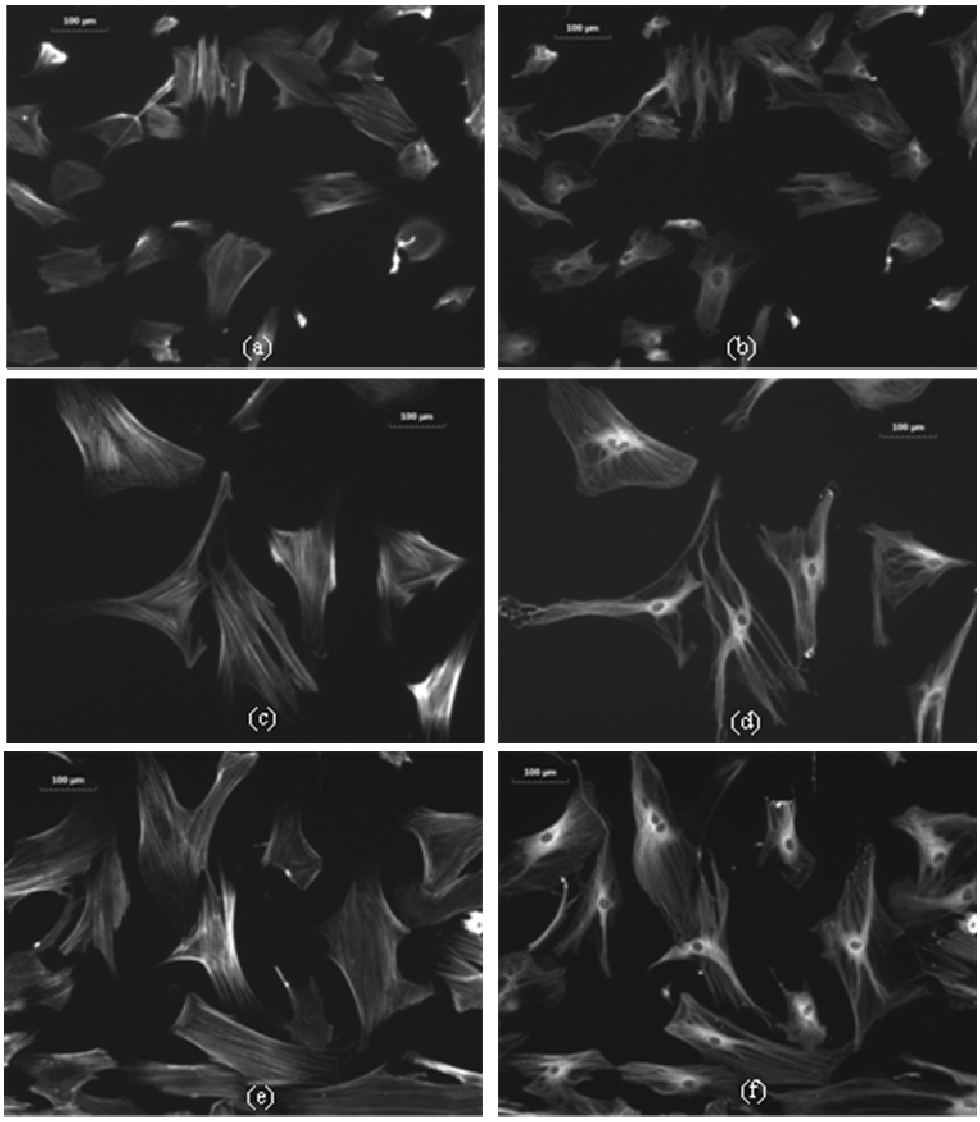

Figure 6.1. LDL-treated VSMC actin stained with phalloidin at 1,3, and 5 days (a,c,e) and LDL-treated VSMC microtubules stained with anti-alpha tubulin at 1,3, and 5 days (b,d,f). Images were captured using a fluorescent microscope at 20x magnification, and processed using HCImage software.

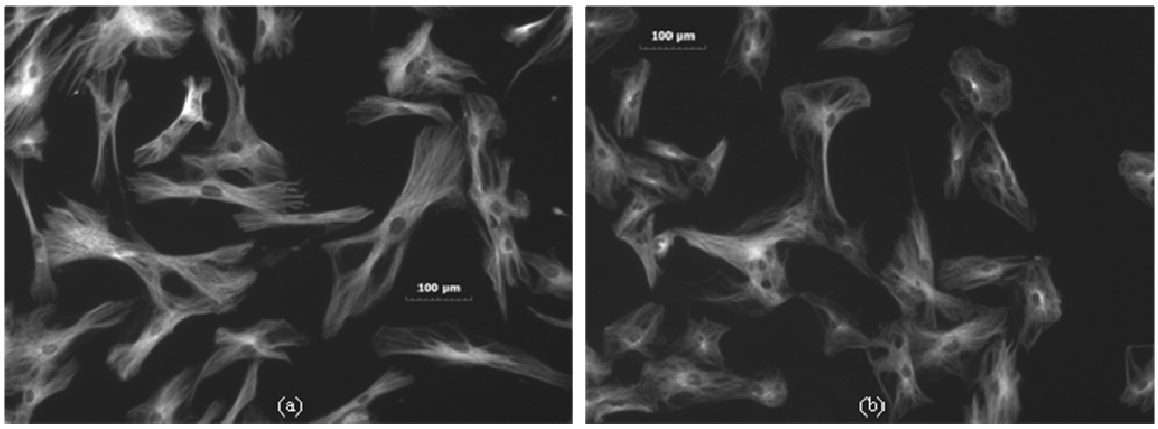

Figure 6.2 (a) OxLDL-treated VSMC microtubules stained with anti-alpha tubulin at day 3 (b) Control VSMC microtubules stained with anti-alpha tubulin at day 3

At 5 days, the oxLDL group displayed fewer actin stress fibers in the central cell regions, along with continued microtubule dispersion. In contrast, control VSMCs exhibited greater actin fiber content, and a concentrated microtubule aster in the perinuclear region with longer microtubules radiating from it, Figure 6.3.

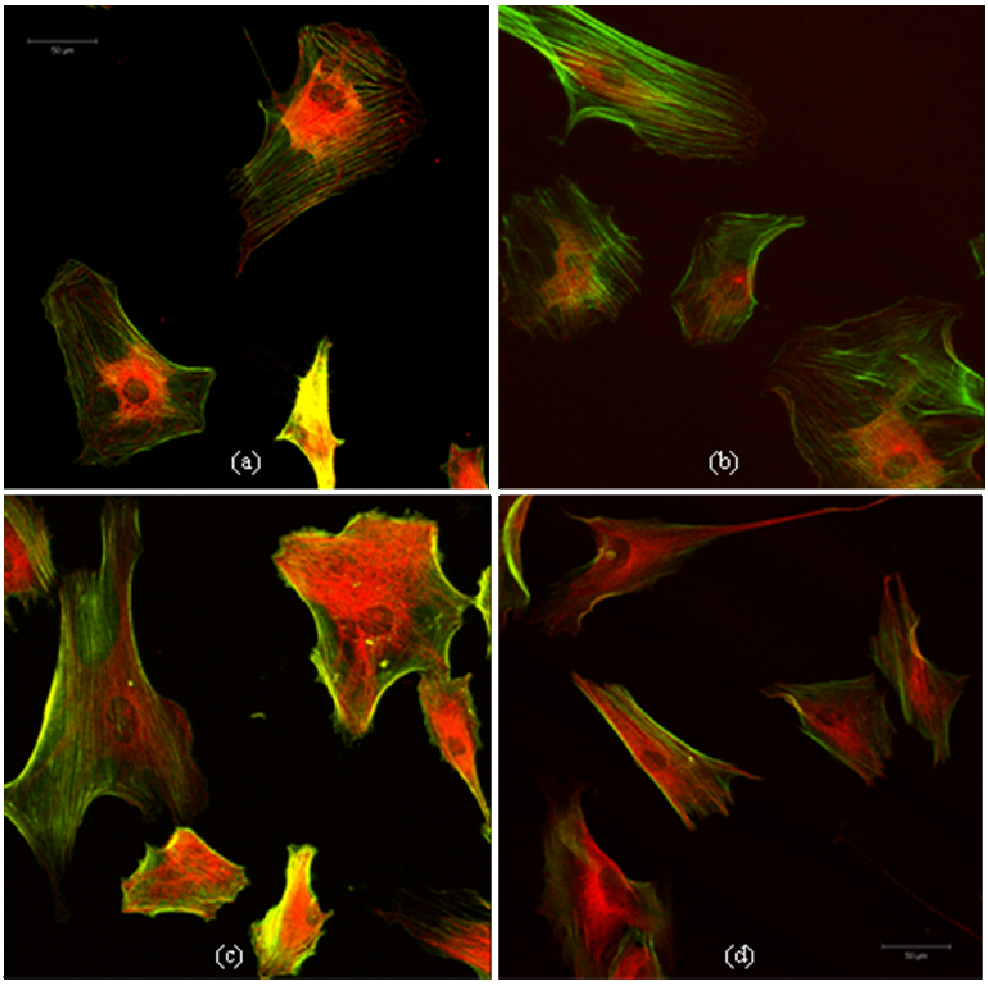

Figure 6.3. (a&b) Control VSMCs at day 5, green regions are F-actin, red regions are microtubules ; (c&d) OxLDL-treated VSMCs at day 5, green regions are F-actin, red regions are microtubules.

Staining of oxLDL-treated VSMCs with CellMask^{TM} revealed substantial lipid staining throughout the cytoplasm, particularly in dense microtubule regions, in both permeabilized and unpermeabilized VSMCs at day 5, Figure 6.4, d,e,f. In contrast, control VSMCs stained with CellMask exhibited lipid staining only in the perinuclear region, again colocalized with dense microtubule structure, Figure 6.4, a,b,c.

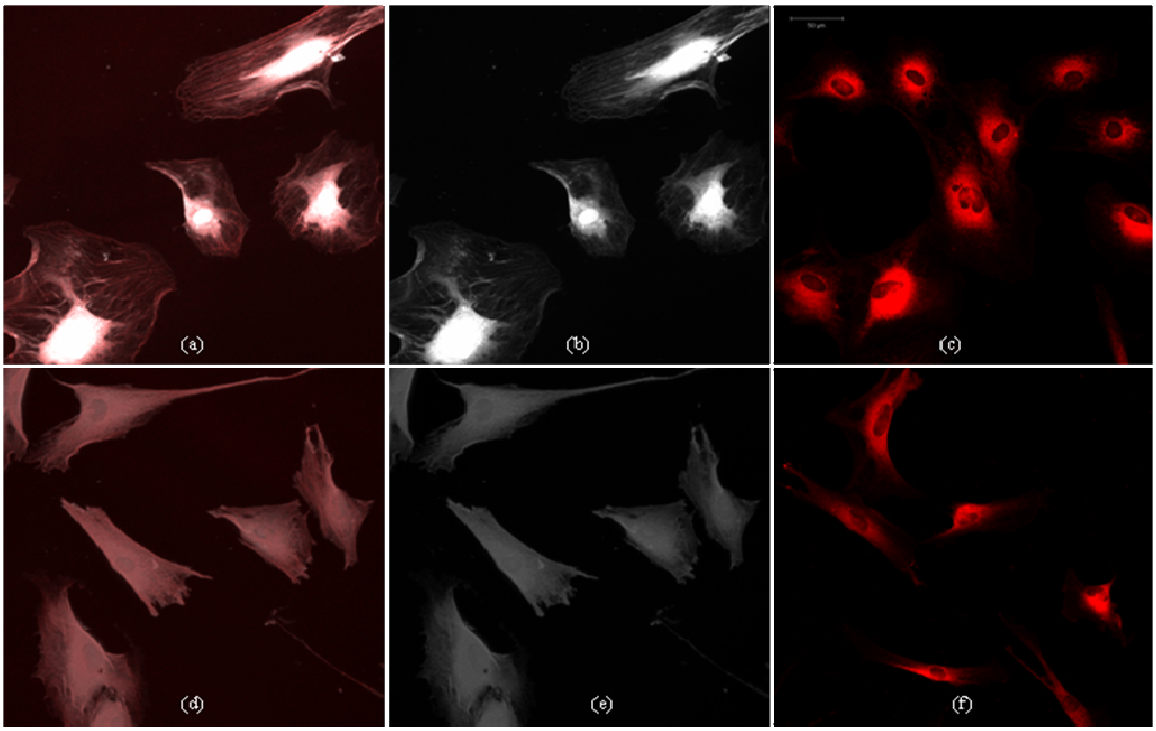

Figure 6.4. Confocal microscopy images of (a) membrane permeabilized control VSMCs stained with CellMask (white) and anti-beta tubulin (red), showing staining predominantly in the central region of each cell, and colocalization of CellMask staining with microtubules, (b) Membrane permeabilized control VSMCs stained with CellMask (white), (c) unpermeabilized control VSMCs fixed and stained with CellMask (red), (d) membrane permeabilized oxLDL-treated VSMCs stained with CellMask (white) and anti-beta tubulin (red), showing staining throughout each cell, and colocalization of CellMask staining with microtubules, (e) Membrane permeabilized oxLDL-treated VSMCs stained with CellMask (white), and (f) unpermeabilized oxLDL-treated VSMCs fixed and stained with CellMask (red).

The mean cell dimensions were similar in oxLDL-treated VSMCs (140 and 50 µm along the major and minor axes, respectively), and control VSMCs (120 and 50 µm along the major and minor axes, respectively), n=25.

OxLDL-treated VSMCs had mean elastic moduli of (4.4 ± 3.1, 1.6 ± 0.7, and 1.6 ± 0.8 kPa at 1, 3, and 5 days, respectively), Figure 6.5. A mean elastic modulus of (3.1 ± 1.4, 2.9 ± 1.6, and 3.6 ± 1.4 kPa at 1, 3, and 5 days, respectively) was determined for control VSMCs, Figure 6.5. Two-way ANOVA revealed a statistically significant effect of time after allowing for the effects of treatment (p=0.029) and a statistically significant interaction between time and treatment (p=0.012). Subsequent pairwise analyses revealed a significant difference between oxLDL and control at day 5 (p=0.003) and significant differences within the oxLDL group when comparing days 1 vs. 3 and 1 vs. 5, (p=0.001) for each.

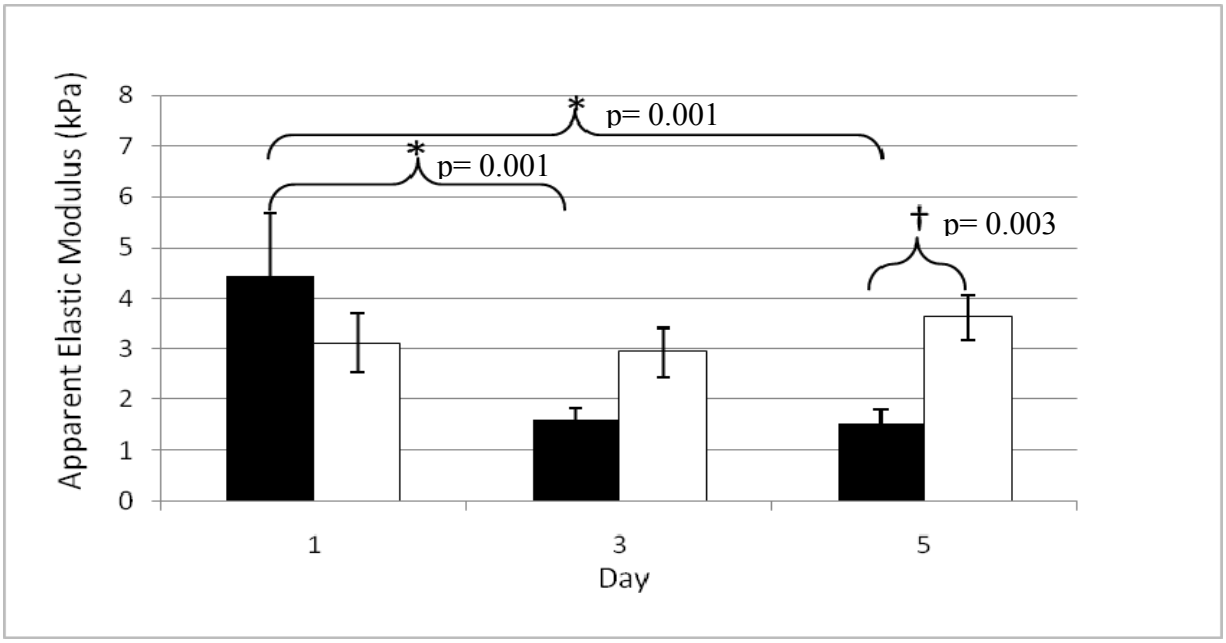

Figure 6.5. Apparent elastic moduli of oxLDL-treated VSMCs (black) and controls (white) at 1,3, and 5 days. Data represent means ± SD.

Analysis of indentation loop hysteresis, showed a significant effect of time after allowing for the effects of treatment ($p=0.012$), treatment after allowing for the effects of time ($p=0.026$), and significant interaction between time and treatment ($p<0.001$). Subsequent pairwise analyses revealed a significant difference between oxLDL and control ($p<0.001$) at day 5 and significant differences within the oxLDL group when comparing days 1 vs. 5 and 3 vs. 5, ($p<0.001$ for each), Figure 6.6. OxLDL-treated VSMCs had mean hysteresis values of (0.24 ± 0.1, 0.31 ± 0.2, and 0.64 ± 0.3 at 1, 3, and 5 days, respectively), Figure 6.6. Control VSMCs had mean hysteresis values of (0.3 ± 0.1, 0.3 ± 0.2, and 0.25 ± 0.1 at 1, 3, and 5 days, respectively), Figure 6.6

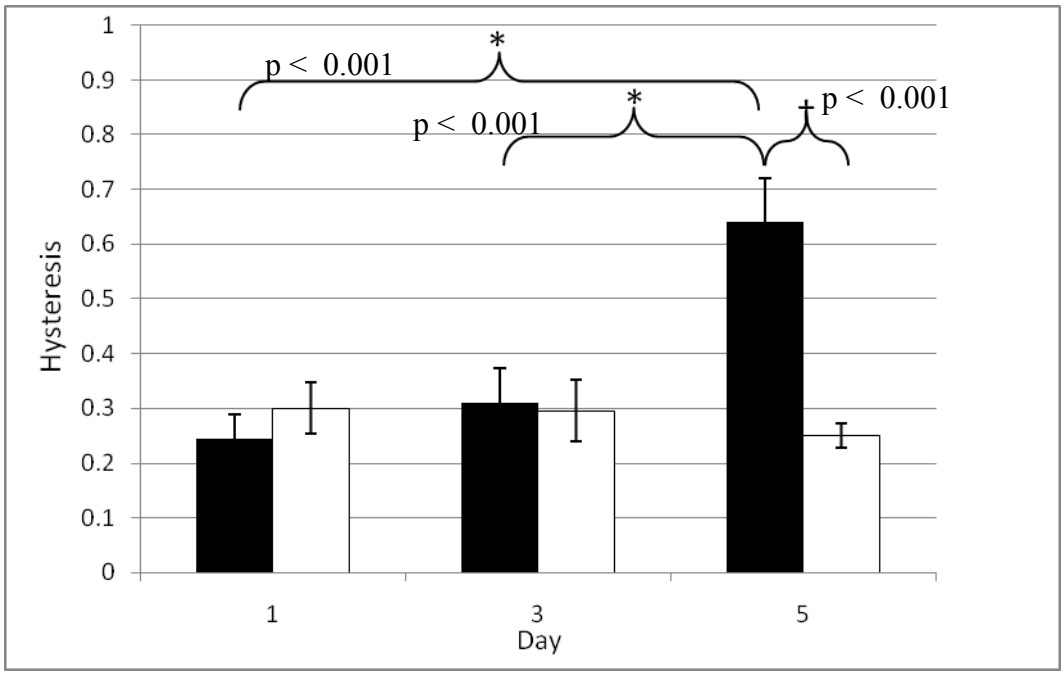

Figure 6.6. Indentation loop hysteresis of oxLDL-treated VSMCs (black) and controls (white) at 1,3, and 5 days. Data represent means ± SD.

Nonspecific adhesion between VSMCs and the AFM probe was significantly greater ($p < 0.001$) at 5 days for oxLDL-treated VSMCs compared to controls, (2.3 ± 0.9 pN vs. 0.9 ± 0.4 pN, respectively).

In quantifying stress relaxation via the parameter G(120), there was a significant interaction between time and treatment ($p=0.008$). Subsequent pairwise analysis revealed a significant difference between oxLDL and control at day 5 ($p=0.001$), Figure 6.7. OxLDL-treated VSMCs had mean G(120) values of (0.25 ± 0.1, 0.31 ± 0.1, and 0.18 ± 0.1 at 1, 3, and 5 days, respectively), Figure 6.7. Control VSMCs had mean G(120) values of (0.18 ± 0.2, 0.31 ± 0.1, and 0.4 ± 0.1 at 1, 3, and 5 days, respectively), Figure 6.7.

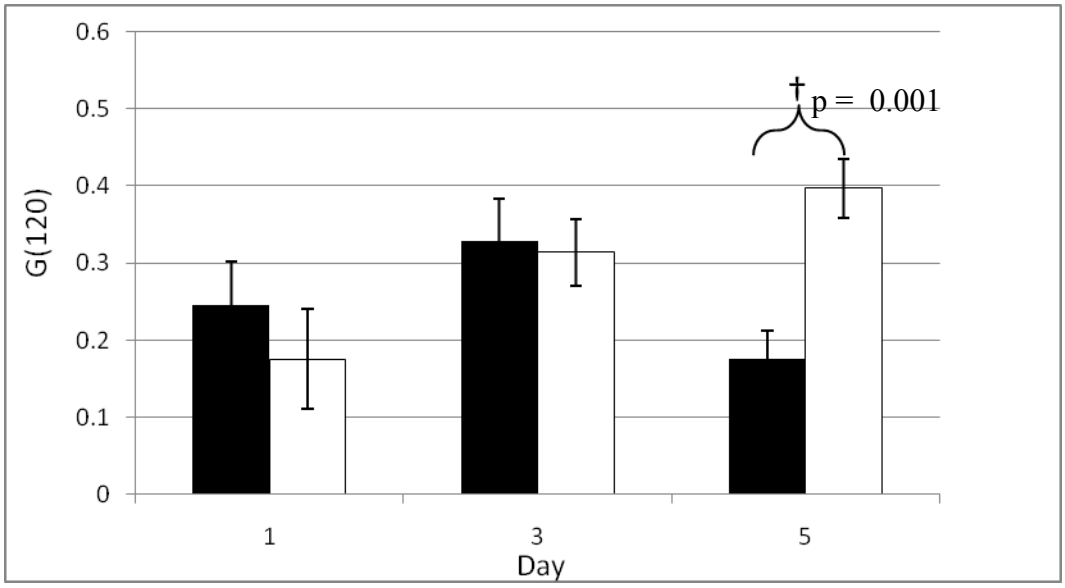

Figure 6.7. G(120) of oxLDL-treated VSMCs (black) and controls (white) at 1,3, and 5 days. Data represent means ± SD.

For the power-law relaxation exponent, α, there was a significant interaction between time and treatment (p=0.005), with subsequent pairwise analysis revealing a significant difference between oxLDL and control at day 5 (p<0.001), Figure 6.8. OxLDL-treated VSMCs had mean α values of (-0.12 ± 0.1, -0.12 ± 0.1, and -0.17 ± 0.1 at 1, 3, and 5 days, respectively), Figure 6.8. Control VSMCs had mean α values of (-0.14 ± 0.04, -0.13± 0.06, and -0.08 ± 0.02 at 1, 3, and 5 days, respectively), Figure 6.8.

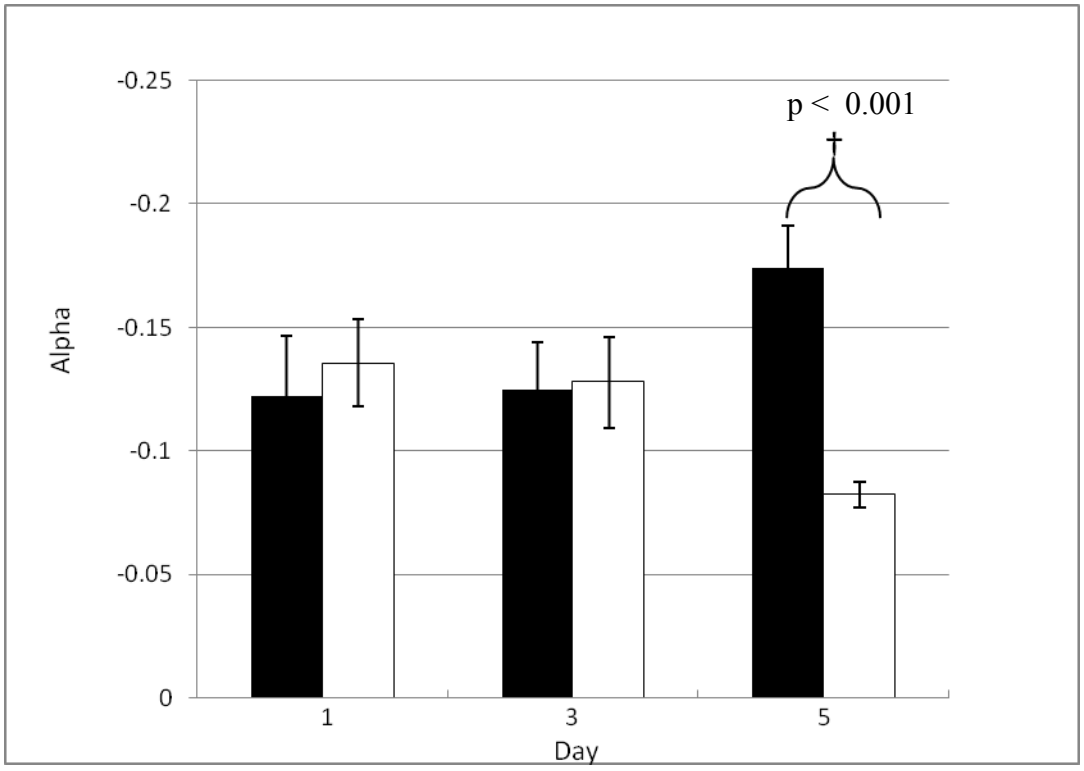

Figure 6.8. Power-law exponent, α, of oxLDL-treated VSMCs (black) and controls (white) at 1,3, and 5 days. Data represent means ± SD.

Both the QLV reduced relaxation function and the power-law model fit the stress relaxation data well ($R^2 = 0.98 \pm 0.02$ and 0.96 ± 0.05, respectively). OxLDL-treated VSMCs had greater C values, and lower τ_1 values at all three timepoints, while τ_1 was greater in the oxLDL group at 1 and 3 days, but lower at day 5, Table 5.1.

Table 5.1. QLV reduced relaxation function parameters.

Day	Group	C	τ1	τ2
1	Control	0.45±0.21	0.16±0.12	150±160
	oxLDL	0.73±1.2	0.09±0.04	380±290
3	Control	0.33±0.32	0.13±0.21	170±260
	oxLDL	0.70±1.2	0.06±0.02	300±310
5	Control	0.15±0.06	0.09±0.07	480±390
	oxLDL	1.0±1.7	0.05±0.03	220±250

No significant difference in cell adhesion was observed between oxLDL and control VSMCs following stress relaxation tests at day 5, (1.34 vs. 1.87 nN, respectively, $p=0.20$).

Strong correlations were found between the different measures of viscous energy dissipation, G(120), α, C, and to a lesser extent, indentation hysteresis, used in the current study (gray shaded cells in Table 5.2). Apparent elastic modulus showed moderate correlations with viscous measures (green shaded cells in Table 5.2). Lateral force measurements were strongly correlated with measures of viscous dissipation (yellow shaded cells in Table 5.2).

Table 5.2 Correlation coefficients of VSMC mechanical parameters.

	E	G120	C	α	Hys	μ
E	1.00					
G120	0.20	1.00				
C	-0.29	-0.61	1.00			
α	0.41	0.76	-0.61	1.00		
Hys	-0.46	-0.49	0.41	-0.76	1.00	
μ	-0.25	-0.66	0.86	-0.72	0.58	1.00

Discussion

The study of single cell mechanics has gained considerable interest in recent years, as researchers have begun to recognize the importance of cellular mechanical properties in regulating many physiological processes. Among the key tasks within this field of study is the determination of what stimuli, either mechanical or chemical, affect cellular mechanical properties. With regard to vascular function and disease progression, oxLDL is known to have numerous effects, including the potential to alter cytoskeletal structure in both ECs and VSMCs. Based upon these prior observations, the purpose of the current study was to determine whether oxLDL caused mechanical changes to VSMCs in an *in vitro* environment

After 5 days of exposure, oxLDL-treated VSMCs displayed fewer actin stress fibers, increased cytoplasmic organelle content, and lamellopoid-like protrusions. All of these observations are characteristic of cell cycle and phenotypic changes [45, 251]. It has been proposed that oxLDL causes a shift towards a synthetic phenotype via the induction of cell cycle proteins [252], with involvement of MAPK pathways [253]. The decreased cell stiffness of VSMCs observed in this study, due to a reduction in actin stress fiber content, would agree with previous VSMC mechanical measurements relating to phenotype [126, 250]. The reduced actin stress fibers in the oxLDL-treated cells would also mean an increased role of the viscous cytoplasm in governing viscoelastic behavior, providing a possible explanation for the reduced viscosity and more fluid-like behavior of the oxLDL group in the present study.

The precise effects of microtubule dispersion in the mechanical behavior of oxLDL-treated VSMCs are unclear. However, it is possible that the highly organized microtubule asters found in the central region of control VSMCs contributed to the greater stiffness and viscosity. Previous research in our laboratory demonstrated that VSMCs treated with the microtubule stabilizing agent paclitaxel, showed significantly increased viscosity[249]. . The microtubule dispersion observed in the oxLDL group may be a result of their role in cell motility, cell cycle changes, or intracellular organelle transport [254, 255], which rely on the dynamic instability of microtubules. Together, it can be speculated that relative stability or instability of the microtubular network may play a key role in cellular viscoelastic behavior.

The CellMask stain used in this study is amphipathic, that is, it is largely hydrophobic, but includes a hydrophilic moiety at one end in order to anchor onto phospholipid membranes. It is for this reason, that the observed staining patterns likely reflect the presence of cytoplasmic organelles, which are surrounded by phospholipid membranes. Increased synthetic organelle content within oxLDL-treated VSMCs may actually serve to increase cytoplasmic viscosity [256]. It is not known what effect, if any, this may have had in the current study, but nonetheless this provides an interesting question for further investigation. The increased nonspecific adhesion for oxLDL-treated cells at 5 days between the AFM probe and cell, may relate to previous observations that oxLDL upregulates adhesion receptors, and that VSMCs isolated from atherosclerotic arteries have been found to exhibit greater levels of adhesion to underlying substrates [257, 258].

Cytoskeletal and morphological changes of VSMCs in response to oxLDL treatment have been observed previously [171, 259]. Both minimally modified LDL (mmLDL) and more highly oxidized oxLDL were shown to induce actin disruption in VSMCs, with the former binding to LDL receptors, while the latter binds to scavenger receptors [260]. Previous studies have shown that VSMCs treated with 50ug/ml of oxLDL in the presence of ITS-supplemented media show significantly increased cell proliferation [252]. However, oxLDL has been shown to have dramatically varying effects on VSMCs, ranging from increased proliferation at concentrations of 35 and 50 μg/ml, to apoptosis at concentrations over 100 μg/ml.[252, 261] *In vivo*, VSMCs contribute to the development of atherosclerotic plaques in several different ways, including cell proliferation, migration, and apoptosis. In light of this and the varying *in vitro* results reported in the literature, it is clear that the effects of oxLDL on VSMCs are highly dependent on numerous variables, including concentration, extent of LDL oxidation, and exposure time.

In the current study, changes to actin an microtubule structure were associated with significant changes in viscoelastic mechanical measurements. Based upon the immunfluorescence staining results, oxldl-treated and control VSMCs were mechanically tested at 1, 3, and 5 day timepoints. LDL-treated VSMCs were not mechanically tested, due to the lack of observed cytoskeletal or morphological effects. When compared to controls, oxLDL-treated VSMCs showed significantly increased relaxation rate and percentage (alpha and G(120)) at 5 days. Indentation loop hysteresis was significantly greater for oxLDL compared to controls at 5 days, with an increasing trend over time.

Together with apparent elastic modulus also being significantly lower in the oxLDL group compared to controls at 5 days, these data suggest increasing fluid-like behavior of VSMCs when subjected to prolonged oxLDL treatment, with the opposite occurring in control cells, most likely due to serum withdrawal and contractile protein upregulation [250].

Both the QLV reduced relaxation function and the power-law model used in this study provided very good fits to the data (R^2=0.96 and 0.98, respectively). For the reduced relaxation function, the mean short term time constant, τ_1, was lower for oxLDL-treated VSMCs compared to controls at each timepoint, and in both groups, decreased at each successive timepoint. In viscoelastic materials, relaxation time constants generally decrease with lower viscosity or greater elasticity. When approached from this perspective, the decrease in τ_1 in the oxLDL cells can be viewed as resulting from decreased viscosity, in light of the decreased elastic behavior, as quantified via apparent elastic modulus. However, in control VSMCs, decreasing τ_1 more likely resulted from increasing contribution from elastic elements (e.g. actin fibers). The mean long term time constant, τ_2, consistently increased with time for control groups, while it consistently decreased for ox-LDL groups. Recent evidence suggests that actin stress fibers are viscoelastic in their behavior, with retraction behavior after severing characterized by a viscoelastic element with a spring and dashpot in parallel [262]. In the current study, an increasing long term time constant in the control group, τ_2, may reflect the viscous behavior of the actin stress fibers over longer time periods, while the decreasing τ_2 in oxldl-treated cells reflects the disappearance of these fibers, and a heightened role of

other cellular constituents in determining viscoelastic behavior. It should be noted that too much weight should not be assigned to the precise values found for the short and long term time constants, as QLV time constants, especially τ_2, can vary greatly [224].

The range of power-law exponents describing VSMC relaxation behavior in the current study demonstrate a weak frequency dependence in agreement with previous studies examining power-law behavior of other cell types [263]. The power-law exponent, α, while not an indicator of physical mechanisms governing relaxation behavior, does provide a simple means of comparing the physical rates of relaxation between different materials. Values of the power-law exponent in the current study indicate that after 5 days, oxLDL-treated VSMCs display more fluid-like behavior (i.e., stronger frequency dependence), when compared to controls, in agreement with the reduced relaxation function damping constant, C.

When comparing the mechanical parameters calculated from the experiments in this study, strong correlations emerged between the different measures of viscous behavior, which provides further support for the validity of each. The relatively lower correlation between apparent modulus and viscous measures underscores the idea that indentation measurements do not capture all relevant viscoelastic properties, and cannot be solely relied upon to quantify cellular mechanical behavior. Lateral force measurements were found to correlate positively with measures of viscous energy dissipation, although the sample size was relatively small (n=10) and variations within lateral force measurements were minute as well. Nonetheless, this observation may result

from greater contact area between cell and probe during lateral force measurements in less viscous (more fluid-like) cells.

Plasma oxLDL levels are a strong predictor of acute coronary heart disease events[264] and restenosis after stent placement[265]. The lipoprotein concentration used in this study was close to that found in serum of human subjects with coronary artery disease [266]. However, oxLDL levels found within subendothelial space in vascular lesions are likely to have much higher levels of oxLDL than those found in blood, due to antioxidation defenses within the bloodstream [267]. Further investigation is necessary to determine any physiological changes that may result from oxLDL-associated mechanical changes. From the perspective of arterial mechanics, oxLDL-induced cellular phenotypic shifts, as hypothesized to have occurred in the current research, would likely cause a drop in cell stiffness. However, there would also likely be increased ECM deposition, thereby explaining the previously observed correlation between oxLDL levels and decreasing arterial compliance [268, 269].

Conclusions

Data from the current study indicate that oxLDL can induce significant changes to the viscoelastic properties of VSMCs *in vitro,* including decreased stiffness and viscosity. The potential clinical implications of this finding warrant further research.

CHAPTER SEVEN

CONCLUSIONS AND RECOMMENDATIONS

Conclusions

The current research was motivated by the desire to gain a better understanding of VSMC mechanical and frictional behavior at the single cell level, and to develop useful techniques to quantify that behavior and its responses to clinically relevant conditions and stimuli. The atomic force microscope was chosen as a platform for this research due to the ability to perform measurements on living cells in media, versatility in mechanical and frictional measurement, imaging capabilities, and commercial availability**.**

The first aim of this research was to determine whether or not VSMC phenotypic shifts resulted in cellular mechanical changes. A better understanding of the concurrent changes to VSMC mechanical properties that occur with phenotypic shifts can help elucidate the role of VSMC mechanics in the development of vascular diseases. In the current study, the mechanical properties of adherent cultured rat aortic VSMCs were assessed by atomic force microscopy (AFM). Serum starvation in DMEM was used to induce a phenotypic shift toward a contractile state *in vitro,* while control groups were kept in DMEM with 10% FBS. Cellular indentation with the AFM was conducted, and the resulting force curves were fit using the Hertz model. The Hertz model allows for computation of an apparent elastic modulus for each cell. In addition, viscous energy dissipation (hysteresis) was calculated for each indentation curve. It was concluded that serum starvation caused a statistically significant increase in apparent elastic modulus

after 5 days, as well a statistically significant decrease in hysteresis after 3 days in culture. Furthermore, serum starved VSMCs became more elongated than controls, which exhibited more spreading. Use of the Hertz model was validated by calculating apparent elastic modulus as a function of indentation depth, over the range of depths used in this study. This demonstrated sufficient linearity in elastic modulus, one of the key assumptions of the Hertz model. Indentation force maps over the surface of the cells revealed relatively small variations in elastic modulus over the central region of the cell, validating the usage of a single indentation point with a sufficiently large probe. The current mechanical data are in agreement with previously published research dealing with the relationship between phenotypic state and mechanical properties of non-adherent VSMCs. If these observed trends in VSMC mechanical property alterations were to hold true *in vivo*, such changes could affect the processes of mechanotransduction and/or arterial mechanical properties, thereby contributing to the progression of vascular disease. As proliferative VSMCs are typically associated with a disease state, this study served as proof of concept that significant mechanical differences exist between "healthy" and diseased VSMCs.

The second aim was to determine the role of specific cytoskeletal components in determing VSMC stress relaxation behavior. Given that the first phase of research showed that significant mechanical changes can occur during phenotypic changes, an understanding of the roles of specific cytoskeletal components responsible for such changes was needed. Furthermore, given the viscoelastic behavior of living cells, the Hertzian elastic modeling commonly used for AFM cell mechanics research was deemed

inadequate on its own. As a means to quantify viscoelastic properties, a novel method of AFM stress relaxation experimentation and modeling was developed. Various cytoskeletal agents with known effects on actin or microtubules, including cytochalasin D, jasplakinolide, paclitaxel, and nocodazole, were used to alter the cytoskeletal architecture of the VSMCs. Stress relaxation experiments were performed on the VSMCs using AFM. Indentation was performed with a 5 μm spherical probe at 50 μm/s in order to approximate a step strain. The quasilinear viscoelastic (QLV) reduced relaxation function, as well as a simple power-law model, and the standard linear solid (SLS) model, were fit to the AFM stress relaxation data. As a necessary condition for use of the reduced relaxation function, strain independence was investigated and confirmed. Statistical comparisons of stress relaxation behavior were performed using the percentage of relaxation (G(120) and rate of relaxation (power-law exponent, α). In addition, the reduced relaxation function yields two time constants, and a unitless measures of damping, while the SLS model yields two time constants as well. Actin depolymerization via cytochalasin D resulted in significant increases in both rate of relaxation and percentage of relaxation, while actin stabilization via jasplakinolide did not affect stress relaxation behavior. Microtubule depolymerization via nocodazole resulted in nonsignificant increases in rate and percentage of relaxation, while microtubule stabilization via paclitaxel caused significant decreases in both rate and percentage of relaxation. Both the QLV reduced relaxation function and the power-law model provided excellent fits to the data ($R^2 = 0.98$), while the SLS model was less adequate ($R^2 = 0.91$). Failure of the SLS model to properly fit the data, illustrate the

divergence in mechanical characteristics of living cells from many common viscoelastic materials. Data from the current study indicate the important role of not only actin, but also microtubules, in governing VSMC viscoelastic behavior. Depolymerizatin of actin leads to more fluid-like behavior of the cell. Based upon these data, as well as previously published research, the role of microtubules in governing cellular viscoelastic behavior appears to be highly dependent on specific experimental conditions, and more complex than that of actin. From a clinical perspective, the significant mechanical changes induced by paclitaxel are relevant, due to its usage in drug eluting stents that are already available on the market. Further research into potential adverse physiological effects of these mechanical changes is necessary. Additionally, this research underscores the need and benefit of characterizing cell mechanics using viscoelastic, rather than purely elastic models.

The third aim was to develop a method to measure surface cellular frictional properties. With the advancement of the field of biotribology, considerable interest has arisen in the study of cell and tissue frictional properties. Much interest exists in the determination of how cells crawl, migrate, and flow through narrow spaces *in vivo*. From the perspective of medical device development, the frictional properties between a rigid surface and underlying cells and tissues is of a particular clinical interest. As with many bearing surfaces, it is likely that contact asperities exist at the size scale of single cells and below. Thus, a technique to measure cellular frictional properties would be beneficial from both a clinical and a basic science perspective. In the current study, an atomic force microscope with a 5 μm diameter borosilicate spherical probe was used to

measure the surface frictional properties of vascular smooth muscle cells (VSMCs). A technique commonly used for frictional measurement of synthetic materials, known as lateral force microscopy (LFM), was adapted for use with VSMCs in media. A 5 μm borosilicate spherical probe, a 10 μm reciprocating path length over the major axis of single cells, speeds of 2 and 20 μm/s, and normal forces up to approximately 100 nN were used for experimental parameters. All experiments were performed in DMEM. Various treatments were used to alter cell structure, in order to better understand the cellular components and mechanisms responsible for governing frictional properties. Actin depolymerization, and therefore cell softening, was induced using cytochalasin D, while crosslinking (cell stiffening) was achieved using paraformaldehyde fixation. In addition, the main constituents of the VSMC glycocalyx, chondroitin sulfate and heparan sulfate, were partially degraded via enzymatic treatment with the enzymes chondroitinase and heparinase, respectively. In some experiments, the AFM probe was chemically modified via SAMs, to make the surface hydrophobic or hydrophilic, or else give a positive or negative charge. It was found that untreated VSMCs had a frictional coefficient of approximately 0.06. This frictional coefficient also appears to be greatly affected by cellular rigidity, with softer cells treated with cytochalasin D having a lower coefficient of friction than paraformaldehyde treated cells. This positive correlation between cell stiffness and frictional coefficient is also what has been found for whole tissues. No changes to frictional properties resulted from glycocalyx degradation, and data from chemically modified probes were inconclusive. The technique of measuring frictional properties at the surface of cells using lateral force microscopy appears to be a

viable one, with potential for investigation of various probe chemistries in the future. However, further research is required to determine the exact nature of the interactions between the AFM probe and cell surface, as well as the sensitivity of this technique. This includes treatment to manipulate the cell surface and/or AFM probe. Investigation into the mode of lubrication is also warranted. Data from the current study indicate the possibility of an elastohydrodynamic or mixed lubrication regime, but further research is needed before any definitive conclusions can be drawn.

The fourth and final research aim was the application of the elastic, viscoelastic, and frictional measurement techniques developed in the prior 3 aims, toward the investigation of frictional and mechanical effects resulting from clinically relevant VSMC stimuli. For this purpose, the lipoproteins LDL and oxLDL were chosen. Both LDL and oxLDL are well known to be associated with vascular disease development. Past studies have shown that oxLDL in particular can cause cytoskeletal changes to VSMCs *in vitro*. In light of this evidence, it was hypothesized in the current study that oxLDL-associated cytoskeletal changes would have also effect VSMC mechanical properties. This hypothesis was tested using AFM-based elastic and viscoelastic measuring techniques, including stress relaxation, Hertz indentation, and hysteresis measurement. In addition to these mechanical measurements, imaging of cytoskeletal components (actin and microtubules) was carried out using fluorescent and confocal microscopy. VSMCs were serum deprived (with the addition of ITS media supplement) for 72 hours prior to lipoprotein supplementation It was found that *in vitro*, oxLDL at 50 μg/ml induced cytoskeletal and morphological changes in VSMCs similar to those

associated with a transition towards a synthetic phenotype. Specifically, oxLDL treatment was associated with a reduction in actin stress fiber content, as well as increased microtubule and organelle dispersion. No changes were observed in LDL or control VSMCs, and as a result, LDL groups were not mechanically tested. After 5 days of exposure, oxLDL caused significant reductions in apparent elastic modulus, and significantly increased rate and percentage of stress relaxation, when compared to untreated controls. These findings raise the possibility that similar VSMC mechanical changes may result from oxLDL exposure *in vivo.* Strong correlations were found among the different measures of viscous energy dissipation, supporting the validity of their usage. Furthermore, there was a strong positive correlation between cellular frictional coefficients, and mechanical damping. This finding seems to contradict the results from aim 3, however it should be noted that different chemical treatments were used in the two studies, and their effects on cellular surface chemistry and frictional behavior are as yet unknown. Data pertaining to frictional effects of oxLDL were inconclusive. The results from this aim represent the collective and successful usage of the AFM-based measurement techniques developed over the course of the prior aims. Using these techniques, it was demonstrated that oxLDL causes significant changes in both elastic and viscoelastic behavior. As such, these measurement techniques or variations thereof, can serve as an *in vitro* test bed for evaluation of the effects of various stimuli on cellular mechanics in future studies. One of the most important points raised by this study, is the need to use several mechanical measurement techniques in combination, when evaluating the effects of a stimulus, as no single measure captures al l pertinent data.

Based upon the results of this research, it can be concluded that numerous clinically relevant stimuli, including oxLDL (aim 4) and paclitaxel (aim2) exposure, affect VSMC mechanical properties in a significant manner. In addition the role of various cytoskeletal components in governing mechanical behavior has been further elucidated. In both aims 1 and 4 of this study, evidence was found that VSMC phenotypic shifts are associated with mechanical changes, the physiological effects of which require further exploration. Perhaps most importantly, AFM-based techniques and associated mechanical models have been identified that will allow for easily repeatable assessment of any number of clinically relevant stimuli related to vascular disease. It is believed that a test platform such as this will allow for the evaluation of not only pharmaceutical and biological agents, but also of mechanical contact from different materials and surface chemistries with potential applications for endovascular devices. From a mechanical standpoint, implantation of vascular devices represents a complex system with numerous variables and components. Using these AFM techniques, it will be possible to provide data for the creation of better computational and experimental models of the mechanical interactions between endovascular devices and underlying cells.

Recommendations

1. **Simultaneous AFM mechanical testing and live cell fluorescence imaging**. One of the most significant drawbacks of the AFM cell techniques described in this research, is the reliance on the investigator on conventional light microscopy for identification of target cells and probe positioning. Development of reliable methods for fluorescent staining of live cell cytoskeletal components would not only make cell identification far less difficult, but would also allow the correlation of cytoskeletal structure within specific cells with the mechanical properties of that cell. This would represent a vast improvement over the current methodology, in which cell populations exposed to a given treatment are heterogeneous in their response, creating great difficulty in discerning if and how a given cell has responded, and how that response is manifested mechanically.

2. **AFM dynamic mechanical analyses**. The AFM has been used in the past to conduct dynamical mechanical tests on living cells, as have various other techniques, such as magnetic twisting cytometry . Utilization of such techniques would allow comparison with the stress relaxation data from the current research, as viscoelastic behavior over a certain frequency spectrum could be compared and validated using the separate techniques. If necessary, refinement of the current mechanical models and identification of better models could be accomplished.

3. ***In vitro* screening of biomaterials and biomolecules**. The current AFM techniques carry great potential for use as an *in vitro* tool to screen clinically relevant biomolecules (e.g. pharmaceuticals, cytokines, lipoproteins) and biomaterials (e.g. stent materials and coatings) for mechanical effects and frictional behavior on VSMCs. In particular, further exploration of lipoproteins, and their effects on cytoskeletal structure and cell mechanics is warranted, in light of the current research findings. Attention should be focused on the identification of agents that inhibit any observed changes to cellular structure and mechanics, with the eventual goal being the identification of targeted therapies that block mechanical changes. Such an approach may help bring some of the clinical benefits of cellular mechanics research to fruition.

4. **Investigate the roles of intermediate filaments, focal adhesions, cytoplasmic properties, and cell contractility on cellular mechanical behavior.** The current research focused primarily on the mechanical effects actin and microtubules. However, these components are by no means the only factors in governing cellular mechanical behavior. Strength of attachment (via focal adhesions), intermediate filaments (typically effecting large strain behavior), cytoplasmic content, and especially in the case of vascular smooth muscle cells, contractility, all warrant future investigation. In each of these areas, existing methods and techniques exist that could be employed for investigation of their role in overall cell mechanics. Doing so will provide a more comprehensive picture of VSMC

mechanical behavior than that provided by the current research.

5. **Mechanical investigation of different cell types**. The only cell type investigated in the current research was VSMCs. However, the usefulness of these AFM techniques should be investigated using other cell types as well. It is not known whether the specific techniques and models employed in the current research will be applicable over a wide range of cell types, or if they are VSMC specific. From the perspective of a vascular researcher, the most obvious candidate would be vascular endothelial cells, given their large role in vascular disease development.

6. **2.5-D or 3-D cell culture for mechanical analysis.** Another significant drawback of the current AFM techniques, is the fact that the cells were adherent to a flat substrate (2-D culture). Although this is usually preferable to non-adherent cells (for instance tested using micropipette techniques) it still leaves a great deal to be desired in terms of replicating the *in vivo* cell environment. One possible solution to this is the fabrication of 2.5-D cell culture wells, in which cells are seeded within a depressed region of a substrate, allowing for attachment on all sides with the exception of the top plane, which would then be accessible to an AFM probe. Mechanical testing of cells in a full 3-D environment would most likely necessitate the use of techniques other than AFM, but this is certainly a research goal worth pursuing.

7. **Comparison with whole tissue (arterial) mechanics**. In the current research, the effects of various treatments on VSMC mechanical properties have been investigated. Utilizing these data, an interesting avenue of investigation would be quantifying the effects of these same treatments (e.g. paclitaxel, oxLDL) on whole arterial tissue, whether *in vivo* or *ex vivo*. Doing so will provide insight into the role of VSMC mechanics in the behavior of the artery as a whole.

8. **Frictional measurements using modified probes/cell modifications.** Although frictional measurements using chemically modified AFM probes were thus far unsuccessful, this is still an area that warrants further investigation. Building of SAMs on AFM probes is a relatively easy and reproducible process, and further investigation to better understand probe/cell interactions in the context of lateral force microscopy is warranted. Different probe materials could also be examined, in addition to chemical modification similar to that done in the current research. This is of particular importance when dealing with the effect of different stent materials on underlying cells. Varying probe speeds and mechanical loads will also yield useful data pertaining to cellular lubrication mechanisms. Lastly, modification of the cell surface could be looked at as an alternative to probe modification. Careful selection of chemical treatments that alter either the glycocalyx or plasma membrane will also provide insight into these areas.

9. **Use of primary cells.** In the current study, cells were generally utilized between passages 4 and 8. Although this is within the commonly accepted passage range for VSMC *in vitro* work, there is still the possibility of substantial changes taking place in between the time of isolation, and passage 4. As soon as cells are removed from their *in vivo* environment, certain changes will be irreversible. So, in addition to the use of earlier passage cells, this fact makes development of a 2.5 or 3D mechanical testing scaffold all the more important.
   (as suggested in #6 above) in order to replicate the *in vivo* environment as closely as possible.

10. **Quantitative analysis of cytoskeletal structure**. In the current research, descriptions of cytoskeletal architecture were largely qualitative. Future work should focus on the development of methods to quantitatively characterize the amount and orientation of cytoskeletal difference cytoskeletal components, and the correlation of those variables with viscoelastic measurements.

APPENDICES

Appendix A

Additional AFM Indentation Data

To obtain a measure of individual cell stiffness, the apparent elastic moduli of the cells were calculated using the modified Hertz models for a pyramidal indenter [173]:

$$F = \frac{1}{2^{\frac{1}{2}}} \frac{E}{(1-\upsilon^2)} \tan(\alpha)\delta^2$$

where F is the measured force (N), δ is indentation depth (m), E is apparent elastic modulus (Pa), υ is Poisson's ratio (0.5) [187], and α is cone angle of the pyramidal indenter (35°). The mean apparent elastic moduli of early passage VSMCs measured using a pyramidal probe were 72.0 ± 24.9 and 80.5 ± 18.3 kPa for serum-fed and 3-day serum-starved groups respectively ($p = 0.207$). For late-passage VSMCs measured using a pyramidal probe, the mean apparent elastic moduli were 60.2 ± 14.2 and 70.0 ± 21.4 kPa for the serum-fed and 3-day serum-starved groups respectively ($p = 0.161$), Figure A.1. Based on these data from the pyramidal AFM probes, there were no statistically significant differences in apparent elastic modulus between early-passage and late-passage serum-fed VSMCs ($p = 0.197$), or early- and late-passage 3-day serum-starved VSMCs ($p = 0.163$). However, late passage VSMCs did exhibit non-significant decreases in modulus.

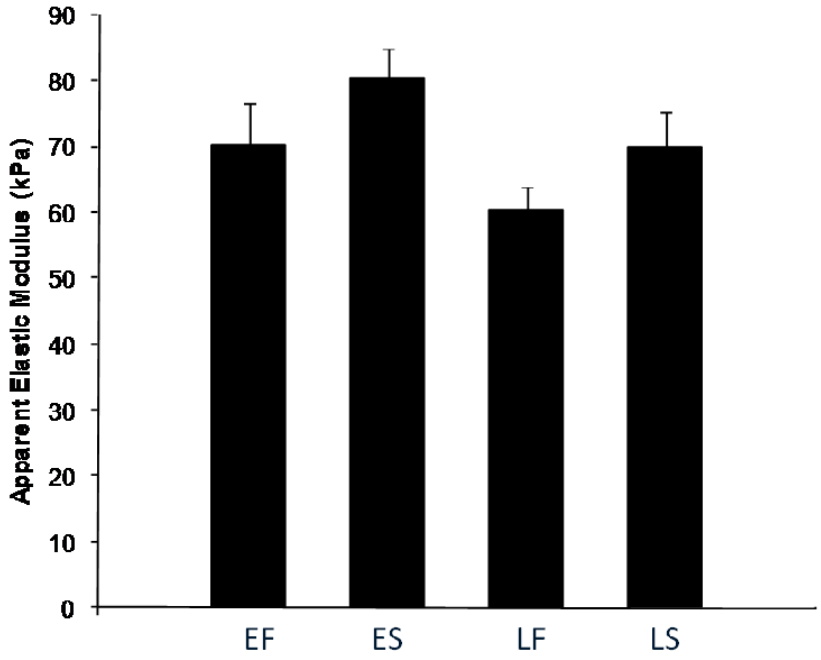

Figure A.1. VSMC apparent elastic moduli measured using a pyramidal probe. E=Early passage, L=Late passage, F=Serum fed, S=Serum starved. Data represent mean ± SE.

Elastic modulus values were significantly greater than those obtained with spherical probes for both early-passage serum-fed VSMCs ($p < 0.001$) and early-passage 3-day serum-starved VSMCs ($p < 0.001$). The cell-to-cell apparent elastic modulus COV had a mean of 28.1 ± 5.9% and 32.0 ± 9.5% for pyramidal and spherical AFM probe groups respectively. The mean COV for moduli measured at a single point were 12.9 ± 12.0% and 6.0 ± 5.3% for pyramidal tips and spherical tips respectively. Cell-to-cell apparent elastic modulus COVs and repeated indentation COVs for each experimental group are summarized in Table A.1.

Table A.1. Cell-to-Cell and Repeated Point Elastic Modulus COVs
pyr=pyramidal tip, sphere=spherical tip

	Cell-to-Cell COV (%)	Repeated Point COV (%)
Early Passage (Serum-fed, pyr)	35.2	24.3
Early Passage (3-day Serum-starved, pyr)	22.7	8.2
Early Passage (Serum-fed, sphere)	20.6	4.1
Early Passage (3-day Serum-starved, sphere)	42.3	4.2
Early Passage (5-day Serum-fed, sphere)	36.8	10.3
Early Passage (5-day Serum-starved, sphere)	28.4	5.3
Late Passage (Serum-fed, pyr)	23.7	8.1
Late Passage (Serum-starved, pyr)	30.6	11.3
All Pyramidal (mean ± SD)	28.0 ± 5.9	12.9 ± 12.0
All Spherical (mean ± SD)	32.0 ± 9.5	6.0 ± 5.3
All Serum-fed (mean ± SD)	29.0 ± 8.1	12.5 ± 12.4
All Serum-starved (mean ± SD)	31.0 ± 8.2	6.1 ± 4.1

Hysteresis was statistically significantly lower for early passage 3-day serum-starved VSMCs in both the pyramidal probe groups (0.62 ± 0.20 and 0.30 ± 0.10 for serum-fed and serum-starved respectively, $p < 0.001$) and the spherical probe groups (0.41 ± 0.08 and 0.32 ± 0.09 for serum-fed and serum-starved respectively, $p = 0.007$). Hysteresis was also statistically significantly lower in 5-day serum-starved than in serum-fed VSMCs ($p < 0.001$). There was a non-statistically significant decrease in hysteresis for late-passage serum-starved VSMCs compared to late-passage serum-fed VSMCs ($p = 0.181$). Serum-fed early-passage VSMCs exhibited statistically significantly greater levels of hysteresis than serum-fed late passage VSMCs ($p<0.001$), while no statistical difference was observed between serum-starved late- and early-passage VSMCs ($p = 0.469$). Hysteresis data are compared in Figure A.2.

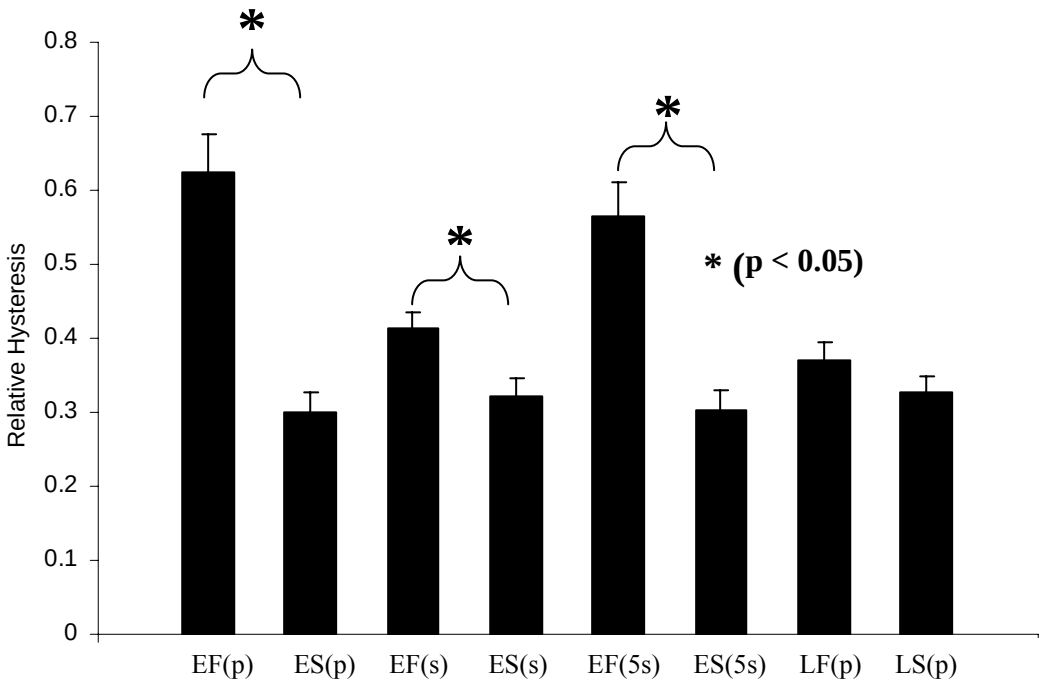

Figure A.2. Hysteresis of early (E) and late passage (L) serum fed (F) and serum starved (S) rat aortic SMCs measured with pyramidal (p) and spherical (s) AFM probes at an approach speed of 10.0 μm/s. Data are presented as mean ± SE.

There has recently been discussion in the literature regarding the efficacy of various AFM probe geometries in determining cellular mechanical properties [173]. It has been reported that mean modulus values yielded from a pyramidal AFM probe are greater than those yielded from a spherical probe [173]. Data from the current study are in agreement on this matter. It is likely that modulus data from spherical probes are more accurate, due to the relative ease of characterizing spherical contact geometry compared to pyramidal geometry, as well as the larger contact area, lesser strains at lower indentation depths, and lower COVs on a repeated point of indentation. In terms of cell-

to-cell elastic modulus variation, the present study yielded mean COVs of 28.0 ± 5.9 and 32.0 ± 9.5% for pyramidal and spherical AFM probe groups respectively, which are both towards the lower end of previously reported COVs from AFM cell indentations studies [174].

The effect of probe speed on measured elastic modulus values was investigated using a spherical indenter. Single cells were indented 5 times consecutively at both 10 μm/s and 0.5 μm/s. Apparent elastic modulus was non-significantly greater at 10 μm/s for each group tested, Figure A.3.

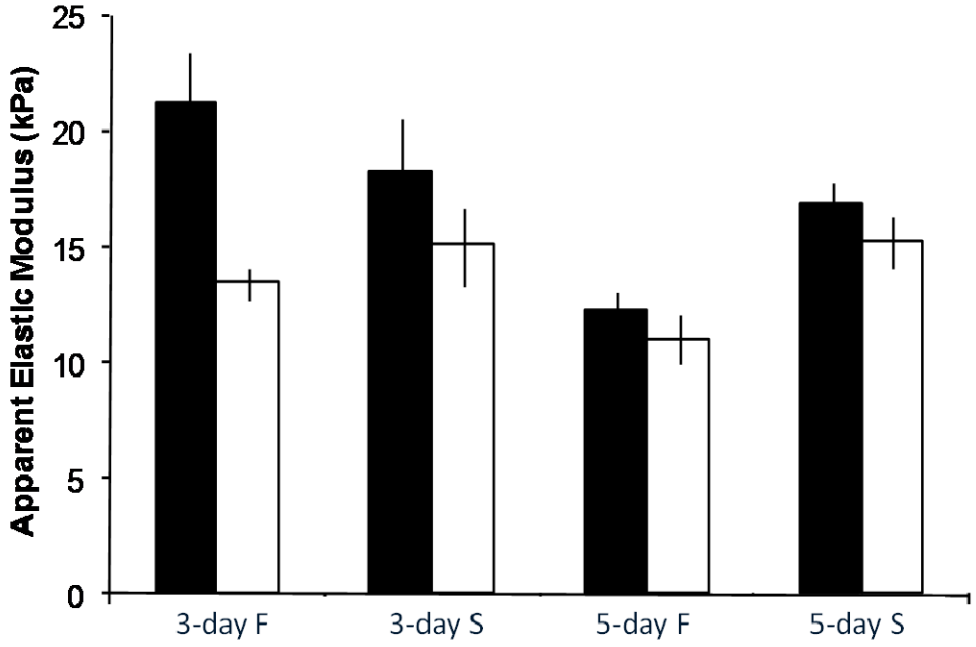

Figure A.3. VSMC apparent elastic moduli measured at indentation speeds of 10 μm/s (black) and 0.5 μm/s (white). F = Serum-fed, S=Serum-starved. Data presented as mean ± SD.

The mean COV for moduli measured at a single point were 12.9 ± 12.0% and 6.0 ± 5.3% for pyramidal tips and spherical tips respectively in the present study. Pyramidal AFM probes do however retain the advantage of enabling the user to easily switch between force and imaging mode without a change of tips and thus allow the creation of intracellular force maps and measurements of localized nanoscale mechanical property variations. The larger spherical probes are more suitable for providing "averaged" values for whole-cell mechanical behavior [146].

In vitro aging has previously been used as a model for examining changes in mechanical properties of epithelial cells in an AFM study, with the finding that *in vitro* aging led to increased cell stiffness [144]. However, in the present study, cells were found to have a slightly *decreased* modulus after *in vitro* aging (~ 15 passages). This discrepancy may be accounted for by the fact that in the current study the "early passage" cells were from passages 5 to 8, perhaps beyond the point of initial *in vitro* phenotypic changes. Data from the current study indicate that late-passage VSMCs did not respond in as significant a manner to serum starvation as early-passage VSMCs, as there were no statistically significant changes in either modulus or hysteresis. It is therefore likely, that past a certain length of time in culture, redifferentiation of VSMCs becomes increasingly difficult, and *in vitro* aging of cells renders them unusable for studies of this nature.

Appendix B

IL-6 and HIL-6 Experiments

Interleukin-6 (IL-6) and Hyper-IL-6 (HIL-6) treatment did not result in any significant changes to VSMC mechanical properties, as measured by AFM indentation and stress relaxation experiments. HIL-6 is a "designer cytokine" produced and provided by the laboratory of Professor Stefan Rose-John at the Institute of Biochemistry at the Christian Albrechts Univerity Kiel. It consists of IL-6 chemically joined to its soluble receptor, sIL-6R. Il-6 was added at a concentration of 1000 ng/ml for a period of 24 hours, while HIL-6 was added at a concentration of 10 ng/ml for 24 hours. These concentrations were based on clinically relevant serum levels of IL-6, and upon the fact that HIL-6 is 100 to 1000 times more active than IL-6 alone. Despite prior evidence that IL-6 substantially alters the cytoskeletal makeup of VSMCs, no significant effects were observed during the current research.

Appendix C

Chemical Modification of AFM Probes

Gold coated 5 um diameter spherical particle tips were utilized for the formation of self-assembled monolayers (SAMs), Figure A.4. This technique enables the creation of an AFM probe with specified chemical properties (e.g. hydrophilic/phobic, charged). For these experiments, a hydrophilic surface was created using the hydroxyl (-OH) terminated alkanethiol 11-hydroxy-1-undecanethiol (Asemblon, Redmond, WA), and a hydrophobic surface was created using the methyl ($-CH_3$) terminated alkanethiol 1-Dodecanethiol (Asemblon). In addition, a positively charged surface was created using the amine-terminated alakenthiol 11-Amino-1-undecanethiol, and a negatively charged surface was created using the carboxyl-terminated alkanethiol, 11-Mercaptoundecanoic Acid (Both from Asemblon). Briefly, 1 mmol ethanol solutions of each respective alkanethiol were made, in which the 5 μm colloidal gold coated 0.12 N/m AFM probes (NovaScan) were submerged overnight. Probes were left in the alkanethiol solution until usage.

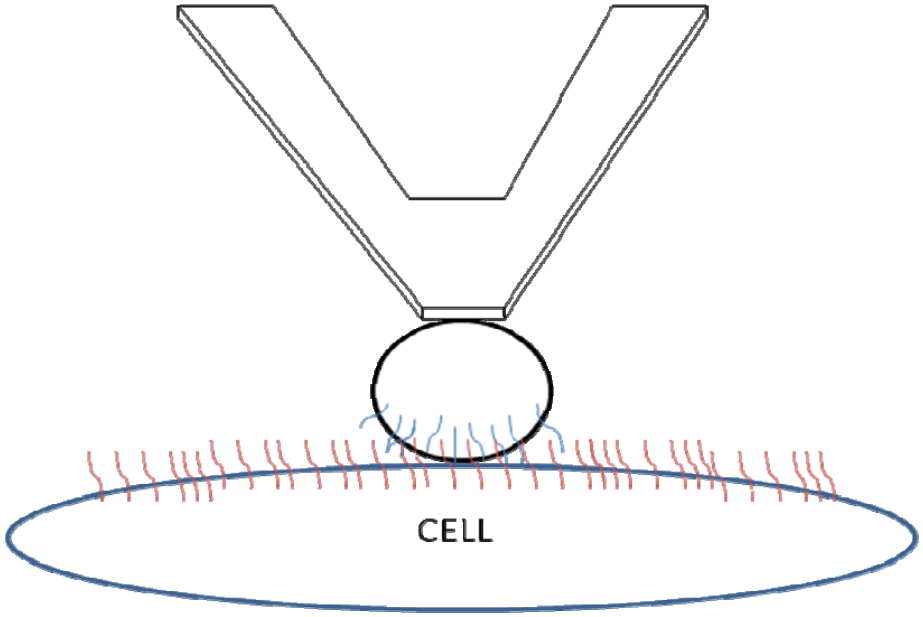

Figure A.4. Interactions between the SAM adhered to the AFM probe, and molecules at the cell surface, may allow for the elucidation of the molecular mechanisms affecting cell surface shear.

The data yielded from these experiments was unusable, although it is not known whether this is a result of instrumentation (AFM) problems or methodological difficulties. Using chemically modified AFM probes for the examination of cell surface frictional phenomena may be a viable technique for future research.

Appendix D

Membrane Permeabilization

Triton X-100 and Escin used for permeabilization of VSMC cell membrane. Triton-X resulted in complete skinning of cell, and was therefore ruled out. Escin, used at concentrations of 1000, 100, and 10 uM, permeabilized cell membrane successfully. However, immunofluorescence imaging revealed significant changes to cytoskeletal structure at higher concentrations (1000 and 100 uM), when cells were placed in PBS, DMEM, or intracellular medium. Lower escin concentrations did not alter cellular mechanical properties in any way. After reviewing these data, this aim was dropped from the current research.

Appendix E

MATLAB Scripts

Hertz Modeling Scripts:

AFMConvertAvgCells.m (reads in text files of raw AFM force curves, and converts to for force-distance or force-indentation)

```
function [Forces, M, FileNums]= AFMConvertAvgCells(Name, startnum, endnum, RampSize, spring, ds, type)

%function [Forces, M, FileNums]= AFMConvertAvgCells(Name, startnum, endnum, RampSize, spring, ds, type)
%
% AFMConvertAvgCells.m reads in text files of the raw AFM force curves (in
% Volt units) and converts it to force-distance or force-indentation
% curves. Be sure to export the data in the AFM software by doing Save As
% ASCII and make sure your do NOT export the header.
%
% Name is the basename of the files you are reading in (for example: if
%       your files are called CellForces051106.000.txt to
%       CellForces051106.099.txt then the basename is 'CellForces051106')
% startnum is the smallest file number in the range you are reading in
% endnum is the largest file number that you are reading in
% RampSize is the length in nm of the Z piezo ramp
% spring is the spring constant in N/m
% ds is the deflection sensitivity in V/nm (if you input ds = 0 and type =
%       'forces', the program will calculate the deflection sensitivity
%       from the data in the first file)
% type is either 'forces', for HRFS data, or 'indent', for nanoindentation
%       data.
%
% Forces is the matrix of distances and forces of the converted data (i.e.
%       [distApproach FApproach distRetract ForceRetract distApproach...])
% M is the raw data from each file
% FileNums is the list of the file numbers that got converted

FileNums = [];
M = [];
reply = 'y';
display('Commands:');
display ('y = yes: include this curve,');
display ('n = no: do not include this curve,');
display ('p = pass: include this curve and just do the rest of the curves (stop prompting me!),');
display ('q = quit: do not include this curve and do only the curves up to this point');
display ('b = back: go back one curve');
display('if something goes wrong and you want to stop the program completely without saving anything type cntrl-C')
```

```
reply2 = input('Name of input file of numbers? [if none, just press enter] ', 's');

if isempty(reply2),
   i = 0;
   while i <(endnum-startnum+1),
      i = i+1;
      if startnum+i-1<10
         FileName = strcat(Name,'.00', num2str(startnum+i-1),'.txt');
      elseif startnum+i-1<100
         FileName = strcat(Name,'.0', num2str(startnum+i-1),'.txt');
      else
         FileName = strcat(Name,'.', num2str(startnum+i-1),'.txt');
      end
      FileName
      fid=fopen(FileName,'r');
      if fid ~= -1
         tline1=fgetl(fid); %Read-off first line containing titles
         temp = fscanf(fid, '%f %f', [2 inf])';
         if reply ~= 'p',
            plot([linspace(RampSize, 0, length(temp))' linspace(0, RampSize, length(temp))'], temp);
            reply = input('Do you want to include this curve? y/n/p/q/b [y]: ', 's');
            if length(reply)>1,
               reply = input('           only one character please! y/n/p/q/b [y]: ', 's');
            end
            if isempty(reply)
               reply = 'y';
            end
         end
         if reply == 'y' || reply =='p',
            FileNums = [FileNums; startnum+i-1];
            M= [M temp];
         elseif reply == 'q'
            break
         elseif reply == 'b'
            i = i-2;
         end
      end
      fclose('all');
   end
else
   FileNums = load(reply2);
   for i = 1:length(FileNums),
      if FileNums(i)<10
         FileName = strcat(Name,'.00', num2str(FileNums(i)),'.txt');
      elseif FileNums(i)<100
         FileName = strcat(Name,'.0', num2str(FileNums(i)),'.txt');
      else
         FileName = strcat(Name,'.', num2str(FileNums(i)),'.txt');
      end
      FileName
      fid=fopen(FileName,'r');
      tline1=fgetl(fid); %Read-off first line containing titles
      temp = fscanf(fid, '%f %f', [2 inf])';
```

```
        M= [M temp];
        fclose('all');
    end
end
[Rrows, Rcolumns]=size(M);
NumSets=Rcolumns/2;
Samples=Rrows;
Data=M(:,:);
Forces =zeros(Samples, 4*NumSets);

for i = 1:NumSets,
    Zext = linspace(RampSize, 0, Samples)';
    Zret = linspace(0, RampSize, Samples)';
%         Defext = UnSlopeBaseCells(Zext, Data(:, i*2-1), 20)*ds;
%         Defret = UnSlopeBaseCells(Zret, Data(:, i*2), 20)*ds;
%         Defext = UnSlopeBaseCells(Sepext, Defext, 100);
%         Defret = UnSlopeBaseCells(Sepret, Defret, Samples-100);
    if type == 'forces',
        Data(:, i*2-1) = UnSlopeBaseCells2(Zext, Data(:, i*2-1), 50, 100);
        Data(:, i*2) = UnSlopeBaseCells2(Zret, Data(:, i*2), Samples-150, Samples-50);
        if ds ==0,
            temp = polyfit(Data(Rrows-50:Rrows-20, i*2-1), Zext(Rrows-50:Rrows-20), 1);
            ds = -temp(1)
        end
        Defext = (Data(:, i*2-1)-mean(Data(45:55, i*2-1)))*ds;
        Defret = (Data(:, i*2)- mean(Data(Samples-55:Samples-45, 2*i)))*ds;
    Sepext = Zext + Defext;
    Sepret = Zret + Defret;
    Defext = Defext -ones(Rrows, 1)*mean(Defext(50:100, :));
    Defret = Defret -ones(Rrows, 1)*mean(Defret(Rrows-30:Rrows-20, :));
    Sepext = Sepext -ones(Rrows, 1)*mean(Sepext(Rrows-30:Rrows-20, :));
    Sepret = Sepret -ones(Rrows, 1)*mean(Sepret(50:100, :));


    elseif type == 'indent',

    Defext = (Data(:, i*2-1))*ds;
    Defret = (Data(:, i*2))*ds;
    Sepext = Zext + Defext;
    Sepret = Zret + Defret;

    Startbase = 40;
    %Check for wacky up-down baseline from missing data during trigger mode
    %measurements when the tip is a bit too close to the sample
    while abs(Defext(Startbase)-Defext(Startbase+1))> 0.8*ds,
        Startbase = Startbase + 2;
    end
    Endbase = Startbase+50;

% If you have a lot of base line drift, then uncomment the next line to
% take out the base line drift ( you might need to change region of points
% you are fitting)
```

```
   [Defext Defret] = UnSlopeBaseCells3(Sepext, Defext, Startbase, Endbase, Sepret, Defret);

% Smooth out the data for contact point finding methods. NOTE: this is only
% used to find the 0 point. The actual data that is returned is not smoothed
% out or processed.
   DefextSmooth = Defext;
   for j=51:Samples-50,
      DefextSmooth(j) = mean(Defext(j-50:j+50));
   end

% PICK YOUR CONTACT POINT FINDING METHOD! Uncomment out the part of code
% for the the method you want to use...

   % Threshold method for picking contact point
   thresh = 2; %Threshold in nm for picking the 0 point. Change this depending on the noise level of your
data
   j = Startbase+50;
   while min(DefextSmooth(j:Samples))< thresh+min(DefextSmooth(Startbase+50:Samples)) & j<Samples
      j = j+1;
   end
   pt0val = Sepext(j);
   [Defext Defret] = UnSlopeBaseCells3(Sepext, Defext, Startbase+20, j-50, Sepret, Defret);
      DefextSmooth = Defext;
   for j=51:Samples-50,
      DefextSmooth(j) = mean(Defext(j-50:j+50));
   end

   j = Startbase+50;
   while min(DefextSmooth(j:Samples))< thresh+min(DefextSmooth(Startbase+50:Samples)) & j<Samples
      j = j+1;
   end
   pt0val = Sepext(j);

   % two region fit over whole data with moving break point.
%     DefextDeriv = polyderiv(DefextSmooth(Startbase:Samples), Zext, 10)';
%     [point0 pt0val] = FindZeroPt(Zext(Startbase+50:Samples-30), DefextDeriv(50:length(DefextDeriv)-
30), 0, 1);
%     point0= point0+Startbase+50;
%     pt0val = Sepext(point0);
%
   % moving window with 2 region fit to find contact point
%     DefextDeriv = polyderiv(DefextSmooth, Zext, 10)';
%     [point0 pt0val] = FindZeroPt2(Zext, DefextDeriv, 0, 1, 200, 100, 500);
%     pt0val = Sepext(point0);

   Sepext = -(Sepext-pt0val);
   Sepret = -(Sepret-pt0val);
   Defext = Defext ;
   Defret = Defret ;

   end
```

```
    Forces(:, i*4-3:i*4) = [Sepext Defext*spring Sepret Defret*spring];
end
```

AVERAGELOTSFORCESCELLS.m (calculates elastic modulus and hysteresis from indentation curves)

```
function [Averages, Stiffness, Eall, Hys, FilesRemoved] = AverageLotsForcesCells(Data, Files,
NumPoints)
% function [Averages, Stiffness, Eall, FilesRemoved] = AverageLotsForcesCells(Data, Files, NumPoints)
%
% AverageLotsForcesCells.m assumes Data is a matrix where the columns are
% alternating distance vectors and force vectors of data. It basically
% averages all the force curves in the matrix Data.
%
% Data is a matrix of force curves (i.e. [distances_1 Force_1 distances_2
% Force_2...] where distances_i is the vector of distances at which the
% forces in vector Force_i were taken)
%       NOTE: it is therefore assumed that Data has an even number of
%       columns
% Files is the list of file numbers (from AFMConvertAvgCells.m output)
% NumPoints is the number of points that you would like to resample at.
%
% Averages is the matrix of averaged data resampled so that it has
% NumPoints points
% Stiffness is the average and standard deviation of the elastic modulus
% for each cell or group of curves. It is calculated using the Hertz model
% Eall is the elastic modulus calculated for each individual curve
% FilesRemoved is a list with any file number that was removed from the
% averaging set by the user.

[Rows Cols] = size(Data);
Averages = [];
Stiffness = [];
CellNumber = 0;
cell = -1;
j = 1;
Approach = [];
Retract = [];
Eall = [];
Hys = [];
FilesRemoved = [];
reply2 = 'y';
InputFile = input('Input file name? [none]: ', 's');
if isempty(InputFile),
    ManualMode = 1;
else
    InputList = load(InputFile);
    SpeedNum = 1;
    TotalCells = length(InputList)/SpeedNum;
    ManualMode = 0;
```

```
end
if ManualMode,
   SpeedNum = str2num(input('How many different speeds did you use per cells? [3] ', 's'));
   TotalCells = 0;
end
reply2 = input('Check curves individually? y/n [n]: ', 's');
if isempty(reply2)
   reply2 = 'p';
elseif length(reply2)~= 1
   reply2 = input('ERROR: please answer y or n: ', 's');
end
if reply2 == 'n' || reply2 == 'p',
   reply2 = 'p';
else
   figure(1)
   hold off
end
if isempty(SpeedNum),
   SpeedNum = 3;
end
speed = 0;
while j <=length(Files),
   Approach = [];
   Retract = [];
   cell = cell +1;
   CellNumber = floor(cell/SpeedNum)+1
   if speed ==SpeedNum,
      speed =0;
   end
   speed = speed+1
   if ManualMode,
      file1 = (input('       First File Number: ', 's'));
      if file1 == 'q',
         break
      end
      temp = 1;
      if file1 ~= 's'
         file2 = (input('       Second File Number: ', 's'));
         if file2 == 'q',
            break
         end
         file1 = str2num(file1);
         file2 = str2num(file2);
      end
   elseif cell+1> TotalCells
      break
   else
      file1 = InputList(cell+1, 1);
      file2 = InputList(cell+1, 2);
   end
   temp =1;
   if file1>file2,
      display('ERROR: the first file number should be smaller than the second one')
```

```
   temp  =0;
end
while temp==1 & j<=length(Files)
   if  Files(j)<file1,
      j = j+1;
   elseif Files(j)<=file2,
      if reply2 ~= 'p',
         hold off
         plot(Data(:, j*4-3), Data(:, j*4-2));
         axis([-1000 1000 -5 20]);
         reply2 = input('Is this curve ok? y/n/p [y]: ', 's');
         if isempty(reply2)
            reply2 = 'y';
         elseif length(reply2) ~= 1,
            reply2 = input('ERROR: please answer y, n, or p only... y/n/p? ', 's');
         end
         if reply2 ~= 'n'
            Approach = [Approach Data(:, j*4-3:j*4-2)];
            Retract = [Retract Data(Rows:-1:1, j*4-1:4*j)];
            j = j+1;
         else
            reply2 = input('Try to fix it? y/n [y]: ', 's');
            if isempty(reply2)
               reply2 = 'y';
            elseif length(reply2)~= 1,
               reply2 = input('ERROR: please answer y or n only... y/n? ', 's');
            end
            if reply2 == 'n',
               FilesRemoved = [FilesRemoved; Files(j)];
               j = j+1;
            else
               xoff = 0;
               yoff =0;
               reply2 = 'n';
               while reply2 == 'n',
                  reply2 = input('x offset: ', 's');
                  xoff = xoff+str2num(reply2);
                  plot(Data(:, j*4-3)+xoff, Data(:, j*4-2)+yoff);
                  axis([0 1000 0 20]);
                  reply2 = input('y offset: ', 's');
                  yoff = yoff+str2num(reply2);
                  plot(Data(:, j*4-3)+xoff, Data(:, j*4-2)+yoff);
                  axis([0 1000 0 20]);
                  reply2 = input('is it ok now? y/n/q [y]: ', 's');
                  if isempty(reply2)
                     reply2 = 'y';
                  elseif length(reply2) ~= 1,
                     reply2 = input('ERROR: please answer y, n, or q only... y/n/q? ', 's');
                  end
               end
               if reply2 == 'y',
                  Approach = [Approach Data(:, j*4-3:j*4-2)];
                  Retract = [Retract Data(Rows:-1:1, j*4-1:4*j)];
```

```
                j = j+1;
                if j>=length(Files)
                    temp = 2;
                end
            else
                FilesRemoved = [FilesRemoved; Files(j)];
                j = j+1;
            end
        end
    end

    else
        Approach = [Approach Data(:, j*4-3:j*4-2)];
        Retract = [Retract Data(Rows:-1:1, j*4-1:4*j)];
        j = j+1;
        if j>length(Files)
        temp = 2;
        end
    end
else
    temp = 2;
end
end

if (isempty(Approach) ~=1)
    [x F Fs E Estd Et] = AverageForces(Approach, NumPoints);
    Averages = [Averages x F Fs];
    Stiffness = [Stiffness; E Estd];
    %       if Estd/E > 0.5,
    %           [E Estd]
    %           plot(x, F, '.')
    %           hold on
    %           [r c] = size(Approach);
    %           plot(Approach(:, 1:2:c), Approach(:, 2:2:c))
    %           pause
    %       end
    Eall = [Eall; Et];
    dx = x(2)-x(1);
    HysAp = sum(F(1:NumPoints))* dx;
    [x F Fs] = AverageForces(Retract, NumPoints);
    dx = x(2)-x(1);
    Hys = [Hys; (HysAp-sum(F(1:NumPoints))*dx)/HysAp];
    Averages = [Averages x(NumPoints:-1:1) F(NumPoints:-1:1) Fs(NumPoints:-1:1)];
else
    display('I was supposed to average files: ')
    file1
    display('through ')
    file2
    display('but I''m at file')
    Files(j)
    display('Either none of those files were good or there is a problem with the script input file?');
    pause
```

```
        Averages = [Averages zeros(NumPoints, 3)];
        Stiffness = [Stiffness; 0 0];
    end
end
```

Stress Relaxation Scripts:

HDRLOAD.m (reads in raw stress relaxation data)
Script from The MATHWORKS (Natick, MA)
http://www.mathworks.com/support/tech-notes/1400/1402.html

```
function [data] = hdrload(file)


% HDRLOAD Load data from an ASCII file containing a text header.
%    [header, data] = HDRLOAD('filename.ext') reads a data file
%    called 'filename.ext', which contains a text header.  There
%    is no default extension; any extensions must be explicitly
%    supplied.
%
%    The first output, HEADER, is the header information,
%    returned as a text array.
%    The second output, DATA, is the data matrix.  This data
%    matrix has the same dimensions as the data in the file, one
%    row per line of ASCII data in the file.  If the data is not
%    regularly spaced (i.e., each line of ASCII data does not
%    contain the same number of points), the data is returned as
%    a column vector.
%
%    Limitations:  No line of the text header can begin with
%    a number.  Only one header and data set will be read,
%    and the header must come before the data.
%
%    See also LOAD, SAVE, SPCONVERT, FSCANF, FPRINTF, STR2MAT.
%    See also the IOFUN directory.


% check number and type of arguments
if nargin < 1
  error('Function requires one input argument');
elseif ~isstr(file)
  error('Input must be a string representing a filename');
end


% Open the file.  If this returns a -1, we did not open the file
% successfully.
fid = fopen(file);
```

```
if fid==-1
  error('File not found or permission denied');
  end


% Initialize loop variables
% We store the number of lines in the header, and the maximum
% length of any one line in the header.  These are used later
% in assigning the 'header' output variable.
no_lines = 0;
max_line = 0;


% We also store the number of columns in the data we read.  This
% way we can compute the size of the output based on the number
% of columns and the total number of data points.
ncols = 0;


% Finally, we initialize the data to [].
data = [];


% Start processing.
line = fgetl(fid);
if ~isstr(line)
  disp('Warning: file contains no header and no data')
  end;
[data, ncols, errmsg, nxtindex] = sscanf(line, '%f');


% One slight problem, pointed out by Peter vanderWal: If the
% first character of the line is 'e', then this will scan as
% 0.00e+00. We can trap this case specifically by using the
% 'next index' output: in the case of a stripped 'e' the next
% index is one, indicating zero characters read.  See the help
% entry for 'sscanf' for more information on this output
% parameter. We loop through the file one line at a time until
% we find some data.  After that point we stop checking for
% header information. This part of the program takes most of the
% processing time, because fgetl is relatively slow (compared to
% fscanf, which we will use later).
while isempty(data)|(nxtindex==1)
  no_lines = no_lines+1;
  max_line = max([max_line, length(line)]);
  % Create unique variable to hold this line of text information.
  % Store the last-read line in this variable.
  eval(['line', num2str(no_lines), '=line;']);
  line = fgetl(fid);
  if ~isstr(line)
    disp('Warning: file contains no data')
```

```
   break
   end;
  [data, ncols, errmsg, nxtindex] = sscanf(line, '%f');
  end % while


% Now that we have read in the first line of data, we can skip
% the processing that stores header information, and just read
% in the rest of the data.
data = [data; fscanf(fid, '%f')];
fclose(fid);


% Create header output from line information. The number of lines
% and the maximum line length are stored explicitly, and each
% line is stored in a unique variable using the 'eval' statement
% within the loop. Note that, if we knew a priori that the
% headers were 10 lines or less, we could use the STR2MAT
% function and save some work. First, initialize the header to an
% array of spaces.
header = setstr(' '*ones(no_lines, max_line));
for i = 1:no_lines
  varname = ['line' num2str(i)];
  % Note that we only assign this line variable to a subset of
  % this row of the header array.  We thus ensure that the matrix
  % sizes in the assignment are equal. We also consider blank
  % header lines using the following IF statement.
  if eval(['length(' varname ')~=0'])
    eval(['header(i, 1:length(' varname ')) = ' varname ';']);
    end
  end % for


% Resize output data, based on the number of columns (as returned
% from the sscanf of the first line of data) and the total number
% of data elements. Since the data was read in row-wise, and
% MATLAB stores data in columnwise format, we have to reverse the
% size arguments and then transpose the data.  If we read in
% irregularly spaced data, then the division we are about to do
% will not work. Therefore, we will trap the error with an EVAL
% call; if the reshape fails, we will just return the data as is.
eval('data = reshape(data, ncols, length(data)/ncols)';', '');
data(:,2) = [];
```

STRESSRELAX.m (normalizes and truncates stress relaxation data)

```
% function [data_final, depth, delta_strain] = stressrelax(data, defsens, ramp)
function [data_final] = stressrelax(data)


lintime = linspace(0.01,120,12000)';
baseline_shift = mean(data(1:100));
data_shift = (data-baseline_shift);
data_small = data_shift(1:1000);
[y n] = max(data_small);
data_norm = (data_shift(n+1)).\(data_shift(n+1:n+12000));
sum(data_norm);
for i = 1:length(data_norm),
   if data_norm(i) < 0
      data_norm(i) = 0.01;
   end
end
sum(data_norm);
data_log = [log10(data_norm(1:12000))];
logtime = log10(lintime(1:12000));
time_resample = evenspc(logtime,logtime,100);
sum(data_log);
data_resample = evenspc(data_log,logtime,100);



% data_final = [[1; 10.^data_resample] [0; 10.^time_resample]];

% sum(data_temp);
% for i = 10:length(data_temp),
%     if data_temp (i) > mean(data_temp(i-2):data_temp(i-1))+1*std(data_temp(i-2):data_temp(i-1))
%        data_temp(i) = mean(data_temp(i-2):data_temp(i-1))+1*std(data_temp(i-2):data_temp(i-1));
%     elseif data_temp(i) < mean(data_temp(i-2):data_temp(i-1))-1*std(data_temp(i-2):data_temp(i-1))
%       data_temp(i) = mean(data_temp(i-2):data_temp(i-1))-1*std(data_temp(i-2):data_temp(i-1));
%
%     end
% end
%
% sum(data_temp);
data_final = [10.^data_resample 10.^time_resample];
% lintime2 = linspace(0,120,12000)';
% depth = [data_norm lintime2];
% delta_strain = (((defsens*y)-(defsens*data_norm(12000)))/depth)*100;
G120=data_final(100)

end
```

EVENSPC.m (called by stressrelax.m)

```
function [F, x] = evenspc(f, d, N)
%
% [F, x] = evenspc(f, d, N)
%
% Creates an evenly-spaced force vector
%
% f = vector of forces
% d = vector of distances
% length(f) must be the same as length(d)
% N = length of desired output force vector
%
% Example:
% forces = [1000 300 600 150];
% dists  = [100 70 20 5];
% F = evenspc(forces, dists, 200);
%
% F will be a force vector with 200 components representing
% forces at evenly-spaced distances from 100 down to 5.
% x will be a vector with 200 components representing the distance at which
% forces in F are done.
%
L = length(f);
[m, n] = size(f);
flag = 0;
if d(L)>d(1),
    d = d(L:-1:1);
    f = f(L:-1:1);
    flag =1;
end
increment = (d(L) - d(1)) / (N-1);
if n==1,
    F = zeros(N,1);
    x = linspace(d(1), d(L), N)';
else
    F = zeros(1,N);
    x = linspace(d(1), d(L), N);
end

F(1) = f(1);
F(N) = f(L);
for i=2:N-1,
  dist = d(1) + increment * (i-1);
  j = 1;
  if (i==N)
     j = L-1;
  else
   while (d(j+1) > dist & j<L-1),
        j = j + 1;
   end
```

```
  end
  % dist is now between d(1,j) and d(1,j+1)
  % let lambda be equal to "how far between" on a
  % scale of 0..1.
  lambda = (dist - d(j)) / (d(j+1) - d(j));
  % linearly interpolate the force based on lambda
  force = f(j+1) * lambda + f(j) * (1-lambda);
  F(i) = force;
end
if flag ==1,
   F = F(N:-1:1);
   x = x(N:-1:1);
end
```

THEGFUNCTION.m (Used in conjunction with QLVFIT.m to fit QLV reduced relaxation function data to stress relaxation data).

```
 function G = TheGFunction(a, t)
G = 0*t;
C = a(1);
tau1 = a(2);
tau2 = a(3);
dtau = (tau2-tau1)/800;
taus = linspace(tau1, tau2,800)';
for i = 1:length(t),
%     fun1 = @(tau) (exp(t(i)/tau)/tau);
%     fun2 = @(tau) (1/tau);
%     int1 = quad(fun1, tau1, tau2);
%     int2 = quad(fun2, tau1, tau2);
    int1 = sum(exp(-t(i)./taus)./taus)*dtau;
    int2 = sum(1./taus)*dtau;
    G(i) = (1 + C.*int1)./(1+ C.*int2);
end
```

QLVFIT.m (Used in conjunction with THEGFUNCTION.m to fit QLV reduced relaxation function data to stress relaxation data).

```
% QLVfun2 = @ (a,t) [1+a(1).*quad((exp(-t./a(2))./a(2)),a(3),a(4))] ./ [1+a(1).*quad((1./a(2)),a(3),a(4))];

%
lintime = linspace(0.01,120,12000)';
logtime = log10(lintime);
t = evenspc(logtime,logtime,100);

% t=logspace(-2,2.079,100)';
StartingVals = [1 0.05 100];
coefEsts = nlinfit(meanjasp(:,2), meanjasp(:,1), @TheGFunction, StartingVals)
xgrid = logspace(-2,2.079,100);
plot(xgrid, meanjasp(:,1), '.')
plot(xgrid, TheGFunction(coefEsts, xgrid), 'r');
hold on
fit = TheGFunction(coefEsts, xgrid)';
R = corr2(fit, meanjasp(:,1));

R2 = R^2
```

EXPONENTIALFIT.m (Used to fit power-law model to stress relaxation data)

```
t= logspace(-2,2.079,100)';
Expfun = @(a,t) a(1).*(t.^a(2));
StartingVals = [1 0];
coefEsts = nlinfit(t, CWilson5_final(:,1), Expfun, StartingVals)
xgrid = logspace(-2,2.079,100);
line(xgrid, Expfun(coefEsts, xgrid), 'Color','g');
fit = Expfun(coefEsts, xgrid)';
R = corr2(fit, CWilson5_final(:,1));
R2 = R^2
```

SLSFIT.m (Fits standard linear solid model to stress relaxation data)

```
t= logspace(-2,2.079,100)';
% a(1)=ER, a(2)=taustress, a(3)=taustrain
SLSfun = @(a,t) a(1).*(1-(1-a(2)./a(3)).*exp(-t./a(3)));
StartingVals = [1 1 1];
coefEsts = nlinfit(t, CWilson_final(:,1), SLSfun, StartingVals)
xgrid = logspace(-2,2.079,100);
line(xgrid, SLSfun(coefEsts, xgrid), 'Color','m');
fit = SLSfun(coefEsts, xgrid)';
R = corr2(fit, CWilson_final(:,1));
R2 = R^2
```

Friction Scripts:

loadFRICFILES.m (loads raw friction data)

```
% loadForceFiles

function [F]=loadForceFiles(pathName, baseName, ff, lf)
iflag_main=0;


%
F = [];
 num_datas=512;
 num_lines=16; %aspect ratio
% ff=51; %first file number
% lf=78; %last file number
% path='C:\Delphine"s Stuff\Lab Stuff\AFMData\10-19-04\102004_AggcolIS\'; %path for loading files

numfiles = lf-ff+1;

n=1;
for j=ff:lf

   if j<10,
      S=strcat(pathName, baseName,'.00',num2str(j),'.txt');
   end

   if j>=10,
      S=strcat(pathName, baseName,'.0',num2str(j),'.txt');
   end

   if j>=100,
      S=strcat(pathName, baseName,'.',num2str(j),'.txt');
   end
 S
 fid=fopen(S,'r');
    tline1=fgetl(fid); %Read-off first line containing titles
   for i=1:num_lines,
      line = fgetl(fid);
      stuff = sscanf(line, '%f', inf);
      temp_m(i, :) = stuff;
   end
    F = [F; temp_m];
    tline1=fgetl(fid); %Read-off first line containing titles
    tline1=fgetl(fid);
   for i=1:num_lines,
      line = fgetl(fid);
```

```
        stuff = sscanf(line, '%f', inf);
        temp_m(i, :) = stuff;
    end
     F = [F; temp_m];
     tline1=fgetl(fid); %Read-off first line containing titles
     tline1=fgetl(fid);
    for i=1:num_lines,
        line = fgetl(fid);
        stuff = sscanf(line, '%f', inf);
        temp_m(i, :) = stuff;
    end
     F = [F; temp_m];
    %for i=1:num_datas*num_lines
    %    line=fgetl(fid);
    %    stuff=sscanf(line,'%f %f %f');
    %    temp_m(:,i)=stuff;
    %end

%     if j == ff
%         F = load(S);
%     else
%         F = [F; load(S)];
%     end

    fclose('all');
end
```

AVERAGEHEIGHTFRICCELL.m (calculates friction values)

```
function [Friction, StDevFric, avFric, stdFric] = AverageHeightFricCell(Datas, lines)
% [AvgHeight StDevHeight Height Friction StDevFric] =
% AverageHeightFric(Datas, Positions, lines, stagg, endagg)
% % Datas is the set of data with trace, retrace of the friction signal,
% and height.
% % Postitions is either 'midd' or 'side'. 'midd' is if your pattern is
% in
% % the middle of the image (so for example, if you have polymer in the
% % middle and some SAM outside). 'side' assumes that your pattern takes
% up
% % one side of the image (so for example the polymer is on the left side
% and
% % the SAM is on the right side of the image)
% lines is the number of lines per set of data (8, or 16 usually)
% stagg is the index at which the pattern starts
% endagg is the index at which the pattern ends (if you are using
% 'side' position then endagg doesn't matter)
%
% see also AverageHeight (if you only have height data and no friction)

[rows cols] = size(Datas);
numData = rows/(3*lines);

HeightDatas = zeros(lines, cols);
StepHeights = zeros(lines, 1);
TraceDatas = HeightDatas;
ReTraceDatas = HeightDatas;
Frics = zeros(lines,cols);

blck = lines*3;

Height = zeros(numData*lines,1);
AvgHeight = zeros(numData,1);
StDevHeight = AvgHeight;
Friction = zeros(numData*lines,1);
StDevFric = Friction;

for i = 1:numData,
   HeightDatas = Datas(i*blck-blck+1:i*blck, :);
   TraceDatas = Datas(i*blck-blck+lines+1:i*blck-blck+2*lines, :);
   ReTraceDatas = Datas(i*blck-blck+2*lines+1:i*blck-blck+3*lines, :);
      Frics = (TraceDatas-ReTraceDatas)/2;
         Friction((i-1)*lines+1: i*lines) = mean(Frics, 2);
         StDevFric((i-1)*lines+1: i*lines) = std(Frics, 0, 2);
         avFric(i) = mean(mean(Frics, 2));
         stdFric(i) = std(mean(Frics, 2));
         temp = [];
```

```
        for j = 1:lines
            if Friction((i-1)*lines+j) < avFric(i)+2*stdFric(i) & Friction((i-1)*lines+j) > avFric(i)-
2*stdFric(i)
                temp = [temp; Friction((i-1)*lines+j)];
            else
                sprintf('deleted block %i line %i', i, j)
            end
        end
        avFric(i) = mean(mean(temp, 2));
        stdFric(i) = std(mean(temp, 2));

%           Friction((i-1)*lines+j,1) = mean(Frics(stagg+20:cols-50),
% 2);
% %           Friction((i-1)*lines+j,2) = mean(Frics(50:stagg-20), 2);
% %           StDevFric((i-1)*lines+j,1) = std(Frics(stagg+20:cols-50),
% 2);
%           StDevFric((i-1)*lines+j,2) = std(Frics(50:stagg-20), 2);
       AvgHeight(i) = mean(Height((i-1)*lines+1:i*lines));
      StDevHeight(i) = std(Height((i-1)*lines+1:i*lines));
   end
end
```

Appendix F

Reagent Dilutions

Cytochalasin D (Sigma):

507.62 g/mol
Start w/ 1 mg in powder form
Dilute into 1 ml DMSO (1 mg/ml)
Aliquot into 20 vials, each with 50 uL
For 10 uM, add 25 uL from vial to 5 ml of media in well

Nocodazole (Sigma):

301 g/mol
Start w/ 10 mg in powder form
Dilute into 2 ml DMSO (5 mg/ml)
Aliquot into 20 vials, each with 0.1 ml
For 20 uM, add 6 uL from vial to 5 ml of media in well

Paclitaxel (Sigma):

853.9 g/mol
Start w/ 5 mg in powder form
Dilute into 1 ml DMSO (5 mg/ml)
Aliquot into 10 vials, each with 100 uL
For 10 uM, add 8.5 uL from vial to 5 ml media

Jasplakinolide (Sigma):

710 g/mol
Start w/ 50 ug
Dilute into 0.1 ml DMSO (0.5 mg/ml)
Aliquot into 5 vials, each with 20 ul
For 1 uM: dilute 7 ul from stock into 5 ml media

Amine-Terminated SAM (11-Amino-1-undecanethiol) (Asemblon):

1 mmol = 0.0024 g/ 10 ml

Carboxyl-Terminated SAM (11-Mercaptoundecanoic Acid) (Asemblon):

1 mmol = 0.0022 g/10 ml

Hydroxy-Terminated SAM (11-Hydroxy-1-undecanethiol) (Asemblon):

1 mmol = 0.002 g / 10 ml

Methyl-Terminated SAM (1-Dodecanethiol) (Asemblon):

1 mmol = 0.002 g / 10 ml

CellMask Plasma Membrane Stain (Invitrogen):

Stock is 5 mg/ml in DMSO (total of 100 uL = 500 ug)
Stock Conc. = 5 ug/uL
Working Conc. = 5 ug/ml
Dilute 1 ul stock per ml working solution, or 1.5 ul per ml for 7.5 ug/ml
Incubate for 10 minutes @ 37 C

OxLDL (Biomedical Technologies):

(Comes in 1 ml vial with 2 mg per vial) for 0.05 mg/ml, add 0.025 ml per ml DMEM; for 0.025 mg/ml, add 0.0125 ml per ml DMEM; for 0.01 mg/ml, add 0.005 ml per ml DMEM

LDL (Biomedical Technologies):

(Comes in 5 mg per 1.0 ml per vial); for 0.05 mg/ml, add 0.01 ml per ml DMEM; for 0.025 mg/ml, add 0.005 ml per ml DMEM; for 0.01 mg/ml, add 0.002 ml per ml DMEM

Chondroitinase ABC (Sigma):

Reconstitute in a 0.01% aqueous bovine serum albumin solution. Subsequent dilutions can be made into a buffer containing 50 mM Tris, pH 8.0, 60 mM sodium acetate, and 0.02% bovine serum albumin. Solutions should be prepared fresh.
Sodium acetate = 82.03 g/mol
Sodium acetate (60mM) = 4.9 g/L = 0.005 g/ml = 0.05 g/10ml
Tris = 121.1 g/mol
Tris (50mM) = 6 g/L = 0.006 g/ml = 0.06 g/10ml
0.01% BSA = 0.0001 g/ml = 0.001 g/10ml

Heparinase III (Sigma):

This enzyme can be reconstituted in 20 mM Tris-HCl pH 7.5, containing 0.1mg/ml BSA and 4 mM CaCl2

$CaCl_2$ = 111 g/mol
$CaCl_2$ (4mM) = 0.444 g/L = 0.0004 g/ml = 0.004 g/10ml
Tris (20 mM) = 2.4 g/L = 0.002 g/ml = 0.02 g/10ml

REFERENCES

1. Lusis, A.J., *Atherosclerosis.* Nature, 2000. **407**(6801): p. 233-41.

2. Lucas, A.R., R. Korol, and C.J. Pepine, *Inflammation in atherosclerosis: some thoughts about acute coronary syndromes.* Circulation, 2006. **113**(17): p. e728-32.

3. Shaw, A. and Q. Xu, *Biomechanical stress-induced signaling in smooth muscle cells: an update.* Curr Vasc Pharmacol, 2003. **1**(1): p. 41-58.

4. Owens, G.K., M.S. Kumar, and B.R. Wamhoff, *Molecular regulation of vascular smooth muscle cell differentiation in development and disease.* Physiol Rev, 2004. **84**(3): p. 767-801.

5. Dzau, V.J., R.C. Braun-Dullaeus, and D.G. Sedding, *Vascular proliferation and atherosclerosis: new perspectives and therapeutic strategies.* Nat Med, 2002. **8**(11): p. 1249-56.

6. Kaperonis, E.A., et al., *Inflammation and atherosclerosis.* Eur J Vasc Endovasc Surg, 2006. **31**(4): p. 386-93.

7. Steffens, S. and F. Mach, *Inflammation and atherosclerosis.* Herz, 2004. **29**(8): p. 741-48.

8. Jerome, W.G., *Advanced atherosclerotic foam cell formation has features of an acquired lysosomal storage disorder.* Rejuvenation Res, 2006. **9**(2): p. 245-55.

9. Navab, M., et al., *The Yin and Yang of oxidation in the development of the fatty streak. A review based on the 1994 George Lyman Duff Memorial Lecture.* Arterioscler Thromb Vasc Biol, 1996. **16**(7): p. 831-42.

10. Knowles, J.W., et al., *Enhanced atherosclerosis and kidney dysfunction in eNOS(-/-)Apoe(-/-) mice are ameliorated by enalapril treatment.* J Clin Invest, 2000. **105**(4): p. 451-58.

11. Aikawa, M., et al., *Lipid lowering reduces oxidative stress and endothelial cell activation in rabbit atheroma.* Circulation, 2002. **106**(11): p. 1390-96.

12. Maier, J.A., et al., *Induction of human endothelial cell growth by mildly oxidized low density lipoprotein.* Atherosclerosis, 1996. **123**(1-2): p. 115-21.

13. Gimbrone, M.A., Jr., et al., *Endothelial dysfunction, hemodynamic forces, and atherogenesis.* Ann N Y Acad Sci, 2000. **902**: p. 230-9; discussion 239-40.

14. Davies, M.J., et al., *The expression of the adhesion molecules ICAM-1, VCAM-1, PECAM, and E-selectin in human atherosclerosis.* J Pathol, 1993. **171**(3): p. 223-29.

15. Blankenberg, S., S. Barbaux, and L. Tiret, *Adhesion molecules and atherosclerosis.* Atherosclerosis, 2003. **170**(2): p. 191-203.

16. Adams, D.H. and S. Shaw, *Leucocyte-endothelial interactions and regulation of leucocyte migration.* Lancet, 1994. **343**(8901): p. 831-36.

17. Sakai, A., et al., *P-selectin and vascular cell adhesion molecule-1 are focally expressed in aortas of hypercholesterolemic rabbits before intimal accumulation of macrophages and T lymphocytes.* Arterioscler Thromb Vasc Biol, 1997. **17**(2): p. 310-16.

18. Wong, C.W., T. Christen, and B.R. Kwak, *Connexins in leukocytes: shuttling messages?* Cardiovasc Res, 2004. **62**(2): p. 357-67.

19. Raines, E.W. and N. Ferri, *Thematic review series: The immune system and atherogenesis. Cytokines affecting endothelial and smooth muscle cells in vascular disease.* J Lipid Res, 2005. **46**(6): p. 1081-92.

20. Tousoulis, D., et al., *Pro-inflammatory cytokines in acute coronary syndromes: from bench to bedside.* Cytokine Growth Factor Rev, 2006. **17**(4): p. 225-33.

21. Li, H., M.W. Freeman, and P. Libby, *Regulation of smooth muscle cell scavenger receptor expression in vivo by atherogenic diets and in vitro by cytokines.* J Clin Invest, 1995. **95**(1): p. 122-33.

22. Jawien, A., et al., *Platelet-derived growth factor promotes smooth muscle migration and intimal thickening in a rat model of balloon angioplasty.* J Clin Invest, 1992. **89**(2): p. 507-11.

23. Rectenwald, J.E., et al., *Direct evidence for cytokine involvement in neointimal hyperplasia.* Circulation, 2000. **102**(14): p. 1697-702.

24. Pan, J.H., et al., *Macrophage migration inhibitory factor deficiency impairs atherosclerosis in low-density lipoprotein receptor-deficient mice.* Circulation, 2004. **109**(25): p. 3149-53.

25. Barani, J., et al., *Inflammatory mediators are associated with 1-year mortality in critical limb ischemia.* J Vasc Surg, 2005. **42**(1): p. 75-80.

26. Elhage, R., et al., *Reduced atherosclerosis in interleukin-18 deficient apolipoprotein E-knockout mice.* Cardiovasc Res, 2003. **59**(1): p. 234-40.

27. Pinderski, L.J., et al., *Overexpression of interleukin-10 by activated T lymphocytes inhibits atherosclerosis in LDL receptor-deficient Mice by altering lymphocyte and macrophage phenotypes.* Circ Res, 2002. **90**(10): p. 1064-71.

28. Smith, J.D., et al., *Decreased atherosclerosis in mice deficient in both macrophage colony-stimulating factor (op) and apolipoprotein E.* Proc Natl Acad Sci U S A, 1995. **92**(18): p. 8264-68.

29. Halayko, A.J. and J. Solway, *Molecular mechanisms of phenotypic plasticity in smooth muscle cells.* J Appl Physiol, 2001. **90**(1): p. 358-68.

30. Panettieri, R.A., Jr., *Airway smooth muscle: an immunomodulatory cell.* J Allergy Clin Immunol, 2002. **110**(6 Suppl): p. S269-74.

31. Morikawa, S., et al., *Abnormalities in pericytes on blood vessels and endothelial sprouts in tumors.* Am J Pathol, 2002. **160**(3): p. 985-1000.

32. Stegemann, J.P., H. Hong, and R.M. Nerem, *Mechanical, biochemical, and extracellular matrix effects on vascular smooth muscle cell phenotype.* J Appl Physiol, 2005. **98**(6): p. 2321-27.

33. Frid, M.G., E.P. Moiseeva, and K.R. Stenmark, *Multiple phenotypically distinct smooth muscle cell populations exist in the adult and developing bovine pulmonary arterial media in vivo.* Circ Res, 1994. **75**(4): p. 669-81.

34. Heldin, C.H., A. Ostman, and L. Ronnstrand, *Signal transduction via platelet-derived growth factor receptors.* Biochim Biophys Acta, 1998. **1378**(1): p. F79-113.

35. Holycross, B.J., et al., *Platelet-derived growth factor-BB-induced suppression of smooth muscle cell differentiation.* Circ Res, 1992. **71**(6): p. 1525-32.

36. Adam, P.J., et al., *Positive- and negative-acting Kruppel-like transcription factors bind a transforming growth factor beta control element required for expression of the smooth muscle cell differentiation marker SM22alpha in vivo.* J Biol Chem, 2000. **275**(48): p. 37798-806.

37. Galis, Z.S. and J.J. Khatri, *Matrix metalloproteinases in vascular remodeling and atherogenesis: the good, the bad, and the ugly.* Circ Res, 2002. **90**(3): p. 251-62.

38. Raines, E.W., *The extracellular matrix can regulate vascular cell migration, proliferation, and survival: relationships to vascular disease.* Int J Exp Pathol, 2000. **81**(3): p. 173-82.

39. Hayward, I.P., et al., *Effect of extracellular matrix proteins on vascular smooth muscle cell phenotype.* Cell Biol Int, 1995. **19**(10): p. 839-46.

40. Prockop, D.J. and K.I. Kivirikko, *Collagens: molecular biology, diseases, and potentials for therapy.* Annu Rev Biochem, 1995. **64**: p. 403-34.

41. Rosenbloom, J., W.R. Abrams, and R. Mecham, *Extracellular matrix 4: the elastic fiber.* Faseb J, 1993. **7**(13): p. 1208-18.

42. Ross, R., *The pathogenesis of atherosclerosis: a perspective for the 1990s.* Nature, 1993. **362**(6423): p. 801-9.

43. Clowes, A.W., M.M. Clowes, and M.A. Reidy, *Kinetics of cellular proliferation after arterial injury. III. Endothelial and smooth muscle growth in chronically denuded vessels.* Lab Invest, 1986. **54**(3): p. 295-303.

44. Voss, B. and J. Rauterberg, *Localization of collagen types I, III, IV and V, fibronectin and laminin in human arteries by the indirect immunofluorescence method.* Pathol Res Pract, 1986. **181**(5): p. 568-75.

45. Thyberg, J., et al., *Phenotypic modulation of smooth muscle cells after arterial injury is associated with changes in the distribution of laminin and fibronectin.* J Histochem Cytochem, 1997. **45**(6): p. 837-46.

46. Pickering, J.G., et al., *alpha5beta1 integrin expression and luminal edge fibronectin matrix assembly by smooth muscle cells after arterial injury.* Am J Pathol, 2000. **156**(2): p. 453-65.

47. Molloy, C.J., D.S. Taylor, and J.E. Pawlowski, *Novel cardiovascular actions of the activins.* J Endocrinol, 1999. **161**(2): p. 179-85.

48. Thubrikar, M.J. and F. Robicsek, *Pressure-induced arterial wall stress and atherosclerosis.* Ann Thorac Surg, 1995. **59**(6): p. 1594-603.

49. Jockusch, B.M., et al., *The molecular architecture of focal adhesions.* Annu Rev Cell Dev Biol, 1995. **11**: p. 379-416.

50. Moiseeva, E.P., *Adhesion receptors of vascular smooth muscle cells and their functions.* Cardiovasc Res, 2001. **52**(3): p. 372-86.

51. Liu, S., et al., *Binding of paxillin to alpha4 integrins modifies integrin-dependent biological responses.* Nature, 1999. **402**(6762): p. 676-81.

52. Cipolla, M.J., N.I. Gokina, and G. Osol, *Pressure-induced actin polymerization in vascular smooth muscle as a mechanism underlying myogenic behavior.* Faseb J, 2002. **16**(1): p. 72-6.

53. Low, R.B., et al., *Actin content of normal and of bleomycin-fibrotic rat lung.* Am Rev Respir Dis, 1984. **129**(2): p. 311-16.

54. Antoniades, H.N., *Human platelet-derived growth factor (PDGF): purification of PDGF-I and PDGF-II and separation of their reduced subunits.* Proc Natl Acad Sci U S A, 1981. **78**(12): p. 7314-17.

55. Li, C. and Q. Xu, *Mechanical stress-initiated signal transductions in vascular smooth muscle cells.* Cell Signal, 2000. **12**(7): p. 435-45.

56. Ohya, Y., et al., *Stretch-activated channels in arterial smooth muscle of genetic hypertensive rats.* Hypertension, 1998. **31**(1 Pt 2): p. 254-58.

57. Mills, I., et al., *Strain activation of bovine aortic smooth muscle cell proliferation and alignment: study of strain dependency and the role of protein kinase A and C signaling pathways.* J Cell Physiol, 1997. **170**(3): p. 228-34.

58. Bornfeldt, K.E. and E.G. Krebs, *Crosstalk between protein kinase A and growth factor receptor signaling pathways in arterial smooth muscle.* Cell Signal, 1999. **11**(7): p. 465-77.

59. Xu, Q., et al., *Induction of mitogen-activated protein kinase phosphatase-1 during acute hypertension.* Hypertension, 1997. **30**(1 Pt 1): p. 106-11.

60. Perlman, H., et al., *Evidence for the rapid onset of apoptosis in medial smooth muscle cells after balloon injury.* Circulation, 1997. **95**(4): p. 981-87.

61. Xu, Q., et al., *Acute hypertension activates mitogen-activated protein kinases in arterial wall.* J Clin Invest, 1996. **97**(2): p. 508-14.

62. Cattaruzza, M., et al., *Deformation-induced endothelin B receptor-mediated smooth muscle cell apoptosis is matrix-dependent.* Cell Death Differ, 2002. **9**(2): p. 219-26.

63. Mayr, M., et al., *Mechanical stress-induced DNA damage and rac-p38MAPK signal pathways mediate p53-dependent apoptosis in vascular smooth muscle cells.* Faseb J, 2002. **16**(11): p. 1423-25.

64. Lee, R.T., et al., *Mechanical strain induces specific changes in the synthesis and organization of proteoglycans by vascular smooth muscle cells.* J Biol Chem, 2001. **276**(17): p. 13847-51.

65. Zou, Y., et al., *Reduced neointima hyperplasia of vein bypass grafts in intercellular adhesion molecule-1-deficient mice.* Circ Res, 2000. **86**(4): p. 434-40.

66. Winslow, R.D., S.K. Sharma, and M.C. Kim, *Restenosis and drug-eluting stents.* Mt Sinai J Med, 2005. **72**(2): p. 81-9.

67. Santin, M., P. Colombo, and G. Bruschi, *Interfacial biology of in-stent restenosis.* Expert Rev Med Devices, 2005. **2**(4): p. 429-43.

68. Kivela, A. and J. Hartikainen, *Restenosis related to percutaneous coronary intervention has been solved?* Ann Med, 2006. **38**(3): p. 173-87.

69. Vernhet, H., et al., *Arterial stenting and overdilation: does it change wall mechanics in small-caliber arteries?* J Endovasc Ther, 2002. **9**(6): p. 855-62.

70. Ott, I., et al., *Procoagulant inflammatory responses of monocytes after direct balloon angioplasty in acute myocardial infarction.* Am J Cardiol, 1998. **82**(8): p. 938-42.

71. Komatsu, R., et al., *Neointimal tissue response at sites of coronary stenting in humans: macroscopic, histological, and immunohistochemical analyses.* Circulation, 1998. **98**(3): p. 224-33.

72. Kornowski, R., et al., *In-stent restenosis: contributions of inflammatory responses and arterial injury to neointimal hyperplasia.* J Am Coll Cardiol, 1998. **31**(1): p. 224-30.

73. Southgate, K.M., et al., *Upregulation of basement membrane-degrading metalloproteinase secretion after balloon injury of pig carotid arteries.* Circ Res, 1996. **79**(6): p. 1177-87.

74. Dollery, C.M., et al., *Expression of tissue inhibitor of matrix metalloproteinases 1 by use of an adenoviral vector inhibits smooth muscle cell migration and reduces neointimal hyperplasia in the rat model of vascular balloon injury.* Circulation, 1999. **99**(24): p. 3199-205.

75. Bauters, C., et al., *Proto-oncogene expression in rabbit aorta after wall injury. First marker of the cellular process leading to restenosis after angioplasty?* Eur Heart J, 1992. **13**(4): p. 556-59.

76. Korkmaz, M.E., et al., *Carbon coating of stents has no effect on inflammatory response to primary stent deployment.* Angiology, 2002. **53**(5): p. 563-68.

77. Gaspardone, A. and F. Versaci, *Coronary stenting and inflammation.* Am J Cardiol, 2005. **96**(12A): p. 65L-70L.

78. Muller-Hulsbeck, S., et al., *Flow patterns from metallic vascular endoprostheses: in vitro results.* Eur Radiol, 2001. **11**(5): p. 893-901.

79. Vernhet, H., et al., *Wall mechanics of the stented rabbit aorta: long-term study and correlation with histological findings.* J Endovasc Ther, 2003. **10**(3): p. 577-84.

80. Sudhir, K., et al., *Mechanical strain stimulates a mitogenic response in coronary vascular smooth muscle cells via release of basic fibroblast growth factor.* Am J Hypertens, 2001. **14**(11 Pt 1): p. 1128-34.

81. Farb, A., et al., *Pathology of acute and chronic coronary stenting in humans.* Circulation, 1999. **99**(1): p. 44-52.

82. Farb, A., et al., *Extracellular matrix changes in stented human coronary arteries.* Circulation, 2004. **110**(8): p. 940-47.

83. Farb, A., et al., *Pathological mechanisms of fatal late coronary stent thrombosis in humans.* Circulation, 2003. **108**(14): p. 1701-6.

84. Del Rizzo, D.F., et al., *Platelet-derived growth factor-induced expression of c-fos in human vascular smooth muscle cells: implications for long-term graft patency.* Ann Thorac Surg, 2002. **74**(1): p. 90-5.

85. Chung, I.M., et al., *Enhanced extracellular matrix accumulation in restenosis of coronary arteries after stent deployment.* J Am Coll Cardiol, 2002. **40**(12): p. 2072-81.

86. Skowasch, D., et al., *Pathogen burden, inflammation, proliferation and apoptosis in human in-stent restenosis. Tissue characteristics compared to primary atherosclerosis.* J Vasc Res, 2004. **41**(6): p. 525-34.

87. Kastrati, A., et al., *Restenosis after coronary stent placement and randomization to a 4-week combined antiplatelet or anticoagulant therapy: six-month angiographic follow-up of the Intracoronary Stenting and Antithrombotic Regimen (ISAR) Trial.* Circulation, 1997. **96**(2): p. 462-67.

88. Virmani, R., *Self-expanding stent deployment strategies may be the key to reducing in-stent restenosis.* Catheter Cardiovasc Interv, 2002. **56**(4): p. 487-88.

89. Cafri, C., et al., *Low-pressure deployment of stents: short- and long-term outcome.* Coron Artery Dis, 2001. **12**(4): p. 313-16.

90. Briguori, C., et al., *In-stent restenosis in small coronary arteries: impact of strut thickness.* J Am Coll Cardiol, 2002. **40**(3): p. 403-9.

91. Lau, K.W., et al., *A stent is not just a stent: Stent construction and design do matter in its clinical performance.* Singapore Med J, 2004. **45**(7): p. 305-11.

92. Moreno, R., et al., *Coronary stenting versus balloon angioplasty in small vessels: a meta-analysis from 11 randomized studies.* J Am Coll Cardiol, 2004. **43**(11): p. 1964-72.

93. Ruygrok, P.N., et al., *Vessel caliber and restenosis: a prospective clinical and angiographic study of NIR stent deployment in small and large coronary arteries in the same patient.* Catheter Cardiovasc Interv, 2003. **59**(2): p. 165-71.

94. Kocijan, A., I. Milosev, and B. Pihlar, *The influence of complexing agent and proteins on the corrosion of stainless steels and their metal components.* J Mater Sci Mater Med, 2003. **14**(1): p. 69-77.

95. Mikhalovska, L.I., et al., *Fibrinogen adsorption and platelet adhesion to metal and carbon coatings.* Thromb Haemost, 2004. **92**(5): p. 1032-39.

96. Huang, N., et al., *Hemocompatibility of titanium oxide films.* Biomaterials, 2003. **24**(13): p. 2177-87.

97. De Scheerder, I., et al., *Evaluation of the biocompatibility of two new diamond-like stent coatings (Dylyn) in a porcine coronary stent model.* J Invasive Cardiol, 2000. **12**(8): p. 389-94.

98. vom Dahl, J., et al., *Effects of gold coating of coronary stents on neointimal proliferation following stent implantation.* Am J Cardiol, 2002. **89**(7): p. 801-5.

99. Heublein, B., K. Pethig, and A.M. Elsayed, *Silicon Carbide Coating N A Semiconducting Hybrid Design of Coronary Stents N A Feasibility Study.* J Invasive Cardiol, 1998. **10**(5): p. 255-262.

100. Malik, N., et al., *Phosphorylcholine-coated stents in porcine coronary arteries: in vivo assessment of biocompatibility.* J Invasive Cardiol, 2001. **13**(3): p. 193-201.

101. Wohrle, J., et al., *Comparison of the heparin coated vs the uncoated Jostent--no influence on restenosis or clinical outcome.* Eur Heart J, 2001. **22**(19): p. 1808-16.

102. Fajadet, J., et al., *Maintenance of long-term clinical benefit with sirolimus-eluting coronary stents: three-year results of the RAVEL trial.* Circulation, 2005. **111**(8): p. 1040-44.

103. Silber, S., *[When are drug-eluting stents effective? A critical analysis of the presently available data]*. Z Kardiol, 2004. **93**(9): p. 649-63.

104. Poon, M., et al., *Rapamycin inhibits vascular smooth muscle cell migration.* J Clin Invest, 1996. **98**(10): p. 2277-83.

105. Marx, S.O., et al., *Rapamycin-FKBP inhibits cell cycle regulators of proliferation in vascular smooth muscle cells.* Circ Res, 1995. **76**(3): p. 412-17.

106. Marchetti, M., *Drug-eluting stents: from evidence to policy.* Expert Rev Med Devices, 2004. **1**(1): p. 49-63.

107. Tanabe, K., et al., *TAXUS III Trial: in-stent restenosis treated with stent-based delivery of paclitaxel incorporated in a slow-release polymer formulation.* Circulation, 2003. **107**(4): p. 559-64.

108. Gomes, W.J. and E. Buffolo, *Coronary stenting and inflammation: implications for further surgical and medical treatment.* Ann Thorac Surg, 2006. **81**(5): p. 1918-25.

109. Tung, R., et al., *Narrative review: drug-eluting stents for the management of restenosis: a critical appraisal of the evidence.* Ann Intern Med, 2006. **144**(12): p. 913-19.

110. Lim, C.T., E.H. Zhou, and S.T. Quek, *Mechanical models for living cells--a review.* J Biomech, 2006. **39**(2): p. 195-216.

111. Janmey, P.A. and D.A. Weitz, *Dealing with mechanics: mechanisms of force transduction in cells.* Trends Biochem Sci, 2004. **29**(7): p. 364-70.

112. Stamenovic, D. and D.E. Ingber, *Models of cytoskeletal mechanics of adherent cells.* Biomech Model Mechanobiol, 2002. **1**(1): p. 95-108.

113. Stamenovic, D., *Microtubules may harden or soften cells, depending of the extent of cell distension.* J Biomech, 2005. **38**(8): p. 1728-32.

114. Humphrey, J.D., *Continuum biomechanics of soft biological tissues.* Proceedings of the Royal Society of London Series a-Mathematical Physical and Engineering Sciences, 2003. **459**(2029): p. 3-46.

115. Ingber, D.E., *Mechanobiology and diseases of mechanotransduction.* Ann Med, 2003. **35**(8): p. 564-77.

116. Ingber, D.E., *Cellular mechanotransduction: putting all the pieces together again.* Faseb J, 2006. **20**(7): p. 811-27.

117. Chicurel, M.E., C.S. Chen, and D.E. Ingber, *Cellular control lies in the balance of forces.* Curr Opin Cell Biol, 1998. **10**(2): p. 232-39.

118. Wang, J.H. and B.P. Thampatty, *An introductory review of cell mechanobiology.* Biomech Model Mechanobiol, 2006. **5**(1): p. 1-16.

119. Wang, N., J.P. Butler, and D.E. Ingber, *Mechanotransduction across the cell surface and through the cytoskeleton.* Science, 1993. **260**(5111): p. 1124-27.

120. Burridge, K. and M. Chrzanowska-Wodnicka, *Focal adhesions, contractility, and signaling.* Annu Rev Cell Dev Biol, 1996. **12**: p. 463-518.

121. Galbraith, C.G., K.M. Yamada, and M.P. Sheetz, *The relationship between force and focal complex development.* J Cell Biol, 2002. **159**(4): p. 695-705.

122. Riveline, D., et al., *Focal contacts as mechanosensors: externally applied local mechanical force induces growth of focal contacts by an mDia1-dependent and ROCK-independent mechanism.* J Cell Biol, 2001. **153**(6): p. 1175-86.

123. Stamenovic, D., et al., *Effect of the cytoskeletal prestress on the mechanical impedance of cultured airway smooth muscle cells.* J Appl Physiol, 2002. **92**(4): p. 1443-50.

124. Sachs, F. and M. Sokabe, *Stretch-activated ion channels and membrane mechanics.* Neurosci Res Suppl, 1990. **12**: p. S1-4.

125. Matsumoto, T., et al., *Smooth muscle cells freshly isolated from rat thoracic aortas are much stiffer than cultured bovine cells: Possible effect of phenotype.* JSME International Journal Series C-Mechanical Systems Machine Elements and Manufacturing, 2000. **43**(4): p. 867-74.

126. Miyazaki, H., Y. Hasegawa, and K. Hayashi, *Tensile properties of contractile and synthetic vascular smooth muscle cells.* Jsme International Journal Series C-Mechanical Systems Machine Elements and Manufacturing, 2002. **45**(4): p. 870-79.

127. Nagayama, K., et al., *Effiect of actin filament distribution on tensile properties of smooth muscle cells obtained from rat thoracic aortas.* J Biomech, 2006. **39**(2): p. 293-301.

128. Engler, A.J., et al., *Surface probe measurements of the elasticity of sectioned tissue, thin gels and polyelectrolyte multilayer films: Correlations between substrate stiffness and cell adhesion.* Surface Science, 2004. **570**(1-2): p. 142-54.

129. Bao, G. and S. Suresh, *Cell and molecular mechanics of biological materials.* Nat Mater, 2003. **2**(11): p. 715-25.

130. Ingber, D.E., *Tensegrity I. Cell structure and hierarchical systems biology.* J Cell Sci, 2003. **116**(Pt 7): p. 1157-73.

131. Stamenovic, D., *Cell mechanics: two regimes, maybe three?* Nat Mater, 2006. **5**(8): p. 597-98.

132. Fung, Y.C., *Biomechanics : mechanical properties of living tissues*. 2nd ed. 1993, New York: Springer-Verlag.

133. Yang, W., et al., *Viscoelasticity of esophageal tissue and application of a QLV model.* J Biomech Eng, 2006. **128**(6): p. 909-16.

134. Costa, K.D., *Single-cell elastography: probing for disease with the atomic force microscope.* Dis Markers, 2003. **19**(2-3): p. 139-54.

135. Simon, A. and M.C. Durrieu, *Strategies and results of atomic force microscopy in the study of cellular adhesion.* Micron, 2006. **37**(1): p. 1-13.

136. Thoumine, O. and A. Ott, *Comparison of the mechanical properties of normal and transformed fibroblasts.* Biorheology, 1997. **34**(4-5): p. 309-26.

137. Ebenstein, D. and L. Pruitt, *Nanoindentation of biological materials.* Nanotoday, 2006. **1**(3): p. 26-33.

138. Dvorak, J.A., *The application of atomic force microscopy to the study of living vertebrate cells in culture.* Methods, 2003. **29**(1): p. 86-96.

139. Santos, N.C. and M.A. Castanho, *An overview of the biophysical applications of atomic force microscopy.* Biophys Chem, 2004. **107**(2): p. 133-49.

140. Alessandrini, A. and P. Facci, *AFM: a versatile tool in biophysics.* Measurement Science & Technology, 2005. **16**(6): p. R65-R92.

141. Butt, H.J., B. Cappella, and M. Kappl, *Force measurements with the atomic force microscope: Technique, interpretation and applications.* Surface Science Reports, 2005. **59**(1-6): p. 1-152.

142. Mathur, A.B., et al., *Endothelial, cardiac muscle and skeletal muscle exhibit different viscous and elastic properties as determined by atomic force microscopy.* J Biomech, 2001. **34**(12): p. 1545-53.

143. Collinsworth, A.M., et al., *Apparent elastic modulus and hysteresis of skeletal muscle cells throughout differentiation.* Am J Physiol Cell Physiol, 2002. **283**(4): p. C1219-27.

144. Berdyyeva, T.K., C.D. Woodworth, and I. Sokolov, *Human epithelial cells increase their rigidity with ageing in vitro: direct measurements.* Phys Med Biol, 2005. **50**(1): p. 81-92.

145. Costa, K.D., A.J. Sim, and F.C. Yin, *Non-Hertzian approach to analyzing mechanical properties of endothelial cells probed by atomic force microscopy.* J Biomech Eng, 2006. **128**(2): p. 176-84.

146. Jaasma, M.J., W.M. Jackson, and T.M. Keaveny, *Measurement and characterization of whole-cell mechanical behavior.* Ann Biomed Eng, 2006. **34**(5): p. 748-58.

147. Takai, E., et al., *Osteoblast elastic modulus measured by atomic force microscopy is substrate dependent.* Ann Biomed Eng, 2005. **33**(7): p. 963-71.

148. Liu, K.K., *Deformation behaviour of soft particles: a review.* Journal of Physics D-Applied Physics, 2006. **39**(11): p. R189-R199.

149. Darling, E.M., S. Zauscher, and F. Guilak, *Viscoelastic properties of zonal articular chondrocytes measured by atomic force microscopy.* Osteoarthritis Cartilage, 2006. **14**(6): p. 571-79.

150. VanVliet, K., *Probing drug-cell interactions.* Nanotoday, 2006. **1**(3): p. 18-25.

151. Kienberger, F., et al., *Molecular recognition imaging and force spectroscopy of single biomolecules.* Acc Chem Res, 2006. **39**(1): p. 29-36.

152. Adams, G.G. and M. Nosonovsky, *Contact modeling - forces.* Tribology International, 2000. **33**(5-6): p. 431-42.

153. Selwyn, A.P., *Prothrombotic and antithrombotic pathways in acute coronary syndromes.* Am J Cardiol, 2003. **91**(12A): p. 3H-11H.

154. Darling, E.M., et al., *A thin-layer model for viscoelastic, stress-relaxation testing of cells using atomic force microscopy: do cell properties reflect metastatic potential?* Biophys J, 2007. **92**(5): p. 1784-91.

155. Okajima, T., et al., *Stress relaxation of HepG2 cells measured by atomic force microscopy.* Nanotechnology, 2007. **18**(8): p 084010.

156. Wu, Q., Y. Andreopoulos, and S. Weinbaum, *From red cells to snowboarding: a new concept for a train track.* Phys Rev Lett, 2004. **93**(19): p. 194501.

157. Gleghorn, J.P., et al., *Boundary mode frictional properties of engineered cartilaginous tissues.* Eur Cell Mater, 2007. **14**: p. 20-8; discussion 28-9.

158. Schwab, A., *Function and spatial distribution of ion channels and transporters in cell migration.* Am J Physiol Renal Physiol, 2001. **280**(5): p. F739-47.

159. Siasos, G., et al., *Shear stress, protein kinases and atherosclerosis.* Curr Med Chem, 2007. **14**(14): p. 1567-72.

160. Dunn, A.C., et al., *Macroscopic friction coefficient measurements on living endothelial cells.* Tribology Letters, 2007. **27**(2): p. 233-38.

161. Singh, A., et al., *Facilitated stent delivery using applied topical lubrication.* Catheter Cardiovasc Interv, 2007. **69**(2): p. 218-22.

162. Holzapfel, G.A., M. Stadler, and T.C. Gasser, *Changes in the mechanical environment of stenotic arteries during interaction with stents: computational assessment of parametric stent designs.* J Biomech Eng, 2005. **127**(1): p. 166-80.

163. Costa, K.D. and F.C.P. Yin, *Analysis of indentation: Implications for measuring mechanical properties with atomic force microscopy.* Journal of Biomechanical Engineering-Transactions of the Asme, 1999. **121**(5): p. 462-71.

164. Brunner, C.A., et al., *Cell migration through small gaps.* Eur Biophys J, 2006. **35**(8): p. 713-19.

165. Ainslie, K.M., et al., *Vascular smooth muscle cell glycocalyx influences shear stress-mediated contractile response.* J Appl Physiol, 2005. **98**(1): p. 242-49.

166. Matsuura, E., G.R. Hughes, and M.A. Khamashta, *Oxidation of LDL and its clinical implication.* Autoimmun Rev, 2008. **7**(7): p. 558-66.

167. Ishigaki, Y., et al., *Impact of plasma oxidized low-density lipoprotein removal on atherosclerosis.* Circulation, 2008. **118**(1): p. 75-83.

168. Tsimikas, S., *Oxidized low-density lipoprotein biomarkers in atherosclerosis.* Curr Atheroscler Rep, 2006. **8**(1): p. 55-61.

169. Chouinard, J.A., et al., *Oxidized-LDL induce morphological changes and increase stiffness of endothelial cells.* Exp Cell Res, 2008. **314**(16): p.3007-16

170. Damiani, E., et al., *Altered expression of alpha-actin, smooth muscle myosin heavy chain-1 and calponin in cultured smooth muscle cells by oxidized low density lipoproteins.* FEBS Lett, 1998. **425**(1): p. 123-25.

171. Massaeli, H., et al., *Oxidized low-density lipoprotein induces cytoskeletal disorganization in smooth muscle cells.* Am J Physiol, 1999. **277**(5 Pt 2): p. H2017-25.

172. Rabinovich, Y., et al., *Atomic force microscopy measurement of the elastic properties of the kidney epithelial cells.* J Colloid Interface Sci, 2005. **285**(1): p. 125-35.

173. Rico, F., et al., *Probing mechanical properties of living cells by atomic force microscopy with blunted pyramidal cantilever tips.* Physical Review E, 2005. **72**(2): p. 02194.

174. Jaasma, M.J., W.M. Jackson, and T.M. Keaveny, *The effects of morphology, confluency, and phenotype on whole-cell mechanical behavior.* Ann Biomed Eng, 2006. **34**(5): p. 759-68.

175. Ingber, D.E., *Tissue adaptation to mechanical forces in healthy, injured and aging tissues.* Scand J Med Sci Sports, 2005. **15**(4): p. 199-201.

176. Poliseno, L., et al., *Resting smooth muscle cells as a model for studying vascular cell activation.* Tissue Cell, 2006. **38**(2): p. 111-20.

177. Han, M., et al., *Serum deprivation results in redifferentiation of human umbilical vascular smooth muscle cells.* Am J Physiol Cell Physiol, 2006. **291**(1): p. C50-8.

178. Kato, M. and M. Kyogoku, *Competence growth factors evoke the phenotypic transition of arterial smooth muscle cells.* Ann N Y Acad Sci, 1990. **598**: p. 232-37.

179. Patel, M.K., et al., *Effect of serum withdrawal on the contribution of L-type calcium channels (CaV1.2) to intracellular Ca2+ responses and chemotaxis in cultured human vascular smooth muscle cells.* Br J Pharmacol, 2005. **145**(6): p. 811-17.

180. Zimmermann, O., et al., *Serum starvation and growth factor receptor expression in vascular smooth muscle cells.* J Vasc Res, 2006. **43**(2): p. 157-65.

181. Sun, Z., et al., *Mechanical properties of the interaction between fibronectin and alpha5beta1-integrin on vascular smooth muscle cells studied using atomic force microscopy.* Am J Physiol Heart Circ Physiol, 2005. **289**(6): p. H2526-35.

182. Bacakova, L., V. Mares, and V. Lisa, *Gender-related differences in adhesion, growth and differentiation of vascular smooth muscle cells are enhanced in serum-deprived cultures.* Cell Biol Int, 1999. **23**(9): p. 643-48.

183. Orlov, S.N., et al., *Apoptosis in serum-deprived vascular smooth muscle cells: evidence for cell volume-independent mechanism.* Apoptosis, 2004. **9**(1): p. 55-66.

184. Kindy, M.S., C.J. Chang, and G.E. Sonenshein, *Serum deprivation of vascular smooth muscle cells enhances collagen gene expression.* J Biol Chem, 1988. **263**(23): p. 11426-30.

185. Chamley-Campbell, J., G.R. Campbell, and R. Ross, *The smooth muscle cell in culture.* Physiol Rev, 1979. **59**(1): p. 1-61.

186. Crick, S.L. and F.C. Yin, *Assessing micromechanical properties of cells with atomic force microscopy: importance of the contact point.* Biomech Model Mechanobiol, 2007. **6**(3): p. 199-210.

187. Smith, B.A., et al., *Probing the viscoelastic behavior of cultured airway smooth muscle cells with atomic force microscopy: Stiffening induced by contractile agonist.* Biophysical Journal, 2005. **88**(4): p. 2994-3007.

188. Dimitriadis, E.K., et al., *Determination of elastic moduli of thin layers of soft material using the atomic force microscope.* Biophys J, 2002. **82**(5): p. 2798-810.

189. A-Hassan, E., et al., *Relative microelastic mapping of living cells by atomic force microscopy.* Biophys J, 1998. **74**(3): p. 1564-78.

190. Worth, N.F., et al., *Vascular smooth muscle cell phenotypic modulation in culture is associated with reorganisation of contractile and cytoskeletal proteins.* Cell Motil Cytoskeleton, 2001. **49**(3): p. 130-45.

191. Oommen, B. and K.J. Van Vliet, *Effects of nanoscale thickness and elastic nonlinearity on measured mechanical properties of polymeric films.* Thin Solid Films, 2006. **513**(1-2): p. 235-42.

192. Simon, A., et al., *Characterization of dynamic cellular adhesion of osteoblasts using atomic force microscopy.* Cytometry Part A, 2003. **54A**(1): p. 36-47.

193. Domke, J., et al., *Substrate dependent differences in morphology and elasticity of living osteoblasts investigated by atomic force microscopy.* Coll Surf B-Biointerfaces, 2000. **19**(4): p. 367-79.

194. Qu, M.J., et al., *Frequency-dependent phenotype modulation of vascular smooth muscle cells under cyclic mechanical strain.* J Vasc Res, 2007. **44**(5): p. 345-53.

195. London, G.M., et al., *Arterial stiffness: pathophysiology and clinical impact.* Clin Exp Hypertens, 2004. **26**(7-8): p. 689-99.

196. Ma, X., Y. Wang, and N.L. Stephens, *Serum deprivation induces a unique hypercontractile phenotype of cultured smooth muscle cells.* Am J Physiol, 1998. **274**(5 Pt 1): p. C1206-14.

197. Li, C. and Q. Xu, *Mechanical stress-initiated signal transduction in vascular smooth muscle cells in vitro and in vivo.* Cell Signal, 2007. **19**(5): p. 881-91.

198. Suresh, S., *Biomechanics and biophysics of cancer cells.* Acta Biomater, 2007. **3**(4): p. 413-38.

199. Lammi, M.J., *Current perspectives on cartilage and chondrocyte mechanobiology.* Biorheology, 2004. **41**(3-4): p. 593-96.

200. Ohashi, T., et al., *Experimental and numerical analyses of local mechanical properties measured by atomic force microscopy for sheared endothelial cells.* Bio-Medical Materials and Engineering, 2002. **12**(3): p. 319-27.

201. VanDijk, A.M., et al., *Mechanics of resting isolated single vascular smooth muscle cells from bovine coronary artery.* Am J Physiol, 1984. **246**(3 Pt 1): p. C277-87.

202. Nagayama, K., S. Yanagihara, and T. Matsumoto, *A novel micro tensile tester with feed-back control for viscoelastic analysis of single isolated smooth muscle cells.* Med Eng Phys, 2007. **29**(5): p. 620-28.

203. Rotsch, C. and M. Radmacher, *Drug-induced changes of cytoskeletal structure and mechanics in fibroblasts: an atomic force microscopy study.* Biophys J, 2000. **78**(1): p. 520-35.

204. Wong, P.K., W. Tan, and C.M. Ho, *Cell relaxation after electrodeformation: effect of latrunculin A on cytoskeletal actin.* Journal of Biomechanics, 2005. **38**(3): p. 529-35.

205. Laudadio, R.E., et al., *Rat airway smooth muscle cell during actin modulation: rheology and glassy dynamics.* Am J Physiol Cell Physiol, 2005. **289**(6): p. C1388-95.

206. Tian, B., J.A. Kiland, and P.L. Kaufman, *Effects of the marine macrolides swinholide A and jasplakinolide on outflow facility in monkeys.* Invest Ophthalmol Vis Sci, 2001. **42**(13): p. 3187-92.

207. Bubb, M.R., et al., *Effects of jasplakinolide on the kinetics of actin polymerization. An explanation for certain in vivo observations.* J Biol Chem, 2000. **275**(7): p. 5163-70.

208. Wu, H.W., T. Kuhn, and V.T. Moy, *Mechanical properties of L929 cells measured by atomic force microscopy: effects of anticytoskeletal drugs and membrane crosslinking.* Scanning, 1998. **20**(5): p. 389-97.

209. Wang, N., *Mechanical interactions among cytoskeletal filaments.* Hypertension, 1998. **32**(1): p. 162-65.

210. Enomoto, T., *Microtubule disruption induces the formation of actin stress fibers and focal adhesions in cultured cells: possible involvement of the rho signal cascade.* Cell Struct Funct, 1996. **21**(5): p. 317-26.

211. Stamenovic, D., *Effects of cytoskeletal prestress on cell rheological behavior.* Acta Biomater, 2005. **1**(3): p. 255-62.

212. Nishimura, S., et al., *Microtubules modulate the stiffness of cardiomyocytes against shear stress.* Circ Res, 2006. **98**(1): p. 81-7.

213. Tagawa, H., et al., *Cytoskeletal mechanics in pressure-overload cardiac hypertrophy.* Circ Res, 1997. **80**(2): p. 281-89.

214. Yamamoto, S., et al., *Role of microtubules in the viscoelastic properties of isolated cardiac muscle.* J Mol Cell Cardiol, 1998. **30**(9): p. 1841-53.

215. Kikumoto, M., et al., *Flexural rigidity of individual microtubules measured by a buckling force with optical traps.* Biophys J, 2006. **90**(5): p. 1687-96.

216. Felgner, H., R. Frank, and M. Schliwa, *Flexural rigidity of microtubules measured with the use of optical tweezers.* J Cell Sci, 1996. **109 (Pt 2)**: p. 509-16.

217. Jordan, M.A., et al., *Mechanism of mitotic block and inhibition of cell proliferation by taxol at low concentrations.* Proc Natl Acad Sci U S A, 1993. **90**(20): p. 9552-56.

218. Dye, R.B., S.P. Fink, and R.C. Williams, Jr., *Taxol-induced flexibility of microtubules and its reversal by MAP-2 and Tau.* J Biol Chem, 1993. **268**(10): p. 6847-50.

219. Tanaka, T.T. and Y.C. Fung, *Elastic and inelastic properties of the canine aorta and their variation along the aortic tree.* J Biomech, 1974. **7**(4): p. 357-70.

220. Doehring, T.C., E.O. Carew, and I. Vesely, *The effect of strain rate on the viscoelastic response of aortic valve tissue: a direct-fit approach.* Ann Biomed Eng, 2004. **32**(2): p. 223-32.

221. Toms, S.R., et al., *Quasi-linear viscoelastic behavior of the human periodontal ligament.* J Biomech, 2002. **35**(10): p. 1411-15.

222. Provenzano, P., et al., *Nonlinear ligament viscoelasticity.* Ann Biomed Eng, 2001. **29**(10): p. 908-14.

223. Guo, D.C., et al., *Pathogenesis of thoracic and abdominal aortic aneurysms.* Ann N Y Acad Sci, 2006. **1085**: p. 339-52.

224. Doehring, T.C., et al., *Fractional order viscoelasticity of the aortic valve cusp: an alternative to quasilinear viscoelasticity.* J Biomech Eng, 2005. **127**(4): p. 700-8.

225. Bursac, P., et al., *Cytoskeletal remodelling and slow dynamics in the living cell.* Nat Mater, 2005. **4**(7): p. 557-61.

226. Desprat, N., et al., *Creep function of a single living cell.* Biophys J, 2005. **88**(3): p. 2224-33.

227. Fabry, B., et al., *Time scale and other invariants of integrative mechanical behavior in living cells.* Phys Rev E Stat Nonlin Soft Matter Phys, 2003. **68**(4 Pt 1): p. 041914.

228. Koay, E.J., A.C. Shieh, and K.A. Athanasiou, *Creep indentation of single cells.* J Biomech Eng, 2003. **125**(3): p. 334-41.

229. Lundkvist, A., et al. *Viscoelastic properties of healthy human artery measured in saline solution by AFM based indentation technique*. Spring Meeting of the Materials Research Society. 1998. San Francisco, CA: Materials Research Society.

230. Nagatomi, J., et al., *Contribution of the extracellular matrix to the viscoelastic behavior of the urinary bladder wall.* Biomech Model Mechanobiol, 2007. **7**(5): p. 395-404.

231. Moghani, T., et al., *Finite element simulation of elastohydrodynamic lubrication of soft biological tissues.* Computers & Structures, 2007. **85**(11-14): p. 1114-20.

232. Chang, Y.I. and Y.F. Wang, *A preliminary study on the initial elastic adhesion behavior of leucocytes.* Colloids and Surfaces a-Physicochemical and Engineering Aspects, 1998. **140**(1-3): p. 395-401.

233. Welt, F.G. and C. Rogers, *Inflammation and restenosis in the stent era.* Arterioscler Thromb Vasc Biol, 2002. **22**(11): p. 1769-76.

234. Weinbaum, S., J.M. Tarbell, and E.R. Damiano, *The structure and function of the endothelial glycocalyx layer.* Annual Review of Biomedical Engineering, 2007. **9**: p. 121-67.

235. Nilsson, J., et al., *Cell surface components and growth regulation in cultivated arterial smooth muscle cells.* J Cell Sci, 1983. **64**: p. 107-21.

236. den Otter, W.K. and S.A. Shkulipa, *Intermonolayer friction and surface shear viscosity of lipid bilayer membranes.* Biophys J, 2007. **93**(2): p. 423-33.

237. Stamenovic, D. and N. Wang, *Invited review: engineering approaches to cytoskeletal mechanics.* J Appl Physiol, 2000. **89**(5): p. 2085-90.

238. Dunn, A.C., et al., *Friction coefficient measurement of hydrogel materials on living epithelial cells.* Tribology Letters, 2008. **30**(1): p. 13-19.

239. Cobb, J.A., et al., *A novel method for low load friction testing on living cells.* Biotechnol Lett, 2007. **30**(5): 801-6.

240. Han, L., et al., *Lateral nanomechanics of cartilage aggrecan macromolecules.* Biophys J, 2007. **92**(4): p. 1384-98.

241. Varenberg, M., I. Etsion, and G. Halperin, *An improved wedge calibration method for lateral force in atomic force microscopy.* Review of Scientific Instruments, 2003. **74**(7): p. 3362-67.

242. Bacabac, R.G., et al., *Dynamic shear stress in parallel-plate flow chambers.* J Biomech, 2005. **38**(1): p. 159-67.

243. Bowden, F.P. and D. Tabor, *Friction and lubrication of solids*. 1950, Oxford,: Clarendon Press.

244. Karuppiah, K.S.K., et al., *The effect of protein adsorption on the friction behavior of ultra-high molecular weight polyethylene.* Tribology Letters, 2006. **22**(2): p. 181-88.

245. Mahaffy, R.E., et al., *Scanning probe-based frequency-dependent microrheology of polymer gels and biological cells.* Physical Review Letters, 2000. **85**(4): p. 880-83.

246. Jin, Z.M. and D. Dowson, *Elastohydrodynamic lubrication in biological systems.* Proceedings of the Institution of Mechanical Engineers Part J-Journal of Engineering Tribology, 2005. **219**(J5): p. 367-80.

247. Dowson, D., *Developments in Lubrication - the Thinning Film.* Journal of Physics D-Applied Physics, 1992. **25**(1A): p. A334-A39.

248. Ho, S.P., et al., *Experimental and numerical modeling of variable friction between nanoregions in coventional and crosslinked UHMWPE.* J Biomech Eng, 2004. **126**(1): p. 111-19.

249. Hemmer, J., et al., *Role of Cytoskeletal Components in Stress Relaxation Behavior of Adherent Vascular Smooth Muscle Cells* Journal of Biomechanical Engineering-Transactions of the ASME, 2008. In Press.

250. Hemmer, J.D., et al., *Effects of serum deprivation on the mechanical properties of adherent vascular smooth muscle cells.* Proc Inst Mech Eng [H], 2008. **222**(5): p. 761-72.

251. Adiguzel, E., et al., *Migration and growth are attenuated in vascular smooth muscle cells with type VIII collagen-null alleles.* Arterioscler Thromb Vasc Biol, 2006. **26**(1): p. 56-61.

252. Zettler, M.E., et al., *OxLDL stimulates cell proliferation through a general induction of cell cycle proteins.* Am J Physiol Heart Circ Physiol, 2003. **284**(2): p. H644-53.

253. Chien, M.W., et al., *OxLDL induces mitogen-activated protein kinase activation mediated via PI3-kinase/Akt in vascular smooth muscle cells.* J Lipid Res, 2003. **44**(9): p. 1667-75.

254. Etienne-Manneville, S., *Actin and microtubules in cell motility: which one is in control?* Traffic, 2004. **5**(7): p. 470-77.

255. Gerthoffer, W.T., *Mechanisms of vascular smooth muscle cell migration.* Circ Res, 2007. **100**(5): p. 607-21.

256. Mitchison, T.J., G.T. Charras, and L. Mahadevan, *Implications of a poroelastic cytoplasm for the dynamics of animal cell shape.* Semin Cell Dev Biol, 2008. **19**(3): p. 215-23.

257. Faries, P.L., et al., *Vascular smooth muscle cells derived from atherosclerotic human arteries exhibit greater adhesion, migration, and proliferation than venous cells.* J Surg Res, 2002. **104**(1): p. 22-8.

258. Sukhanov, S. and P. Delafontaine, *Protein chip-based microarray profiling of oxidized low density lipoprotein-treated cells.* Proteomics, 2005. **5**(5): p. 1274-80.

259. Cheng, J., et al., *Mechanical stretch inhibits oxidized low density lipoprotein-induced apoptosis in vascular smooth muscle cells by up-regulating integrin alphavbeta3 and stablization of PINCH-1.* J Biol Chem, 2007. **282**(47): p. 34268-75.

260. Mackman, N., *How do oxidized phospholipids inhibit LPS signaling?* Arterioscler Thromb Vasc Biol, 2003. **23**(7): p. 1133-36.

261. Qiao, C., K. Zhang, and J. Xia, *Influence of oxidized low density lipoprotein on the proliferation of human artery smooth muscle cells in vitro.* J Huazhong Univ Sci Technolog Med Sci, 2007. **27**(1): p. 20-3.

262. Kumar, S., et al., *Viscoelastic retraction of single living stress fibers and its impact on cell shape, cytoskeletal organization, and extracellular matrix mechanics.* Biophys J, 2006. **90**(10): p. 3762-73.

263. Fabry, B., et al., *Scaling the microrheology of living cells.* Phys Rev Lett, 2001. **87**(14): p. 148102.

264. Meisinger, C., et al., *Plasma oxidized low-density lipoprotein, a strong predictor for acute coronary heart disease events in apparently healthy, middle-aged men from the general population.* Circulation, 2005. **112**(5): p. 651-57.

265. Naruko, T., et al., *Persistent high levels of plasma oxidized low-density lipoprotein after acute myocardial infarction predict stent restenosis.* Arterioscler Thromb Vasc Biol, 2006. **26**(4): p. 877-83.

266. Holvoet, P., et al., *Circulating oxidized LDL is a useful marker for identifying patients with coronary artery disease.* Arterioscler Thromb Vasc Biol, 2001. **21**(5): p. 844-48.

267. Nakajima, K., T. Nakano, and A. Tanaka, *The oxidative modification hypothesis of atherosclerosis: the comparison of atherogenic effects on oxidized LDL and remnant lipoproteins in plasma.* Clin Chim Acta, 2006. **367**(1-2): p. 36-47.

268. Toikka, J.O., et al., *Decreased large artery distensibility in borderline hypertension is related to increased in vivo low-density lipoprotein oxidation.* Scand J Clin Lab Invest, 2002. **62**(4): p. 301-6.

269. Toikka, J.O., et al., *Large-artery elastic properties in young men : relationships to serum lipoproteins and oxidized low-density lipoproteins.* Arterioscler Thromb Vasc Biol, 1999. **19**(2): p. 436-41.